Heinrich Heine Universität Düsseldorf

Funktionelle und mechanistische Rolle von EIN2 als zentralem Regulator der Ethylensignalkette:

Nukleärer Import und Interaktionsarchitektur mit nachgeschalteten Transkriptions- und Chromatinregulatoren

---

Inaugural-Dissertation

zur Erlangung des Doktorgrades
der Mathematisch-Naturwissenschaftlichen Fakultät
der Heinrich-Heine-Universität Düsseldorf

vorgelegt von

Fabian Wynen

aus Düsseldorf

Düsseldorf, August 2026

aus dem Institut für Biochemische Pflanzenphysiologie
der Heinrich-Heine-Universität Düsseldorf

Gedruckt mit der Genehmigung der
Mathematisch-Naturwissenschaftlichen Fakultät der
Heinrich-Heine-Universität Düsseldorf

Berichterstatter:

1. Prof. Dr. Georg Groth

2. Prof. Dr. Lutz Schmitt

Tag der mündlichen Prüfung:

Abstract

Ethylene is a small, gaseous phytohormone responsible for modulation of several developmental plant processes such as flower senescence, seed germination, and fruit ripening of climacteric fruits. Upon ethylene perception by receptors located in the endoplasmic reticulum membrane, inhibition of the kinase CTR1 triggers proteolytic cleavage of the key regulator EIN2. This, in turn, allows its translocation into the nucleus, where ethylene responses are activated by the transcription factors EIN3 and EIL1. Despite extensive investigation of the ethylene pathway, the molecular mechanisms underlying nucleocytoplasmic transport of EIN2 followed by nuclear events upon EIN2 nuclear entry remained poorly understood. In this work, phenotypical analysis of *Arabidopsis thaliana* mutant seedlings revealed the involvement of the Importin-α superfamily in the nucleocytoplasmic transport of EIN2. Despite the functional redundancy within this family, biophysical *in vitro* and *in planta* characterization revealed distinct binding affinities among individual isoforms, indicating isoform-specific functions for EIN2 nuclear trafficking. Furthermore, a direct interaction between EIN2 and EIN3 was demonstrated for the first time in several biological systems, providing new insights into the molecular mechanisms linking EIN2 nuclear import to transcriptional regulation. Concentration-dependent competition between ENAP1 and EIN3 for binding to EIN2 suggests a more dynamic transcriptional regulation involving sequential protein interactions rather than the formation of a stable ternary complex. Moreover, systematic domain mapping of EIN3 identified distinct protein regions required for homodimerization, nuclear localization, and transcriptional regulation. Together, the findings of this thesis refine our current molecular understanding of the ethylene signaling pathway and provide a mechanistic framework for further functional and structural studies.

Zusammenfassung

Ethylen ist ein kleines gasförmiges Phytohormon, das zahlreiche pflanzliche Entwicklungsprozesse wie die Blütenseneszenz, die Samenkeimung oder die Fruchtreifung klimakterischer Früchte reguliert. Durch Rezeptoren, die in der Membran des endoplasmatischen Retikulums lokalisiert sind, kommt es in Anwesenheit von Ethylen zur Inhibition der Kinase CTR1, wodurch anschließend der Hauptregulator des Ethylensignalwegs, EIN2, proteolytisch gespalten wird. Dadurch wird dessen Translokation in den Zellkern ermöglicht, in dem die Ethylenantwort durch die Transkriptionsfaktoren EIN3 und EIL1 ausgelöst wird. Trotz intensiver Untersuchungen des Ethylensignalwegs blieben die molekularen Mechanismen des nukleozytoplasmatischen Transports von EIN2 sowie die nach dessen Kernimport ablaufenden nukleären Prozesse bislang nur unzureichend verstanden. Im Rahmen dieser Arbeit konnte anhand von phänotypischen Analysen von *Arabidopsis thaliana*-Mutanten gezeigt werden, dass die Importin-α-Superfamilie an dem nukleozytoplasmatischen Transport von EIN2 beteiligt ist. Trotz der funktionellen Redundanz innerhalb dieser Proteinfamilie wurden mithilfe biophysikalischer *in vitro*- und *in planta*-Experimente unterschiedliche Bindungsaffinitäten einzelner Isoformen bestimmt, was auf Isoform-spezifische Funktionen bezüglich des EIN2-Kernimports hindeutet. Darüber hinaus konnte erstmals eine direkte Interaktion zwischen EIN2 und EIN3 in verschiedenen biologischen Systemen nachgewiesen werden, wodurch neue molekulare Einblicke in den Zusammenhang zwischen dem nukleozytoplasmatischen Transport von EIN2 und der nachgeschalteten transkriptionellen Regulation gewonnen wurden. Die beobachtete konzentrationsabhängige Konkurrenz zwischen ENAP1 und EIN3 um die Bindung an EIN2 spricht für einen dynamischeren Mechanismus der Transkriptionsregulation, der mit größerer Wahrscheinlichkeit auf sequenziellen Proteininteraktionen als auf der Bildung eines stabilen ternären Komplexes beruht. Durch die systematische funktionelle Charakterisierung von EIN3 konnten Proteinregionen identifiziert werden, die für die Homodimerisierung, Kernlokalisation sowie die transkriptionelle Regulation erforderlich sind. Die Ergebnisse dieser Arbeit erweitern unser aktuelles molekulares Verständnis des Ethylensignalwegs und liefern einen mechanistischen Rahmen für weiterführende funktionelle und strukturelle Untersuchungen.

Table of Contents

Abstract ..... **III**
Zusammenfassung ..... **IV**
Table of Contents ..... **V**
List of Abbreviations ..... **VI**
List of Figures ..... **IX**
1 Introduction **10**
1.1 The ethylene signaling pathway – an overview 10
1.1.1 Ethylene receptors – the initial instance in ethylene signaling 12
1.1.2 CTR1 – coupling the signal towards cleavage 13
1.2 The ethylene signaling pathway – signal transduction 14
1.2.1 EIN2 – the central player in ethylene signaling 14
1.2.2 Nuclear transport machinery – bridging the ER-nuclear gap 16
1.2.2.1 Importin-alpha (IMPα) superfamily 17
1.2.2.2 Importin-beta (IMPβ) superfamily 19
1.3 The ethylene signaling pathway – ethylene response 22
1.3.1 Ethylene transcription factors – activating ethylene responses 23
1.3.2 EIN3 family – the key regulatory hub in ethylene signaling 23
2 Aim of this thesis **26**
3 Results **27**
3.1 Nucleocytoplasmic transport of EIN2 27
3.2 Molecular events upon EIN2 nuclear entry 60
4 Discussion **102**
5 Literature **114**
6 Acknowledgement **123**
7 Declaration **125**

List of Abbreviations

3-AT	3-amino-1,2,4-triazole
5-TAMRA	5-carboxytetramethylrhodamine
ABA	Abscisic acid
ACC	1-aminocyclopropane-1-carboxylate
AD	Activation Domain
ANOVA	Analysis Of Variance
AP2	Apetala2
ARM	Armadillo-repeat
At	*Arabidopsis thaliana*
BD	Binding Domain
BLI	Biolayer Interferometry
CAS	Cellular Apoptosis Susceptibility
CBF	C-repeat Binding Factor
CER	Cerulean
ChIP-Seq	Chromatin immunoprecipitation sequencing
Cryo-EM	Cryo-Electron Microscopy
CTR1	Constitutive Triple Response 1
DREB	Drought-Responsive Element Binding
EBF1/2	EIN3 Binding F-Box 1/2
EBS	EIN3 Binding Site
E. coli	*Escherichia coli*
EDF	Ethylene response DNA-binding Factor
EIN2-5	Ethylene Insensitive 2-5
EIL1-5	EIN3-like 1-5
ENAP1/2	EIN2 Nuclear Associated Protein 1/2
EPR	Electron Paramagnetic Resonance
ER	Endoplasmic reticulum
ERF	Ethylene Response Factor
ERS1/2	Ethylene Response Sensor 1/2
ETP1/2	EIN2 Targeting Protein 1/2
ETR1/2	Ethylene Resistant 1/2

EU	European Union
FLIM	Fluorescence Lifetime Imaging Microscopy
FP	Fluorescence Polarization
FRET	Förster's Resonance Energy Transfer
GAF	cGMP-specific phosphodiesterase, adenylyl cyclases, and FhlA
GB1	Immunoglobulin-binding domain B1 of streptococcal protein G
GFP	Green Fluorescent Protein
GOI	Gene of Interest
HAT	Histone acetyltransferase
HDAC	Histone deacetylase
HDX-MS	Hydrogen-Deuterium Exchange Mass Spectrometry
HEAT	Huntingtin, Elongation Factor 3, Protein Phosphatase 2A, TOR1
His-tag	Poly-Histidine tag
IBB	Importin-β Binding Domain
IMAC	Immobilized Metal Affinity Chromatography
IMPα	Importin-alpha
IMPβ	Importin-beta
IPTG	Isopropyl-β-D-thiogalactopyranoside
JA	Jasmonic acid
K_D	Dissociation constant
kDa	Kilodalton
MST	Microscale Thermophoresis
NASC	Nottingham Arabidopsis Stock Centre
NES	Nuclear Export Signal
NLS	Nuclear Localization Sequence
NMR	Nuclear Magnetic Resonance
NOP-1	NLS-derived Octa-Peptide-1
NPC	Nuclear Pore Complex
NUP	Nucleoporin
OD_{600}	Optical density at 600 nm
PAB	Poly-A Binding Protein
P-body	Processing Body
qPCR	quantitative Polymerase Chain Reaction

PDB	Protein Database
RAN1	Responsive to Antagonist 1
Ran	RAS-related Nuclear Protein
RanGAP	Ran GTPase Activating Protein
RanBP1	Ran Binding Protein 1
Ran_{GDP}	GDP-bound RAN
Ran_{GTP}	GTP-bound RAN
RAV	Related to Abscisic Acid Insensitivity 3/Viviparous 1
RNA	Ribonucleic acid
SCF	SKP1-Cullin-F-Box
SEC-MALS	Size Exclusion Chromatography-Multi Angle Light Scattering
SPR	Surface Plasmon Resonance
SUB-Y2H	Split-ubiquitin yeast two-hybrid
TAIR	The Arabidopsis Information Resource
TF	Transcription factor
TOR	Target of Rapamycin
UTR	Untranslated region
Y2H	Yeast two-hybrid
YFP	Yellow Fluorescent Protein

List of Figures

Figure 1: Schematic overview of the ethylene signaling pathway 11
Figure 2: Classification of ethylene receptors (ETRs) 12
Figure 3: Triple response phenotype of *A. thaliana* wildtype and *ein2-5* mutant seedlings 15
Figure 4: Different classes of nuclear localization sequences (NLSs) and overall Importin-α (IMPα) architecture 18
Figure 5: Schematic illustration of the Importin-α/β (IMPα/β)-mediated nuclear import cycle 21
Figure 6: Heat map representing the transcription levels of the EIN3 family in different plant tissues 25

1 Introduction

1.1 The ethylene signaling pathway – an overview

Ethylene, a gaseous plant hormone, regulates numerous developmental and stress-related processes, including fruit ripening, leaf abscission, and senescence (Abeles, 1992; Bakshi et al., 2015). The intensely studied signaling pathway comprises a negative feedback loop that regulates ethylene perception initiated by a family of ethylene receptors (ETRs) (Bleecker and Kende, 2000; Chen et al., 2002; Ecker, 1995). In the absence of ethylene, the Raf-like serine/threonine kinase CTR1 (CONSTITUTIVE TRIPLE RESPONSE 1) phosphorylates the key player in ethylene signal transduction, EIN2 (ETHYLENE INSENSITIVE 2), leading to ubiquitination mediated by ETP1/2 (EIN2 TARGETING PROTEIN 1 and 2) and SCF-E3 (SKP1, CULLINS, F-BOX PROTEINS). This regulatory cascade ultimately marks EIN2 for proteasomal degradation (Ju et al., 2012; Kieber et al., 1993; Qiao et al., 2009). In addition, ethylene transcription factors such as EIN3 (ETHYLENE INSENSITIVE 3), EIL1 (EIN3-LIKE 1), and EIL2 undergo ubiquitination by EBF1/2 (EIN3 BINDING F-BOX1 and 2) and SCF-E3 complexes, which cannot be prevented due to diminished EIN2 levels (Guo and Ecker, 2003; Potuschak et al., 2003). Thus, no ethylene response occurs. In contrast, the action of ETRs upon ethylene perception results in the inhibition of CTR1 (Ju et al., 2012). This, in turn, prevents phosphorylation of EIN2 by CTR1, resulting in cleavage of the cytosolic C-terminal part of EIN2 from its transmembrane N-terminal section by a protease that has not been identified yet (Wen et al., 2012). The C-terminal part of EIN2 (C-END; residues 479-1294 in the context of this thesis) is the key player in transducing the signal received at the endoplasmic reticulum (ER) membrane to the nucleus (Wen et al., 2012). Upon cleavage, EIN2 (C-END) is transported from the cytoplasm to and into the nucleus, where it is suggested to activate and stabilize the ethylene transcription factors EIN3, EIL1, and EIL2 together with ENAP1/2 (EIN2 NUCLEAR ASSOCIATED PROTEIN 1 and 2) (Zhang et al., 2017), thus resulting in ethylene responses.

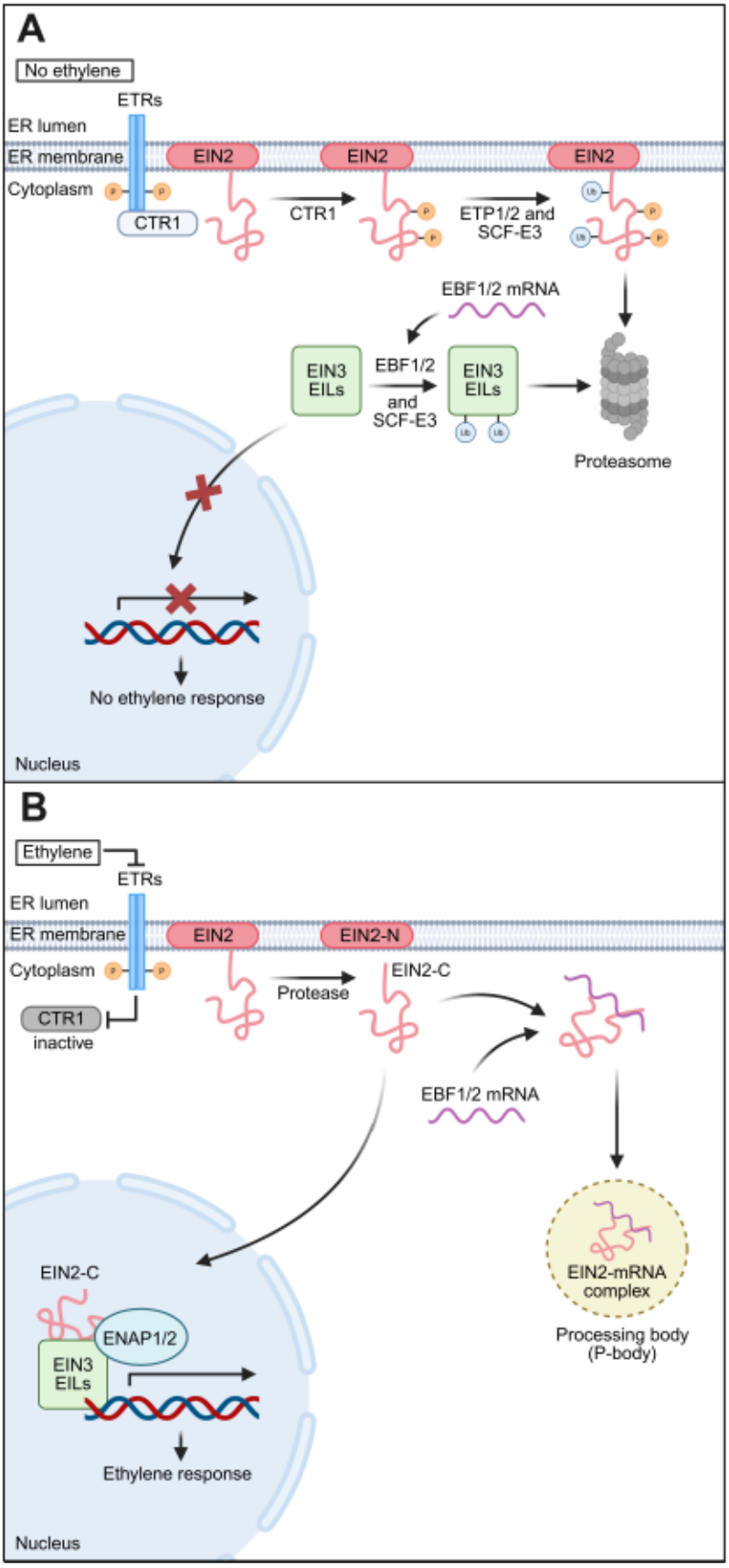

Figure 1: Schematic overview of the ethylene signaling pathway. A) In the absence of ethylene, the Raf-like kinase CTR1 phosphorylates the key regulator EIN2. The phosphorylation of EIN2 leads to ubiquitination of EIN2 by ETP1/2 and SCF-E3 ubiquitin ligase consequently resulting in degradation of EIN2. Additionally, transcription factors belonging to the EIN3 family, especially EIN3 and EIL1, are targeted by EBF1/2 and SCF-E3 complexes for ubiquitination also leading to proteasomal degradation. Thus, no ethylene response occurs. B) Ethylene acts as a negative regulator and is sensed by ethylene receptors (ETRs) located in the ER membrane. The perception of ethylene induces a signaling cascade that leads to inhibition of CTR1. Due to diminished kinase activity of CTR1, EIN2 escapes phosphorylation and instead undergoes proteolytic cleavage by an unidentified protease. Cleavage of EIN2 results in an N-terminal membrane-remaining part (EIN2 (N-END)) and a cytosolic C-terminal domain (EIN2 (C-END)). This, in turn, leads to prevention of EBF1/2 translation mediated by the formation of EIN2-EBF1/2-mRNA complexes in so-called processing bodies (P-bodies) ultimately resulting in accumulation of EIN3/EIL1 protein levels in the nucleus. Additionally, EIN2 is transported into the nucleus, where it is suggested to activate or stabilize the transcription factors in an interplay with ENAP1/2 leading to a transcriptional cascade in response to ethylene. Created with BioRender and reproduced according to (Binder, 2020).

1.1.1 Ethylene receptors – the initial instance in ethylene signaling

Ethylene perception in *Arabidopsis thaliana* is mediated by a family of ER-integrated ethylene receptors consisting of five different proteins: ETR1 (ETHYLENE RESISTANT 1), ETR2, ERS1 (ETHYLENE RESPONSE SENSOR 1), ERS2, and EIN4 (ETHYLENE INSENSITIVE 4). This receptor family possesses an overall architecture consisting of three N-terminally located transmembrane α-helices, followed by a GAF domain (cGMP-SPECIFIC PHOSPHODIESTERASE, ADENYLYL CYCLASES, AND FhlA) and a kinase domain. Additionally, ETR1, ETR2, and EIN4 contain a receiver domain located at the C-terminus (Binder, 2020; Lacey and Binder, 2014). Based on phylogenetic analysis and sequence alignments, the ethylene receptor family can be further divided into two categories: subfamily 1 and subfamily 2 (Hall et al., 2007). Members of the first subfamily, such as ETR1 and ERS1, share the aforementioned structural architecture, whereas ETR2, ERS2, and EIN4 belong to subfamily 2 and possess additional N-terminally located amino acids with yet unknown function (Binder, 2020; Hall et al., 2007; Lacey and Binder, 2014). Moreover, ETR1 exhibits histidine kinase activity *in vitro*, whereas all other receptors possess serine/threonine kinase activity. ERS1 is the only receptor reported to exhibit both histidine and serine/threonine kinase activity *in vitro* (Gamble et al., 1998; Moussatche and Klee, 2004). The receptors function as homodimers and constitute the primary ethylene sensors in the

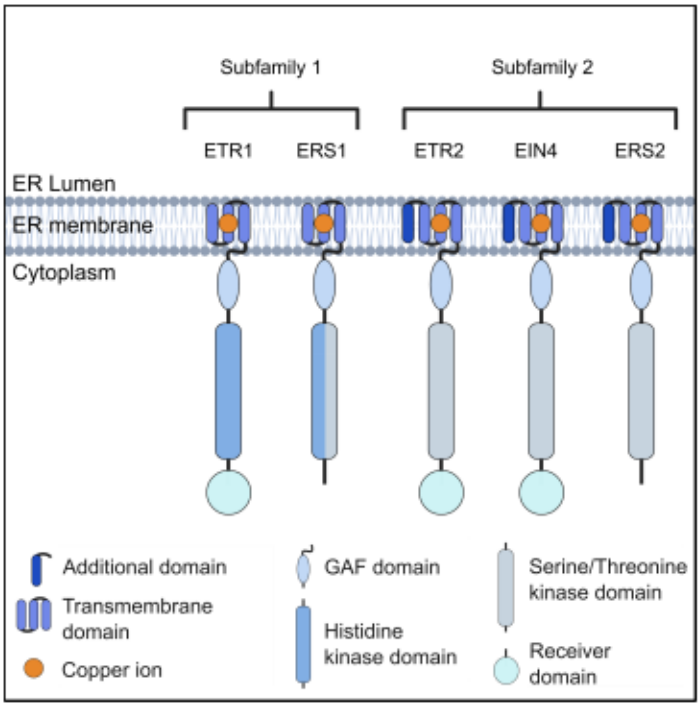

Figure 2: Classification of ethylene receptors (ETRs). The five ETRs encoded in the *A. thaliana* genome are subdivided into subfamily 1 and 2. They share an overall conserved architecture consisting of a transmembrane domain, a GAF domain, and a kinase domain. Members of the subfamily 2 possess an additional N-terminally located domain pointed towards the ER lumen. However, its function remains unclear. ETR1, ETR2, and EIN4 contain a receiver domain at the C-terminus, whereas this domain is lacking in ERS receptors. Despite all receptors possessing a kinase domain, they differ in their activity. *In vitro*, ETR1 exhibited histidine kinase activity, while the other four receptors have serine/threonine kinase activity. Only ERS1 has been reported to exhibit both kinase activities *in vitro*. ETRs are depicted in their inactive monomeric form for clarity. Created with BioRender and reproduced according to (Binder, 2020).

signaling pathway. The dimerization takes place between the transmembrane area and the GAF domain of the receptors and is stabilized by two disulfide bonds in the N-terminal region (Binder, 2020; Grefen et al., 2008). Although ethylene binds to the N-terminal transmembrane region, the conserved cysteines Cys4 and Cys6, forming the disulfide bonds in ETR1, are not necessary for ethylene binding or a functional state of this receptor *in planta* (Chen et al., 2010; Xie et al., 2006). Instead, residues in transmembrane helix 1 (Asp25, Tyr32, Ile35, and Pro36) and transmembrane helix 2 (Ile62, Cys65, and His69) are crucial for ethylene binding to ETR1 since mutations in these residues abolished ethylene binding up to less than 5 % (Rodrıguez et al., 1999; Schaller and Bleecker, 1995; Wang et al., 2006). Especially, Cys65 and His69, located in transmembrane helix 2, were identified as copper binding sites, which is a necessary co-factor for ethylene binding primarily delivered by the ER-localized copper transporter RAN1 (RESPONSIVE TO ANTAGONIST 1) (Hirayama et al., 1999; Hoppen et al., 2019b; Rodrıguez et al., 1999). In addition, direct interactions between ETRs and soluble chaperones ATX1 (ANTIOXIDANT-1) and CCH (COPPER CHAPERONE) were demonstrated by biophysical interaction studies, suggesting another route for copper exchange (Hoppen et al., 2019b). Prior binding studies gave evidence that the stoichiometry is two copper ions per dimer instead of one copper ion (Schott-Verdugo et al., 2019). Despite decades of research and numerous discoveries regarding the ethylene receptors, the molecular mechanisms underlying ethylene signal transduction and the molecular relationship between CTR1 and ETR1 remain largely unknown (Binder, 2020; Zhong and Chang, 2012).

1.1.2 CTR1 – coupling the signal towards cleavage

The *A. thaliana* CTR1 protein is an ER-associated Raf-like kinase with serine/threonine activity consisting of 821 amino acids (Zhong and Chang, 2012). The catalytic activity of CTR1 resides in its C-terminal part, while the N-terminal region, comprising amino acids 1-550, functions as a regulatory domain (Kieber et al., 1993; Zhong and Chang, 2012). The regulatory domain is essential for the interaction with ethylene receptors at their histidine kinase domain, as shown by yeast two-hybrid (Y2H) studies (Clark et al., 1998). This ensures the association of CTR1 at the ER membrane since ER association levels of CTR1 decreased significantly in multiple loss-of-function ethylene receptor mutants (Gao et al., 2003). Although the interaction interface comprises the histidine kinase domain, the activity of this domain is not necessary for interaction with

CTR1 (Gao et al., 2003). As the name suggests, *ctr1* mutant seedlings exhibit the "triple response" phenotype even in the absence of ethylene, although this phenotype is only visible in the presence of ethylene in wildtype seedlings (Zhong and Chang, 2012). The "triple response" is a typical response of wildtype *Arabidopsis thaliana* plants towards ethylene when grown in the dark and is characterized by an exaggerated apical hook, bushy roots, and a shortened hypocotyl (Bleecker et al., 1988; Chang et al., 1993; Guzman and Ecker, 1990; Kieber et al., 1993). Based on these results, CTR1 was identified as a negative regulator of the ethylene signaling pathway, which is inhibited by ethylene receptors (ETRs) upon ethylene perception. Therefore, it is a downstream-acting component of the ETRs but an upstream-functioning component of the key regulator EIN2, which is another interaction partner of CTR1 apart from the ethylene receptors (Ju et al., 2012; Kieber et al., 1993; Zhong and Chang, 2012).

1.2 The ethylene signaling pathway – signal transduction

The ethylene signaling pathway is initiated by ethylene binding to the ETRs at the ER membrane. However, the ethylene response occurs in the nucleus. This raises the question of how the signal, initially perceived at the ER membrane by ETRs, is transduced via the cytoplasm and ends up in the nucleus. This is where EIN2, the central regulator of the ethylene signaling pathway, becomes essential for signal transduction and will be discussed in more detail in the following section.

1.2.1 EIN2 – the central player in ethylene signaling

EIN2 is an ER-localized integral membrane protein containing 1294 amino acids in *A. thaliana* (molecular weight of around 141 kDa) (UniProt Consortium, 2018) and can be divided into two domains: 1) The N-terminal hydrophobic part (residues 1-461) consisting of 12 transmembrane spanning helices and 2) the C-terminal hydrophilic part (residues 462-1294) which is localized in the cytoplasm (Alonso et al., 1999). The N-terminus of EIN2 possesses a 21 % sequence similarity with the Nramp protein family involved in the transport of divalent metal ions, although no such function has been identified in EIN2 yet (Alonso *et al.*, 1999; Zheng and Zhu, 2016). However, recent plant genetic studies combined with Y2H assays discovered a new regulatory factor, *Os*MHZ3 (Mao Hu Zi 3), that is suggested to interact with the N-terminal part of EIN2 from *Oryza sativa* and inhibit the 26S proteasome pathway, thus preventing

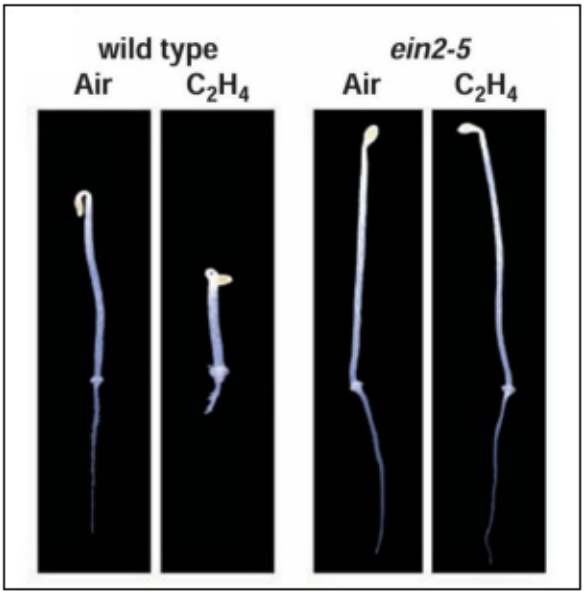

Figure 3: Triple response phenotype of *A. thaliana* wildtype and *ein2-5* mutant seedlings. In the presence of ethylene, wildtype seedlings grown in the dark exhibit the so-called triple response phenotype, indicated by bushy roots, shortened hypocotyl, and an exaggerated apical hook. In contrast, ethylene perception is impaired in ein2-5 mutants leading to normal growth behavior

*Os*EIN2 degradation (Ma et al., 2018; Su and Hou, 2024). Apart from this, the biochemical function of the N-terminus of EIN2 remains mostly unclear and has to be further investigated in the future. In contrast, the C-terminal part of EIN2 has been studied more thoroughly than its N-terminal region. Apart from ethylene signaling, several physiological functions regulated by EIN2 proteins from different species were discovered, such as endosperm and embryo development in *Zea mays* and stomatal closure, hypocotyl elongation, and root meristem proliferation upon glucose depletion in *Arabidopsis thaliana* (Fu et al., 2021; Gallie and Young, 2004; Zhao et al., 2021). Despite its involvement in diverse biological processes (Su and Hou, 2024), EIN2 is primarily recognized as the central regulator of the ethylene signaling pathway. Over the last decades, various *ein2* mutants were discovered that exhibited an insensitivity towards ethylene indicated by the lack of the aforementioned "triple response" phenotype (Alonso *et al.*, 1999; Guzman and Ecker, 1990). Complementation experiments with *ein2* mutants using the C-terminal part of EIN2 (residues 479-1294) restored the ability of ethylene sensing in light-grown and dark-grown seedlings (Alonso et al., 1999; Bisson and Groth, 2010). Therefore, the C-terminal domain of EIN2 is sufficient for ethylene signal transduction, which is achieved in two different ways: On the one hand, EIN2 forms complexes with mRNAs of EBF1 and EBF2, which regulate the proteasomal degradation of the ethylene transcription factors EIN3 and EIL1 (An et al., 2010). These EIN2-mRNA complexes are taken up by so-called processing bodies (P-bodies), in which the mRNA is degraded, leading to translational silencing of the EBF1/2 mRNA and thus, stabilization of EIN3 and EIL1 by preventing the proteasomal degradation of both proteins (Li et al., 2015). The minimal EIN2 sequence required for translational silencing was identified as *At*EIN2$^{654-1272}$. Additionally, the poly-uridylates (poly-U) motifs within the 3' UTR of

the target mRNA were shown to be crucial for this process (Li et al., 2015). Furthermore, EIN2 interacts with exoribonuclease EIN5 and several other poly-adenylate (poly-A) binding proteins (PABs) such as PAB2, PAB4, and PAB8 to relocate the EIN2-mRNA complex into P-bodies (Li et al., 2015; Su and Hou, 2024). On the other hand, EIN2 is translocated into the nucleus, where it stabilizes EIN3 and EIL1. Previous chromatin immunoprecipitation sequencing (ChIP-Seq) studies also identified the nuclear proteins ENAP1 and ENAP2 as interaction partners of both EIN2 and EIN3 (Zhang et al., 2016; Zhang et al., 2017). Since histone acetylation levels were found to be elevated in an EIN2-dependent manner, it was suggested that EIN2 and ENAPs might play a regulative role in histone acetylation (Zhang et al., 2017). Histone acetylation loosens the interaction between DNA and histones, thereby increasing DNA accessibility and promoting transcriptional activation of target genes (He and Lehming, 2003). However, the precise physiological mechanism upon EIN2 translocation into the nucleus remains unclear. Considering the molecular weight of EIN2, it is unable to passively diffuse into the nucleus but must be actively transported (Davis, 1995). Since a highly conserved nuclear localization sequence (NLS) was identified (Bisson and Groth, 2011), it was hypothesized that this motif plays a crucial role in EIN2 translocation, which was further investigated by *in planta* localization studies (Qiao et al., 2012; Wen et al., 2012). C-terminally GFP-tagged EIN2 constructs comprising residues 459-1294 or 479-1294 were found in the cytoplasm, the nucleus, and partially at the ER membrane (Bisson and Groth, 2015; Wen *et al.*, 2012). However, deletion of the NLS abolished nuclear localization completely, indicating the significance of the NLS for EIN2 nuclear import (Bisson and Groth, 2015; Wen et al., 2012). Additionally, the NLS of EIN2 is crucial for the binding and processing of the EBF1/2 mRNA in P-bodies (Li et al., 2015). Furthermore, several ethylene response phenotypes such as elongated hypocotyl of light-grown seedlings were annulled in plants constitutively expressing EIN2 lacking the NLS (Wen et al., 2012). Therefore, a variety of studies implied the relevance of an intact NLS for physiological functionality of EIN2.

1.2.2 Nuclear transport machinery – bridging the ER-nuclear gap

Most proteins must localize to specific subcellular compartments within the cell at defined time points. Due to the compartmentalization of the cell into distinct organelles, the cytoplasm, and the nucleus, the information specifying protein localization is largely

encoded within their amino acid sequence (Görlich and Kutay, 1999; Moroianu, 1997; Xiong et al., 2021). Most nuclear proteins contain so-called nuclear localization sequences that are recognized by nuclear transport receptors for translocation into the nucleus across nuclear pore complexes (NPCs) (Dingwall and Laskey, 1991; Moroianu, 1999). The NPC spans the double membrane of the nuclear envelope and functions as a gatekeeper for proteins. Small proteins with a molecular weight of less than 40-60 kDa can passively diffuse into the nucleus, whereas larger macromolecules must be actively transported through the NPC (Grossman et al., 2012). This active translocation is widely mediated by an interplay of proteins of the Importin-alpha (IMPα) and the Importin-beta (IMPβ) superfamily (Chook and Blobel, 2001), which will be described in more detail in the following sections.

1.2.2.1 Importin-alpha (IMPα) superfamily

The IMPα/β-superfamily serves as the central and best-characterized pathway for nuclear protein transport and is highly conserved from yeast to humans (Xiong et al., 2021). The IMPα superfamily is responsible for cargo recognition and cargo binding by distinct NLS motifs, whereas the IMPβ superfamily takes care of the translocation of IMPα-cargo complexes (Görlich and Kutay, 1999; Quimby and Corbett, 2001). NLSs are typically rich in basic amino acids such as lysine or arginine. Depending on the number of basic clusters, they can be divided into monopartite (single basic amino acid cluster) or bipartite (two basic amino acid clusters separated by a 10-12 amino acid linker) (Kalderon et al., 1984b; Kalderon et al., 1984a; Lange et al., 2007). Kosugi et al. defined six NLS classes capable of specific binding to IMPα proteins from rice (*Oryza sativa*), yeast (*Saccharomyces cerevisiae*), and human (*Homo sapiens*) (Kosugi et al., 2009). Canonical NLSs comprise both monopartite and bipartite motifs. Monopartite NLSs include the consensus sequences KR(K/R)R or K(K/R)RK (class 1) and (P/R)XXKR(^DE)(K/R) (class 2; ^DE denotes any amino acid except from aspartate or glutamate), whereas bipartite NLSs (class 6) are defined by the consensus sequences $KRX_{10\text{-}12}K(KR)(KR)$ or $KRX_{10\text{-}12}K(KR)X(K/R)$. In contrast, three additional NLS classes, which are designated as non-canonical NLS, were discovered with the consensus sequences KRX(W/F/Y)XXAF for class 3, (R/P)XXKR(K/R)(^DE) for class 4, and LGKR(K/R)(W/F/Y) for class 5 (Kosugi et al., 2009). While classes 1-4 and 6 are recognized by IMPα proteins from yeast to human, class 5 was found to be functional only in a plant-specific context (Kosugi et al., 2009). Notably, the NLS of

A

NLS class	Consensus sequence[a]
Class 1	KR(K/R)R or K(K/R)RK
Class 2	(P/R)XXKR(^DE)(K/R)
Class 3	KRX(W/F/Y)XXAF
Class 4	(R/P)XXKR(K/R)(^DE)
Class 5	LGKR(K/R)(W/F/Y)
Class 6	$KRX_{10-12}K(KR)(KR)$ or $KRX_{10-12}K(KR)X(K/R)$

[a]X = any amino acid; ^DE = any amino acid except Asp or Glu

B

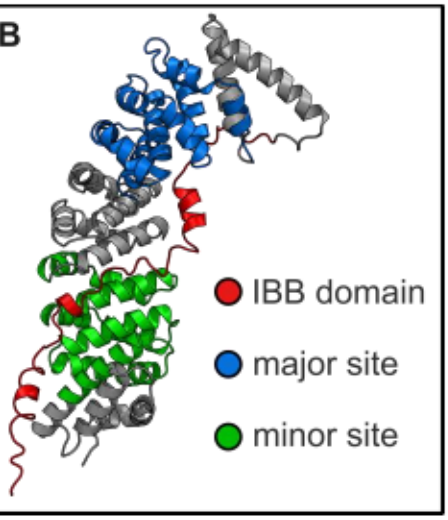

Figure 4: Different classes of nuclear localization sequences (NLSs) and overall Importin-α (IMPα) architecture. A) Overview of the consensus sequences of distinct NLS classes defined by (Kosugi et al., 2009). Class 1, 2, and 6 represent canonical mono- or bipartite NLSs, whereas the other three classes are defined as non-canonical NLSs. Canonical NLSs are reported to bind to the major binding site of IMPα, while classes 3-5 preferentially bind to the minor binding site. Bipartite NLSs (class 6) can bind to both binding clefts. Only class 5 exhibited specificity towards plant importins. Reproduced according to (Chang et al., 2013a). B) Structure prediction of *At*IMPα1 as a representative model illustrating the overall architecture using AlphaFold3 (Abramson et al., 2024). The disordered region comprising residues 497-532 was hidden for clarity. The IBB domain is shown in red, whereas the major and minor binding sites are depicted in blue and green, respectively.

EIN2 comprising the sequence LKRYKRRL does not fit perfectly into any of these classes (Bisson and Groth, 2011; Ju et al., 2012). It would be most likely categorized into class 1 (canonical NLS) but also shows similarities to class 5 (plant-specific NLS). As mentioned above, recognition and interaction of the cargo protein is mediated by the IMPα superfamily (Görlich and Kutay, 1999). The *Arabidopsis thaliana* genome encodes nine different isoforms of Importin-α proteins (IMPα1-9) (Bhattacharjee et al., 2008). The overall architecture of this superfamily is highly conserved and can be divided into two domains with distinct functions: 1) The N-terminal Importin-β binding domain (IBB domain), which is highly flexible, and 2) the C-terminal domain, which comprises ten tandem armadillo (ARM) repeats, with each ARM repeat consisting of three α-helices (Kobe, 1999; Marfori et al., 2012). As the name suggests, the IBB domain is responsible for binding between IMPα and IMPβ proteins to form a ternary complex with the cargo protein, which is subsequently translocated into the nucleus (Görlich et al., 1996a). However, previous structural and binding studies have shown that a basic amino acid-rich region within the IBB domain competes with the cargo protein NLS for binding to both NLS-binding sites of IMPα (Goldfarb et al., 2004). Therefore, besides being the contact site between IMPα and IMPβ, the IBB domain functions as a regulative auto-inhibitory domain (Kobe, 1999; Lott and Cingolani, 2011).

The C-terminal ARM repeats form the interface for recognition and binding of the NLS at the concaves of the protein with ARM repeats 2-4 and 7-9 harboring the two distinct NLS binding sites referred to as major and minor binding sites, respectively (Conti and Kuriyan, 2000; Fontes et al., 2003; Fontes et al., 2000). Canonical NLSs have been shown to preferentially bind to the major binding site, whereas non-canonical NLSs primarily interact with the minor binding site. In contrast, bipartite NLSs are bound at both NLS-binding clefts (Kosugi et al., 2009). Furthermore, the tenth ARM repeat of several IMPα proteins is known to mediate binding of the exportin CAS (CELLULAR APOPTOSIS SUSCEPTIBILITY), which is responsible for nuclear export and recycling of IMPα (Goldfarb et al., 2004; Haasen and Merkle, 2002). Overall, the *At*IMPα isoforms share a high degree of sequence identity (42 %) and sequence conservation (61 %). Nevertheless, the isoforms IMPα8 and IMPα9 differ strongly compared to the other seven isoforms either in sequence identity (less than 30 % for IMPα9) or structural architecture (IMPα8 is lacking the IBB domain) (Tamura and Hara-Nishimura, 2014; Wynen et al., 2025). The observed divergence in amino acid sequence and structural features suggests the evolution of distinct functions beyond nucleocytoplasmic transport. This is further supported by studies demonstrating isoform-specific roles in immunity and *Agrobacterium*-mediated transformation among closely related *At*IMPα isoforms (Bhattacharjee et al., 2008; Palma et al., 2005). It is therefore plausible that IMPα isoforms with lower sequence homology, such as IMPα8 and IMPα9, exhibit an even greater degree of functional specialization beyond nucleocytoplasmic transport.

1.2.2.2 Importin-beta (IMPβ) superfamily

The cargo-recognition by IMPα, marking the initial step in protein translocation, is followed by the formation of a ternary complex comprising IMPβ and the cargo-bound IMPα (Tamura and Hara-Nishimura, 2014). Subsequently, this complex must be translocated across the NPC, in which the IMPβ superfamily plays a pivotal role. They are present in all eukaryotic organisms and play roles in plant development, reproduction, abiotic stress responses, and immunity (Xiong et al., 2021). Unlike the IMPα proteins, whose numbers vary strongly amongst eukaryotic organisms (one in *S. cerevisiae*, four in *D. melanogaster*, six in *H. sapiens*, and nine in *A. thaliana*), the IMPβ superfamily consists in unicellular and multicellular organisms of 14-15 and 18-20 isoforms, respectively (Tamura and Hara-Nishimura, 2014; Xiong et al., 2021).

The *A. thaliana* genome encodes 18 isoforms of the IMPβ superfamily that share strong structural homology despite their relatively low sequence similarity (Tamura and Hara-Nishimura, 2014). IMPβ proteins are composed of a series of HEAT (**H**UNTINGTIN, **E**LONGATION FACTOR 3, PROTEIN PHOSPHATASE 2**A,** and TARGET OF RAPAMYCIN 1 (**T**OR1)) repeats with a length of approximately 40 amino acids per repeat and an average number of 20 repeats per protein (Lott and Cingolani, 2011; Ström and Weis, 2001; Xu et al., 2010). One HEAT repeat consists of two α-helices mimicking a hairpin-like structure that is linked by a smaller α-helical region (Cingolani et al., 2002; Cingolani et al., 1999). Based on their transport direction, they are subdivided into two families: importins and exportins. Exportins mediate the export of cargo out of the nucleus by interacting with a nuclear export signal (NES), whereas importins are responsible for the import of cargo into the nucleus in an interplay with IMPα (Chook and Blobel, 2001; Neville et al., 1997; Ström and Weis, 2001). The binding between IMPβ and IMPα is mediated by the IBB domain of IMPα, which is a crucial regulatory element that ensures the transport of only cargo-loaded IMPα due to its auto-inhibitory function (Kobe, 1999; Lott and Cingolani, 2011). The translocation of the ternary IMPβ/IMPα/cargo complex is mediated by IMPβ through interaction with the NPC (Chook and Blobel, 2001; Moroianu, 1997). Precisely, IMPβ interacts with several of the 30 nucleoporins (NUPs) that form the NPC (Lott and Cingolani, 2011; Rout et al., 2000). The binding motif of nucleoporins responsible for interaction with IMPβ is FxFG (with x mostly being a hydrophobic amino acid or glycine) as revealed by *in vitro* and *in vivo* binding analysis (Chi and Adam, 1997; Damelin and Silver, 2000). Notably, the binding of IMPβ to NUPs occurs at the opposite site compared to IMPβ-IMPα binding, allowing simultaneous interaction and, consequently, translocation of the complex through the NPC (Bayliss et al., 2000). Upon nuclear entry, IMPβ binds to Ran_{GTP} (RAS-RELATED NUCLEAR PROTEIN), a small GTPase, initiating the dissociation of the IMPβ/cargo-bound IMPα complex. The interaction between IMPβ and Ran_{GTP} occurs at HEAT repeats 1-4 and 12-15 as revealed by structure elucidation of Kap95p from yeast (PDB code: 2BKU) (Bischoff and Görlich, 1997; Lee et al., 2005). Since distinct conformational states were observed in crystallographic studies, it is suggested that Ran_{GTP} induces conformational changes allosterically, leading to the dissociation from IMPα (Lott and Cingolani, 2011). Subsequently, the resulting IMPβ/Ran_{GTP} complex has a much higher affinity compared

to the IMPβ/IMPα complex and requires the additional factors RanBP1 (RAN BINDING PROTEIN 1) and RanGAP (RAN GTPase ACTIVATING PROTEIN) to promote GTP hydrolysis (Floer et al., 1997; Görlich et al., 1996b; Moroianu et al., 1996). While only RanGAP activates the intrinsic GTPase activity of Ran, it was shown that RanBP1 stimulates the RanGAP-induced GTPase activity by stabilizing the complex (Bischoff et al., 1995; Bischoff and Görlich, 1997). However, the hydrolysis of Ran_{GTP} into Ran_{GDP} is not necessary for the dissociation of the IMPβ/Ran_{GTP} complex but is crucial for maintaining the energy requirements of active transport (Floer et al., 1997). With the IMPα/cargo complex remaining, release of the cargo is facilitated through an interplay between the IBB domain, nucleoporins, the exportin CAS (belonging to the IMPβ superfamily), and Ran_{GTP}. Nup50, a nucleoporin located towards the nuclear basket of the NPC, was identified to directly bind to IMPα and therefore acts as a catalyst for cargo release (Guan et al., 2000; Matsuura and Stewart, 2005). The dissociation of the resulting IMPα/Nup50 complex and the export of IMPα for recycling is subsequently mediated by the IBB domain and CAS bound to Ran_{GTP}. The resulting trimeric complex consisting of IMPα, CAS, and Ran_{GTP} is highly specific for NLS-free IMPα (Kutay et al., 1997; Lott and Cingolani, 2011; Solsbacher et al., 1998). The IBB domain signals the

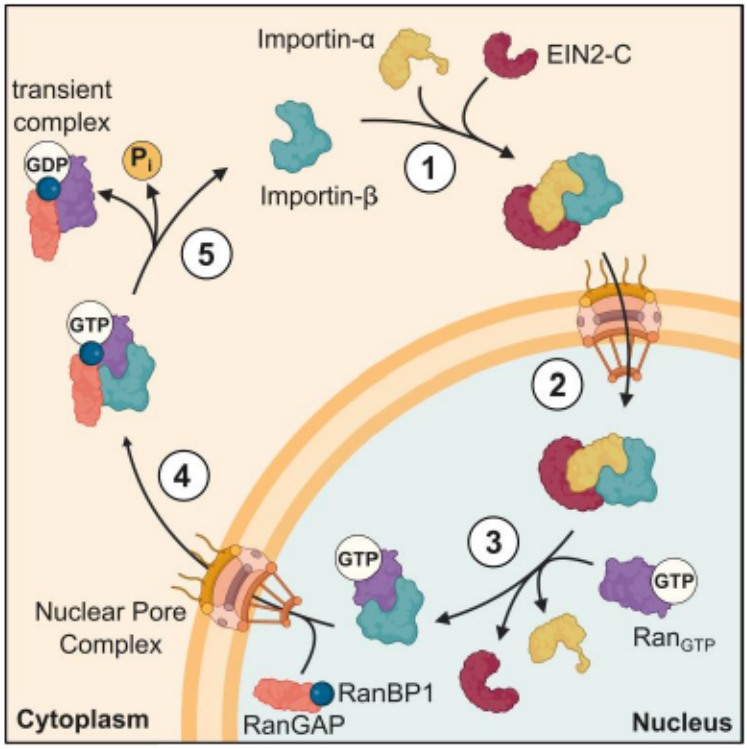

Figure 5: Schematic illustration of the Importin-α/β (IMPα/β)-mediated nuclear import cycle. In the cytoplasm, IMPα binds the nuclear localization sequence of the cargo (EIN2-C) and subsequently interacts with IMPβ through its Importin-β binding (IBB) domain, thereby forming a ternary complex (1). The IMPα/β-cargo complex is translocated into the nucleus through the nuclear pore complex (2). In the nucleus, the GTP-bound form of the Ras-related nuclear protein Ran (Ran_{GTP}) binds to IMPβ, triggering dissociation of the IMPα-cargo complex from IMPβ (3). The IMPβ-Ran_{GTP} complex is subsequently exported back to the cytoplasm, where Ran binding protein 1 (RanBP1) and Ran GTPase activating protein (RanGAP) promote GTP hydrolysis of the complex (4). After hydrolysis, IMPβ dissociates from the transient Ran_{GDP}-RanGAP-RanBP1 complex and is recycled for another round of nuclear import (5). For clarity, the CAS-mediated recycling of IMPα is not shown. Created with BioRender.

cargo-free state of IMPα by promoting a conformational state that enables CAS binding, which is required for recycling (Lott and Cingolani, 2011). However, apart from the IMPα-dependent transport pathway, it is reported that certain cargo are directly transported via the IMPβ superfamily (Jäkel and Gürlich, 1998; Takizawa et al., 1999). Various studies demonstrated the ability of single IMPβ isoforms to transport a variety of specific cargo types, such as *At*IMPβ3 (ortholog of human IMPβ5) or *At*IMPβ4 (ortholog of human IMPβ4), transporting ribosomal proteins or transcription factors, respectively (Liu et al., 2019; Xiong et al., 2020). Besides that, microRNA (miRNA) and transfer RNA (tRNA) were also identified as targets of specific members of the IMPβ superfamily (Park et al., 2005; Xiong et al., 2021). The secret of cargo specificity might be embedded in the protein sequence of IMPβ members, which is supported by the relatively low sequence relations amongst this superfamily (O'Reilly et al., 2011; Tamura and Hara-Nishimura, 2014). Beyond nucleocytoplasmic transport, members of the IMPβ family were discovered to have roles in spindle formation, protein stability, and miRNA biogenesis in yeast and metazoans (Forbes et al., 2015; Funabiki, 2005; Wu et al., 2018). Furthermore, it has been suggested that IMPβ proteins can prevent the 26S proteasome-mediated protein degradation by directly binding lysine-enriched NLSs, thereby shielding lysine residues from E3 ligase-mediated ubiquitination. Therefore, IMPβ proteins fulfill a dual functional role in protection and transport of the NLS bearing cargo (Xiong et al., 2021). However, the actual mechanism of how protein degradation is prevented by IMPβ remains unclear.

1.3 The ethylene signaling pathway – ethylene response

More than 2000 transcription factors (TFs), belonging to numerous TF families, are encoded in the *A. thaliana* genome, reflecting the complexity of transcriptional regulation (Guo et al., 2005; Riechmann et al., 2000; Thirugnanasambantham et al., 2015). Nuclear entry of EIN2 initiates a transcriptional cascade by activating EIN3 and EIL1. These TFs regulate the expression of various downstream genes, including members of the AP2/ERF (Apetala2/Ethylene response factor) family, ultimately amplifying the ethylene response. The following sections first introduce the AP2/ERF family before discussing the EIN3 transcription factor family in more detail.

1.3.1 Ethylene transcription factors – activating ethylene responses

The AP2/ERF transcription factor family accounts for around 7 % of the approximately 2000 TF families in *A. thaliana* and therefore is one of the largest TF families (Vogel et al., 2012). Transcription factors belonging to this family are characterized by an AP2/ERF binding motif that comprises around 60-70 amino acids (Zhai et al., 2022). The AP2/ERF domain is shaped by a three-stranded β-sheet followed by an almost parallel α-helix and is involved in DNA binding. In particular, arginine (R) and tryptophan (W) residues were identified to be crucial for DNA binding (Allen et al., 1998). Based on the number of AP2/ERF domains and their DNA binding motif, the AP2/ERF family is further subdivided into five classes defined by Sakuma et al.: AP2, RAV (Related to Abscisic Acid Insensitivity 3/Viviparous 1), DREB (drought-responsive element-binding factor), ERF, and others (representing an undefined class) (Sakuma et al., 2002). The AP2 family comprises two AP2/ERF motifs, whereas the RAV family contains one AP2/ERF motif in addition to another DNA binding motif, the B3 domain. Similar to RAV, ERFs and DREBs possess only a single AP2/ERF domain (Sakuma et al., 2002; Zhai et al., 2022). With 147 genes identified in *A. thaliana*, the ERF subfamily is the largest one of the AP2/ERF family, with ERF1 (ETHYLENE RESPONSE FACTOR 1) being the best characterized ERF so far (Lorenzo et al., 2003; Nakano et al., 2006; Solano et al., 1998). Although ERFs are regulated by various factors, including JA, ABA, and pathogen infections (Nakano et al., 2006), ethylene - and consequently the EIN3 family - plays a pivotal role in modulating ethylene-responsive gene expression (Chang et al., 2013b; Dolgikh et al., 2019).

1.3.2 EIN3 family – the key regulatory hub in ethylene signaling

In *A. thaliana*, the EIN3 family consists of six members named EIN3 and EIL1-5, which all possess a conserved N-terminally located DNA binding domain that recognizes short DNA sequences called EBS (EIN3 binding sites) (Chao et al., 1997; Guo and Ecker, 2004; Song et al., 2015). Given their sequence identity, EIN3, EIL1, and EIL2 are considered functionally homologous proteins responsible for the regulation of ethylene-responsive genes (Alonso et al., 2003; Chao et al., 1997; Solano et al., 1998). However, *ein3 eil1* double mutants were sufficient to completely abolish ethylene perception considering triple response phenotyping or pathogen resistance. Thus, EIN3 and EIL1 were identified as key regulators of ethylene responses (Alonso et al.,

2003). This is further supported by the fact that, amongst all six family members, EIN3 and EIL1 are the most closely related (Guo and Ecker, 2004). Nevertheless, EIL2 might possess a minor role in ethylene signaling due to its ability to rescue the triple response phenotype of *ein3* single mutants (Chao et al., 1997). This is consistent with transcriptional analyses showing that EIL2 is expressed at relatively low levels and only in the root apical meristem and pollen, in contrast to EIN3 and EIL1 (Dolgikh et al., 2019). Therefore, these findings support the lower significance of EIL2 in ethylene response and suggest a tissue-specific limitation of its functionality. EIL4 and EIL5 were expressed exclusively in dark-grown seedlings, and to date, no function has been assigned to these proteins (Dolgikh et al., 2019; Guo and Ecker, 2004). Despite its relatively high transcription levels compared to EIL2, EIL4, and EIL5, EIL3 has not been assigned a role in ethylene responses but rather in the response to sulfur deficiency (Dolgikh et al., 2019; Wawrzyńska and Sirko, 2014). Accordingly, EIN3 and EIL1 form the key regulatory hub in ethylene signaling, leading to the induction of several hundreds of TFs of different TF families in response to a variety of stresses (Dolgikh et al., 2019). As mentioned before, *ERF1* is one of the first identified EIN3 target genes and is known to be involved in various ethylene responses (Solano et al., 1998). Additionally, EIN3 targets genes that are associated with roles in de-etiolation (*PIF3*) (Zhong et al., 2012), root hair development (*RSL4, ESE1*) (Feng et al., 2017; Zhang et al., 2011) or salt and cold stress responses (*CBF1/2/3*) (Shi et al., 2012). Although EIN3 forms homodimers independently of DNA, dimerization substantially enhances its DNA-binding affinity compared to the monomeric state (Song et al., 2015). Amino acids 113–257 have been identified as crucial for EIN3 homodimerization (Solano et al., 1998). Since elevated histone acetylation levels at H3K14 (H3K14Ac) and non-canonical H3K23 (H3K23Ac) were observed in response to ethylene, histone modifications are proposed to facilitate EIN3-DNA interaction as they play a critical role in the up- and downregulation of gene expression (Zhang et al., 2016; Zhang et al., 2017). Interestingly, the elevation of H3K14Ac and H3K23Ac levels is EIN2-dependent, supporting the pivotal role of EIN2 as the key regulator of ethylene signaling (Zhang et al., 2017). In the nucleus, EIN2 can interact with ENAP1, a nuclear protein containing a SANT domain. The SANT domain is a conserved motif in chromatin remodeling enzymes such as histone acetyltransferases (HATs) or histone deacetyltransferases (HDACs) (Aasland, 1996; Zhang et al., 2016). Notably, EIN3-ENAP1 binding was also

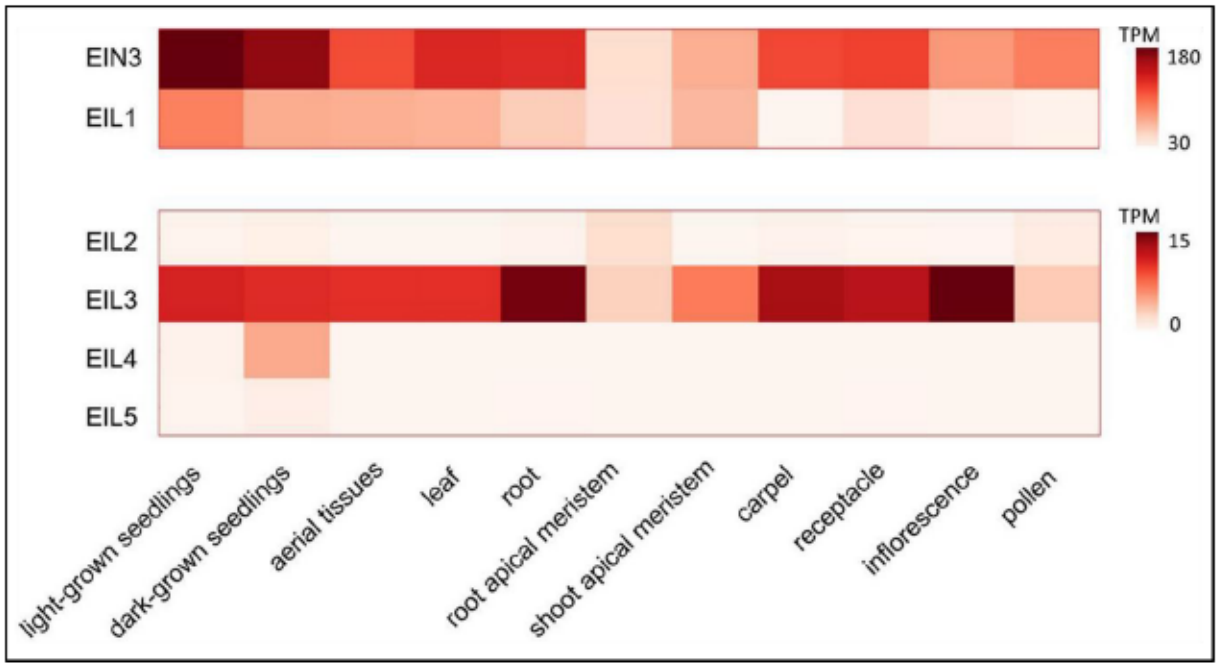

Figure 6: Heat map representing the transcription levels of the EIN3 family in different plant tissues (taken from (Dolgikh et al., 2019)). TPM means transcripts per million.

observed and is suggested to contribute to the elevated acetylation levels (Zhang et al., 2016). However, since neither EIN2 nor ENAP1 contains a histone acetyltransferase domain, it is likely that the ENAP1/EIN2/EIN3 complex recruits HATs to mediate histone acetylation (Dolgikh et al., 2019). Notably, EIN3 can both activate and repress gene expression in response to ethylene, further indicating the importance of histone acetylation in gene regulation. Two HDACs, called SRT1 (SIRTUIN1) and SRT2, were reported to interact with ENAP1 and to be involved in diminishing H3K9 acetylation levels. Specifically, SRT2 functionality was found to be EIN2- and EIN3-dependent (Zhang et al., 2018). The resulting histone deacetylation strengthens histone-DNA interactions, decreases chromatin accessibility, and consequently represses the transcription of target genes (He and Lehming, 2003). Although these results shed light on the nuclear events upon ethylene signaling, the precise molecular mechanisms following EIN2 nuclear entry remain unclear.

2 Aim of this thesis

Due to its pivotal role in several plant developmental processes, including seed germination, senescence, and fruit ripening, the ethylene signaling pathway is of great scientific and agronomic importance. Considering forecasts predicting a growth in population of about 25 % within the next 25 years, the significance of the ethylene signaling pathway becomes even more evident. Although this pathway has been extensively studied over the past decades and considerable insights have been gained, many aspects remain unresolved. Core components of this pathway, as well as the central role of the key regulator EIN2 in mediating signal transduction from the ER membrane to the nucleus, have been identified. Nevertheless, the underlying mechanism of EIN2 translocation upon ethylene perception is still unclear. One objective of this thesis was therefore to gain novel insights regarding the nucleocytoplasmic transport of EIN2. Based on the identification of a functional nuclear localization sequence (NLS) in EIN2, it was hypothesized that the canonical IMPα-IMPβ transport machinery is involved in the nuclear import of EIN2. This work aimed to determine whether specific IMPα isoforms function as nuclear import receptors for EIN2 and to assess the degree of functional redundancy among the nine *At*IMPα isoforms. Furthermore, the molecular basis of EIN2 recognition by IMPα isoforms was investigated to gain a better understanding of cargo selectivity. Apart from the nucleocytoplasmic transport, molecular events downstream of EIN2 nuclear accumulation remain incompletely understood. Although EIN2 is crucial for EIN3 stabilization and activation, it remains unclear whether EIN2 directly interacts with EIN3 or indirectly promotes its stabilization. Therefore, another aim was the investigation of the molecular relationship between EIN2 and EIN3 to characterize the underlying mechanisms of EIN3 activation. Particular emphasis was placed on domain mapping approaches to identify functional regions involved in protein interaction. Together, these studies aimed to provide a mechanistic framework for two central processes of ethylene signaling: the nucleocytoplasmic transport of EIN2 and the molecular regulation of EIN3 following EIN2 nuclear entry.

3 Results

3.1 Nucleocytoplasmic transport of EIN2

Title	The importin-alpha superfamily engages in ethylene signaling by shuttling ETHYLENE INSENSITIVE 2 from the endoplasmic reticulum to the nucleus
Authors	**Fabian Wynen**, Jan Eric Maika, Raphael Josef Eberle, Nina Jahnke, Marcel Wiermer, Laura Hartmann, Rüdiger Simon, Georg Groth
Published in	The FEBS Journal, Volume 293, Issue 3, February 2026 Pages 894-917
Impact Factor	5.5 (2026)
DOI	10.1111/febs.70285
Own contribution	**Methodology** Development and optimization of FP binding studies and triple response approaches **Investigation** Performance of FP experiments and phenotypic plant studies **Formal analysis** Analysis and interpretation of FP and phenotypic plant data **Validation** Verification of experimental results and reproducibility **Visualization** Preparation of figures and graphical representations **Writing - Original draft / Review and Editing** Preparation of the manuscript

Check for updates

The FEBS Journal

FEBS PRESS science publishing by scientists

The importin-alpha superfamily engages in ethylene signaling by shuttling ETHYLENE INSENSITIVE 2 from the endoplasmic reticulum to the nucleus

Fabian Wynen[1], Jan Eric Maika[2], Raphael Josef Eberle[1], Nina Jahnke[3], Marcel Wiermer[4], Laura Hartmann[5], Rüdiger Simon[2] and Georg Groth[1]

1 Institute of Biochemical Plant Physiology, Heinrich-Heine-Universität Düsseldorf, Germany
2 Institute of Development Genetics, Heinrich-Heine-Universität Düsseldorf, Germany
3 Institute for Organic Chemistry and Macromolecular Chemistry, Heinrich-Heine-Universität Düsseldorf, Germany
4 Biochemistry of Plant-Microbe Interactions, Institute of Biology, Freie Universität Berlin, Germany
5 Institute for Macromolecular Chemistry, University of Freiburg, Germany

Keywords
EIN2; ethylene signaling; importin alpha superfamily; NLS-motif; nucleocytoplasmic transport

Correspondence
G. Groth, Biochemical Plant Physiology, Heinrich-Heine-Universität Düsseldorf, Universitätsstraße 1, 40225 Düsseldorf, Germany
Tel: +49 211 81-12822
E-mail: georg.groth@hhu.de

(Received 17 March 2025, revised 11 July 2025, accepted 29 September 2025)

doi:10.1111/febs.70285

Plant hormones are small molecules that modulate a plethora of growth and developmental pathways. Among these molecules, ethylene is known to modulate several important agronomical traits, including fruit ripening and senescence. However, the mechanisms, pathways, and processes of ethylene signaling from the receptors at the endoplasmic reticulum (ER) membrane to the transcriptional regulators in the nucleus remain to be elucidated. Here, we demonstrate that the importin alpha superfamily of nuclear transport receptors plays a pivotal role by transporting ethylene key regulator ETHYLENE INSENSITIVE 2 (EIN2) from the ER into the nucleus. Our findings show that *importin α* (*impα*) single- and triple-mutant seedlings of *Arabidopsis thaliana* retain a normal ethylene response, as evidenced by the typical triple-response phenotype observed in the presence of ethylene. *In vitro* and *in planta* interaction studies demonstrate that EIN2 is recognized as cargo by all nine IMPα isoforms, though with distinct affinities. Specifically, the binding studies reveal that IMPα1/2/3/4/7 are the most relevant isoforms for the nucleocytoplasmic transport of EIN2. Based on computational interaction predictions, we have identified potential binding modes and offer novel mechanistic insights into the interaction between the nuclear localization signal (NLS) motif of EIN2 and the IMPα superfamily. Our results provide novel insights into the mechanism by which the ethylene signal is transmitted from the ER membrane to the nucleus. The data pave the way for a more comprehensive understanding of the ethylene signaling pathway and the central role of EIN2.

Abbreviations
ARM, armadillo repeat domain; At, *Arabidopsis thaliana*; BLI, biolayer interferometry; CER, cerulean; CTR1, CONSTITUTIVE TRIPLE RESPONSE1; EIN2 CEND, ethylene-insensitive protein 2 C-terminal cytosolic part; EIN2, ETHYLENE INSENSITIVE2; ER, endoplasmic reticulum; ETR, ethylene receptor; FLIM-FRET, fluorescence lifetime microscopy and Förster's resonance energy transfer; FP, fluorescence polarization; GAF, cGMP-specific phosphodiesterase, adenylyl cyclases, and FhlA; IBB, importin β binding domain; IMPα, importin α; IMPβ, importin β; K_d, dissociation constant; NLS, nuclear localization signal; NPC, nuclear pore complex; RAN, RAS-RELATED NUCLEAR PROTEIN; YFP, YELLOW FLUORESCENCE PROTEIN.

293, 894–917 © 2025 The Author(s). *The FEBS Journal* published by John Wiley & Sons Ltd on behalf of Federation of European Biochemical Societies.
This is an open access article under the terms of the Creative Commons Attribution License, which permits use, distribution and reproduction in any medium, provided the original work is properly cited.

Introduction

The plant hormone ethylene plays a crucial role in plant growth and development, influencing processes such as fruit ripening, senescence, and adaptive responses of plants to a wide range of biotic and abiotic stresses [1–5]. Ethylene perception and responses are mediated by a family of integral membrane receptors (ETRs) localized at the endoplasmic reticulum (ER)–Golgi network [6–8]. The receptors, which in their functional state form homo- and heteromers at the membrane, act as negative regulators of the signaling pathway, following an inverse-agonist model in which ethylene binding switches off downstream signal transmission [7,9–13]. Receptor-associated Raf-like kinase CONSTITUTIVE TRIPLE RESPONSE1 (CTR1) and ER integral membrane protein ETHYLENE INSENSITIVE2 (EIN2) have been identified as pivotal downstream partners of the receptors and key elements in ethylene signal transmission [14–16]. Both interact with the ethylene receptors at the ER membrane [17–19], but for long it was unclear how the ethylene signal is transmitted from the ER to the nucleus. Bioinformatic sequence analysis revealed a putative nuclear localization signal (NLS) in the C-terminus of EIN2 (residues 1261–1268), supporting the idea that the C-terminal cytosolic part (amino acids 462–1294) is cleaved off the N-terminal transmembrane part in response to the ethylene signal for translocation into the nucleus [20]. Under certain circumstances, the C-terminus of EIN2 is localized in cytoplasmic P-bodies [21,22]. Multiple experimental studies provided mechanistic insights into the processes bridging ethylene transmission from the receptors located in the ER membrane to the nucleus [23,24]. Additionally, binding studies revealed that the EIN2 NLS-motif serves not only in nuclear localization but also provides a critical contact site for the GAF (cGMP-specific phosphodiesterase, adenylyl cyclases, and FhlA) domain of the ETR receptors [25,26]. EIN2 lacking the NLS motif shows strongly reduced affinity for the receptors. Synthetic peptides derived from the EIN2 NLS-motif [25] also impede the interaction of EIN2 and the receptors. Notably, the corresponding peptides markedly impair ethylene responses in plants, such as fruit ripening or senescence [27–30]. Further genetic and molecular studies on the ethylene signaling network revealed that the Raf-like kinase CTR1 directly interacts with and phosphorylates EIN2 at multiple sites in the absence of the plant hormone [31–34]. Conversely, the plant hormone inactivates CTR1, preventing CTR1-dependent phosphorylation of EIN2 [33]. In turn, ER-membrane localized EIN2 is proteolytically processed, and the C-terminal end of EIN2, containing the NLS-motif [20,31], is translocated to the nucleus [31–33]. Deletion of the NLS retained EIN2 CEND in the cytoplasm, suggesting that the NLS sequence is responsible for CEND's nuclear localization [32]. In the nucleus, EIN2 CEND activates the transcription factor EIN3 [22,32] and its paralogs by a mechanism that has yet to be fully elucidated, resulting in the transcription of ethylene response genes [35,36]. The pathways and transport mechanisms of EIN2 CEND to and into the nucleus are not resolved yet. In addition to the previously reported localization of EIN2 in the ER membrane and EIN2 CEND in the nucleus [20,31–33], several studies in *Arabidopsis thaliana* and *Nicotiana tabacum* have described alternative subcellular localization for both [17,31,32,37,38]. For instance, EIN2 has been observed in the nucleus [32], while EIN2-CEND has been detected in the cytoplasm [31,32,37,38] (Fig. 1A).

Macromolecules with a molecular weight larger than 40 kDa (e.g., EIN2 CEND (91.81 kDa)) require an active transport process for translocation across nuclear pore complexes (NPC) that span the double membrane of the nuclear envelope [39–42]. Nuclear import receptors recognize their molecular cargos in the cytoplasm by distinct NLS sequence motifs, carry them across the NPC, and release them in the nucleus [43,44]. Based on their recognition sequence, NLS motifs are classified as either monopartite (a single cluster of basic amino acids) or bipartite (two clusters of basic amino acids separated by a 10–12 amino acid linker) [45]. Sequence-based prediction of NLSs in the cytosolic part CEND of the ethylene key regulator EIN2 reveals that the CEND contains mono- and bipartite NLSs [20], suggesting an interaction with the IMPα superfamily. In the classical nuclear import pathway, which is conserved from yeast to humans [46], a cytoplasmic complex is formed. Thereby, NLS motifs in the cargo proteins are recognized by the nuclear transport receptor importin α (IMPα) which, upon NLS binding, functions as an adaptor and bridges the interaction to the actual nuclear import carrier importin β (IMPβ), which mediates the passage of the ternary complex through the NPC [47–49] (Fig. 1B). Active transport of the IMPα-IMPβ cargo complex across the NPC is mediated by the direct interaction of IMPβ and nucleoporin proteins in the NPC [50,51]. Therefore, a crucial step in nuclear translocation is the specific recognition of the cargo protein by the IMPα receptor, as this complex formation ultimately determines which cargo is transported to the nucleus.

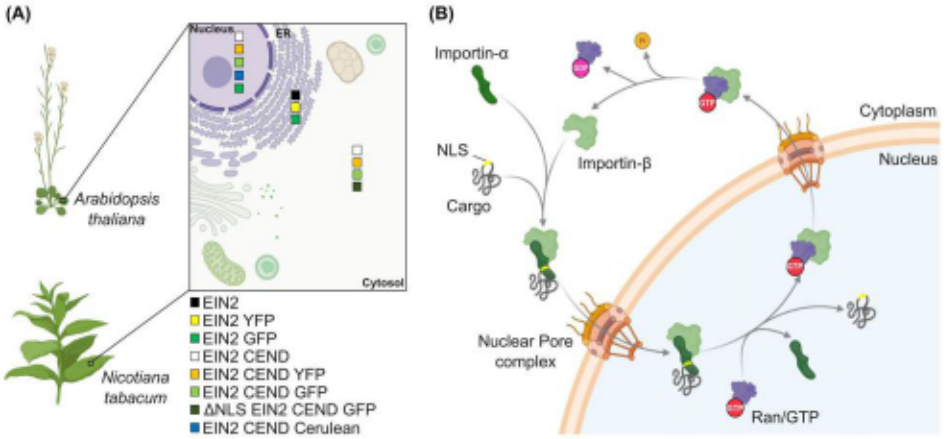

Fig. 1. Mapping EIN2 and EIN2CEND localization in plant cells and the role of IMPα/β in nuclear import. (A) Localization of EIN2 (ETHYLENE INSENSITIVE 2) and EIN2 CEND (ETHYLENE INSENSITIVE 2 C-terminal cytosolic part) based on reported *A. thaliana* and *N. tabacum in planta* experiments. (B) Simplified principle of the importin (IMPα/β mediated nuclear import. During the IMPα/β mediated nuclear import, a cytoplasmic complex between IMPα, cargo nuclear localization signal (NLS), and IMPβ is formed. The IMPα/β-cargo complex translocates into the nucleus through the nuclear core complex. In the nucleus, binding of Ras-related nuclear protein/Guanosine-triphosphate (RAN/GTP) to IMPβ triggers the dissociation of ternary import complexes and drives nuclear cargo release. IMPβ-RAN/GTP complexes exit the nucleus. RAN/GTP hydrolysis and release of Ras-related nuclear protein/Guanosine-diphosphate (RAN/GDP) in the cytoplasm then free IMPβ for the next round of import. Both parts of the figure were created with BioRender.com.

RAS-RELATED NUCLEAR PROTEIN (RAN), a small GTPase that exists in a GTP-bound nuclear and GDP-bound cytoplasmic state [52–54], controls the cargo binding to and release from the IMPα/β heterodimer. Binding of RAN·GTP to IMPβ in the nucleoplasm triggers the dissociation of ternary import complexes and drives nuclear cargo release [55,56]. However, members of the IMPβ protein family can function independently of IMPα adapters to mediate nuclear cargo import [57–59]. Lu *et al.* [60] demonstrated that IMPβ can mediate nuclear traffic of EIN2 CEND in *Arabidopsis thaliana*.

Structural studies have shown that IMPα proteins of different origin show conserved architectures consisting of two functionally and structurally distinct domains [61,62]. The C-terminal armadillo repeat domain (ARM) provides distinct binding sites for cargo NLS motifs. Repeats 2–4 shape the major site, whereas repeats 6–8 form the minor NLS binding site [63–66]. The major site is regarded as the high-affinity binding site for canonical monopartite NLSs, whereas bipartite NLSs bind to both the minor and the major site [67]. The flexible auto-inhibitory N-terminal IMPβ binding domain (IBB) of IMPα contains a sequence related to bipartite NLSs, which competes with NLS cargo for binding to the ARM repeats and facilitates interaction with IMPα upon cargo binding as well as release of the cargo in the nucleoplasm [68,69]. The *A. thaliana* genome encodes eight IMPα isoforms (IMPα1–IMPα7 and IMPα9) that contain both IBB domains and ARM repeats, as well as a single isoform (IMPα8) that contains only ARM repeats [70,71].

Here, we demonstrate in cell biological, biophysical, and *in planta* studies that EIN2-NLS peptides and EIN2 CEND interact with the IMPα superfamily. Our results provide novel mechanistic insights into how EIN2 CEND translocates from the ER membrane to the nucleus, shedding light on processes by which EIN2 integrates and bridges signaling from the ER membrane into the nucleus to trigger stress and developmental responses upon perception of the plant hormone ethylene.

Results

Involvement of individual members of the IMPα superfamily in plant ethylene response

In the presence of ethylene, dark-grown seedlings display the characteristic phenotypic responses known as triple response [9,10,15,72,73]. We hypothesized that nucleocytoplasmic transport and nuclear import of the

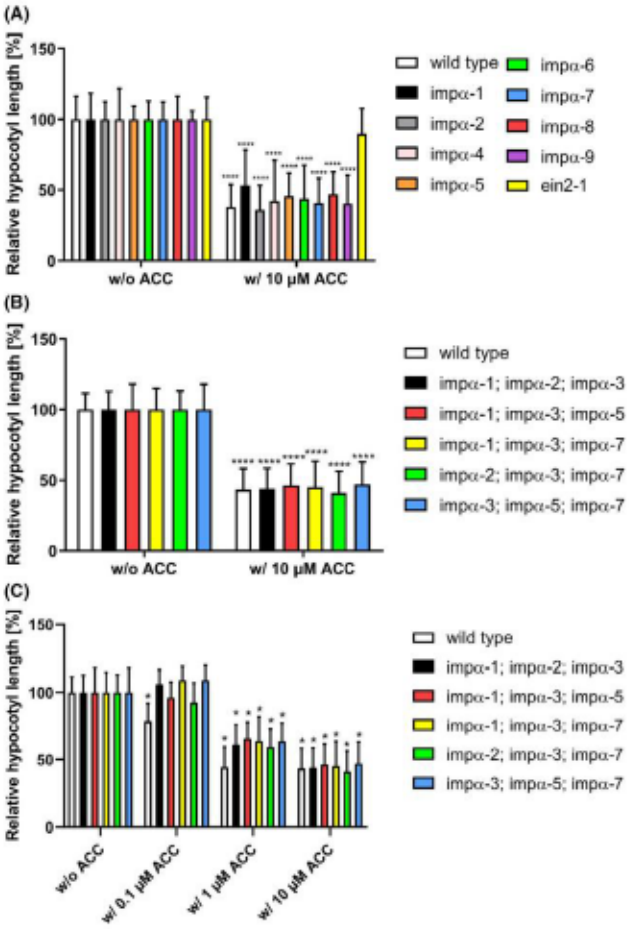

Fig. 2. Triple response experiments with single and triple *impα* loss-of-function mutants. (A) Triple response experiments with single loss-of-function *impα* mutants and (B and C) with triple loss-of-function *impα* mutants. The wild-type Col-0 served as a positive control, while the mutant *ein2-1* functioned as the negative control for the triple response. The *impα3* single mutant did not germinate. The hypocotyl length of each plant line in the absence of the ethylene precursor 1-aminocyclopropane-1-carboxylic acid (ACC) (w/o ACC) was set to 100%, and the hypocotyl length of each line in the presence (w/) of ACC is displayed in percent relative to the respective untreated control. Bars represent the mean ± SD of pooled data from at least 10 seedlings per condition for the single *impα* mutants and at least 20 seedlings per condition for the triple *impα* mutants. For statistical analysis a two-way ANOVA and Dunnett's multiple comparisons test was used. *P-value < 0.05; ****P-value < 0.0001 (w/o ACC vs. respective ACC concentration). In C), one asterisk equals four asterisks for a better overview.

EIN2 cytosolic part (CEND), which bridges ethylene signal transduction from the ER membrane to the nucleus, are mediated by the IMPα-IMPβ transport machinery. This hypothesis is supported by the previously identified NLS motif in the EIN2 C terminus. To investigate whether any of the IMPα isoforms are implicated in ethylene signaling, *A. thaliana* Col-0 (wild-type; positive control), single *loss-of-function* mutants of the IMPα isoforms (*impα1-impα9*) obtained from the Nottingham Arabidopsis Stock Centre (NASC), and ethylene-insensitive mutant *ein2-1* (negative control) were grown in the dark in the presence of the ethylene precursor 1-aminocyclopropane-1-carboxylate (ACC) and subsequently analyzed for their triple response. Fig. 2A illustrates that all single *impα* mutants besides *impα-3*, which was excluded from the study due to seed germination issues, showed the typical triple response, similar to the wild-type Col-0, with a 54–64% decrease in hypocotyl length for Col-0 and the *impα* mutants. In contrast, the triple response was not observed in the *ein2-1* loss-of-function control, which showed only a 10% decrease in hypocotyl length. The findings on the single *impα* mutants indicate that nucleocytoplasmic transport and nuclear import of EIN2 CEND cannot be attributed to a single IMPα isoform, possibly because of functional

redundancy among the IMPα isoforms. This is in line with the high homology and large conservation among the IMPα isoforms, with 42% identity and 61% conservation in the amino acid sequence of canonical IMPα1-8, suggesting that other family members compensate for the loss of one IMPα isoform. IMPα9 possesses here a special position because of a sequence identity <30%. A sequence alignment within the *Arabidopsis thaliana* IMPα family is shown in Fig. S1.

To gain further insights into the role of the IMPα superfamily for ethylene signaling, we studied multiple higher order *IMPα* loss-of-function mutants [74] (Fig. 2). The triple mutants *impα-1;impα-2;impα-3*, *impα-1;impα-3;impα-5*, *impα-1;impα-3;impα-7*, *impα-2;impα-3;impα-7*, and *impα-3;impα-5;impα-7* all showed the typical triple response phenotype when grown in the dark and exposed to the ethylene precursor ACC (Fig. 2B). The decrease in hypocotyl length of the triple mutants ranged from 53% to 59%, which is comparable to the decrease observed for the single *impα* mutants (Fig. 2A). These results from the analysis of multiple loss-of-function mutants support the hypothesis that the IMPα isoforms function redundantly in the nuclear import of EIN2. To check for potential differences in ethylene sensitivity, we supplemented the experiments from Fig. 2B with 0.1 and 1 μM ACC (Fig. 2C). The wild-type Col-0 exhibited a relative reduction in hypocotyl length of 21% even at 0.1 μM ACC, whereas all triple mutants remained unaffected, showing a maximum reduction of 7.5%. At 1 μM ACC, the decrease in wild-type seedlings (55.5%) was comparable to that observed at 10 μM ACC (56.5%). In contrast, the hypocotyl length reduction in the triple mutants ranged from 34% to 41% at 1.0 μM and from 53% to 59% at 10 μM ACC as previously noted. These findings indicate that the mutation of three IMPα isoforms leads to diminished sensitivity in ethylene perception, supporting the pivotal role of the IMPα superfamily in ethylene signaling. However, no differences in ethylene sensing were observed among the various triple mutants, further reinforcing the hypothesis of IMPα redundancy in EIN2 transport. The deletion of an excessive number of IMPα isoforms is likely to have detrimental effects on regular plant growth and development, which has already been observed in the triple mutants (*impα-1;impα-2;impα-3*) [74]. Due to the pivotal role of the IMPα-IMPβ machinery in the nuclear transport of a large number of cargo proteins, we adopted an alternative strategy to investigate the role of IMPα proteins in plant ethylene signal transduction by testing their physical interaction with the ethylene key regulator EIN2.

EIN2 interacts with and binds to all members of the IMPα superfamily

To clarify whether EIN2 is a potential cargo protein of the IMPα superfamily, all nine IMPα isoforms of *A. thaliana* were expressed recombinantly in *E. coli* and purified to homogeneity from the bacterial host (Fig. 3C). Interaction of purified IMPα proteins was probed by fluorescence polarization (FP) measurements with a set of EIN2-NLS peptides and shortened EIN2 CEND (Fig. 3A,B, Table S1). FP takes advantage of the fact that a fluorescent molecule, when excited by polarized light, emits light with a polarization level inversely related to its molecular rotation rate. This feature makes FP a valuable tool for studying the binding of small labeled ligands or peptides to larger proteins and serves as the basis for both direct and competitive binding assays [75].

In these studies, we initially examined the interaction between TAMRA-NOP-1, a peptide that corresponds to the NLS motif of EIN2 and is N-terminally labeled with the fluorescent dye 5-TAMRA (5-carboxytetramethylrhodamine), and the nine *Arabidopsis* IMPα proteins. The results of these binding studies revealed that binding occurred for all nine IMPα isoforms (Fig. 3A). While the majority of the IMPα proteins demonstrated comparable affinities for TAMRA-NOP-1, with dissociation constants (K_ds) in the low micromolar range (3–6 μM), isoforms IMPα5 and IMPα9 showed lower affinities, with K_d values of 12.9 ± 0.9 μM and 13.8 ± 0.9 μM, respectively. Binding affinities of IMPα6 and IMPα8 were only slightly diminished compared to the majority, with K_d values of 8.7 ± 1.5 μM and 7.9 ± 0.2 μM, respectively. In conclusion, these findings indicate that all nine members of the *A. thaliana* IMPα superfamily are capable of binding EIN2 *in vitro* as a cargo and support a physiological role of the IMPα-EIN2 interaction. The IMPα binding affinities indicate that they are not equally crucial for the binding and transport of EIN2 to and into the nucleus or for cytoplasmic trapping of EIN2 CEND. Previous binding studies between several NLS peptides and *A. thaliana* IMPα3 lacking the auto-inhibitory IBB domain [76] have observed affinities in the low micromolar range (0.7–5.4 μM). Based on our findings, the IMPα superfamily can be classified into the following three groups: IMPα1/2/3/4/(7), IMPα6/8, and IMPα5/9. Given the low dissociation constants of the IMPα-EIN2-NLS complexes, isoforms IMPα1/2/3/4/(7) seem to be most relevant for EIN2 nucleocytoplasmic transport.

To substantiate the hypothesis that EIN2 CEND serves as a cargo recognized by the IMPα superfamily

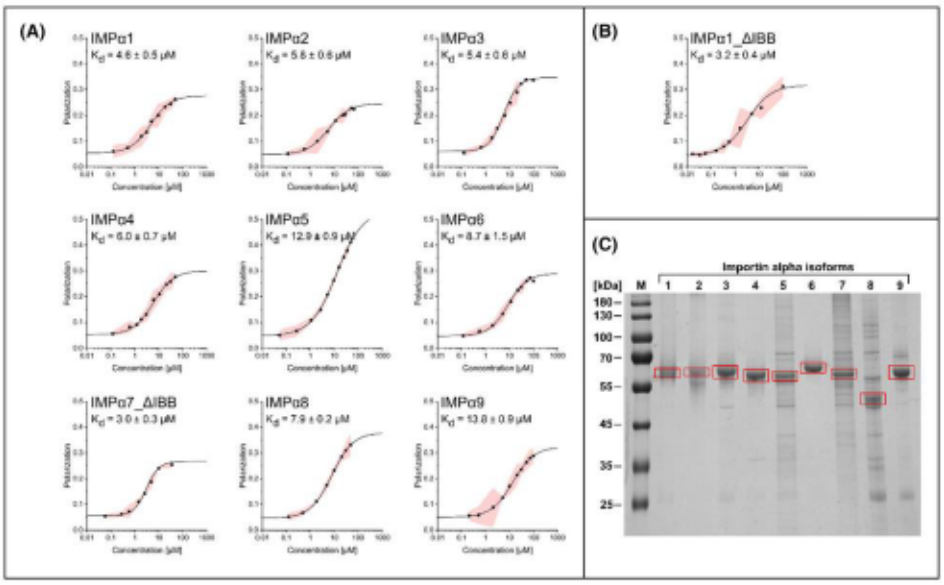

Fig. 3. Fluorescence polarization (FP) measurements of IMPα isoforms 1–9 with the TAMRA-NOP-1 peptide as a proxy for EIN2 CEND. For importin (IMPlα7 a variant lacking the N-terminal importin β binding (IBB) domain was employed as expression and purification of full-length IMPα7 was not successful. The polarization is plotted against the protein concentration in μM. Data points represent mean values with 95% confidence intervals based on three independent measurements. Dissociation constants (K_d) were determined by using the Logistic Fit function in Origin. (A) K_d value determination for IMPα1-9 and IMPα7_ΔIBB. (B) K_d value determination for IMPα1_ΔIBB. Data points represent mean values with 95% confidence intervals based on three independent experiments ($n = 3$). The SDS-PAGE for all purified isoforms is depicted in (C). The red boxes indicate the purified IMPα isoforms.

and to confirm the NOP-1 binding specificity, competitive FP measurements were performed. In these studies, TAMRA-NOP-1 bound to IMPα4 was selected as a representative interaction of the IMPα superfamily. TAMRA-NOP-1 was subsequently displaced by the addition of selected EIN2 CEND-NLS constructs of different lengths. Two of the constructs (NOP-1, EIN2 residues: 1262–1269; N41P-1, EIN2 residues: 1229–1269) were produced synthetically, while CEND construct GB1-*At*EIN2C$^{1215–1281}$ containing a GB1-tag to enhance solubility was produced recombinantly in *E. coli*. The binding curves shown in Fig. 4 clearly demonstrate that all three EIN2 CEND-NLS constructs were able to displace previously bound TAMRA-NOP-1, as indicated by a decrease in fluorescence polarization. Notably, the affinity of the different CEND peptides for IMPα4 decreased with increasing amino acid length. NOP-1 displayed the highest affinity of all EIN2-NLS probes, with a K_d of 4.1 ± 0.4 μM (Fig. 4A), which closely aligns with the observed affinity of IMPα4 for TAMRA-NOP-1 (~6 μM). With the extended EIN2-NLS probe N41P-1 as competitor, a K_d of 8.1 ± 1.1 μM was observed (Fig. 4B), while the most extended CEND probe GB1_*At*EIN2C$^{1215–1281}$ showed binding with a K_d of 22.1 ± 2.8 μM (Fig. 4C). The displacement of pre-bound TAMRA-NOP-1 by all EIN2-NLS CEND probes unequivocally confirms the specific binding of the EIN2-NLS core motif (NOP-1) and longer EIN2 CEND constructs. These results provide further support for the hypothesis that EIN2 CEND serves as a cargo protein of the IMPα superfamily to be transported from the ER to the nucleus via the IMPα-IMPβ machinery.

Next, we used biolayer interferometry (BLI) with an Octet K2 instrument (Fortè Bio, Dallas, USA) to substantiate and further delineate the binding interactions between the IMPα superfamily and the EIN2-NLS motif. BLI measures slight changes in reflected light at a sensor surface upon the formation of molecular complexes. Specifically, it monitors interference patterns of white light, which are reflected from two different

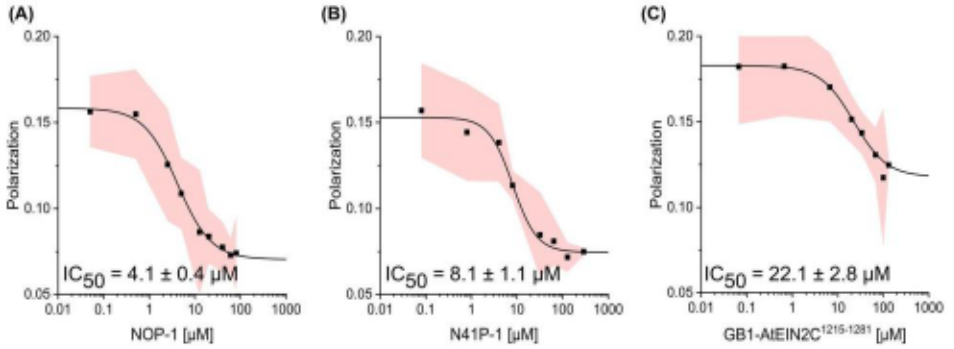

Fig. 4. Competitive fluorescence polarization (FP) measurements with EIN2 peptides of different lengths against TAMRA-NOP-1 bound to IMPα4. The tested EIN2 peptides included (A) NOP1, (B) N41P-1, and (C) GB1-*At*EIN2C$^{1215–1281}$. The concentration of IMPα4 (6 μM) was selected based on the previously determined K_d value of TAMRA-NOP-1 (TAMRA, Carboxytetramethylrhodamin). Polarization was plotted against the competitor concentration in μM. Data points represent mean values with 95% confidence intervals based on three independent experiments ($n = 3$). IC_{50}-values were determined using the Logistic Fit function in Origin.

surfaces: an internal reference layer and a layer of biomolecules immobilized on a biosensor tip [77].

In these binding assays, IMPα1 lacking the IBB domain (ΔIBB_IMPα1) and IMPα4 were selected as representatives of the IMPα superfamily. Prior to their interaction studies with different EIN2 CEND-NLS probes, both importins were biotinylated with the Biotin-PEG4-NHS ester Protein Labeling Kit from Jena Bioscience (Jena, Germany) and immobilized onto streptavidin-coated biosensor tips (Fig. 5).

Following their immobilization, the loaded biosensor tips were dipped into wells containing NOP-1, N41P-1, and GB1-*At*EIN2C$^{1215–1281}$, respectively, which served as EIN2 CEND-NLS probes of varying lengths and complexities. The resulting association and dissociation curves for serial dilutions of NOP-1, N41P-1, and GB1-*At*EIN2C$^{1215–1281}$ with ΔIBB_IMPα1 and IMPα4 are presented in Fig. 5. The analysis of the binding kinetic data and the processing of BLI sensorgrams by the implemented Octet® Analysis Studio Software revealed dissociation constants (K_ds) in the low μM range (2.5–21.4 μM) for NOP-1, N41P-1, and GB1-*At*EIN2C$^{1215–1281}$ (Table 1; Fig. 5A–E), with the basic EIN2-NLS probe (NOP-1) showing the highest affinity (ΔIBB_IMPα1: 2.5 ± 1.0 μM and IMPα4: 7.6 ± 1.1 μM as shown in Fig. 5A,B). These findings agree well with the previously determined binding constants measured by FP.

Curve fitting of the BLI sensorgrams was tested with different binding models. The best fit was obtained with a 1:2 heterogeneous ligand binding model (data not shown). This model assumes analyte binding at two independent ligand sites at the IMPα immobilized on the biosensor surface. Furthermore, each ligand site binds the analyte independently and with a different rate constant. Notably, the dose response curve for the GB1-*At*EIN2C$^{1215–1281}$ interaction with IMPα4 showed a clear biphasic sigmoidal curve (Fig. 5F). Based on this observation, a low and high K_d were determined, with the low K_d in the medium nM range and the high K_d in the higher μM range (Table 1). In this case, the second K_d in the higher μM range may be attributed to the binding of the GB1-tag.

Structural basis for the interaction of the IMPα superfamily with EIN2-NLS motif

Homology modeling of ΔIBB_IMPα1 and IMPα4 was performed to demonstrate the position of the IBB domain in the structure and its effect on the major and minor NLS binding site (Fig. 6A). To further localize EIN2-NLS binding to the IMPαs, structural models of ligand–protein complexes of the IMPα3 core structure (PDB code: 4TNM) lacking the IBB domain with the NOP-1 peptide were generated with AlphaFold2 [78] using *ColabFold* 1.5.5. The resulting models suggest that NOP-1 is bound by the major NLS binding site of IMPα3, which is the preferred binding site for canonical monopartite NLS. Key interactions of IMPα3 with the EIN2-NLS CEND probe were predicted at residues E138, W141, N145, T154, Q180, W183, N187, W226, N230, and D264 (Fig. 6B). To

293, 894–917 © 2025 The Author(s). *The FEBS Journal* published by John Wiley & Sons Ltd on behalf of Federation of European Biochemical Societies.

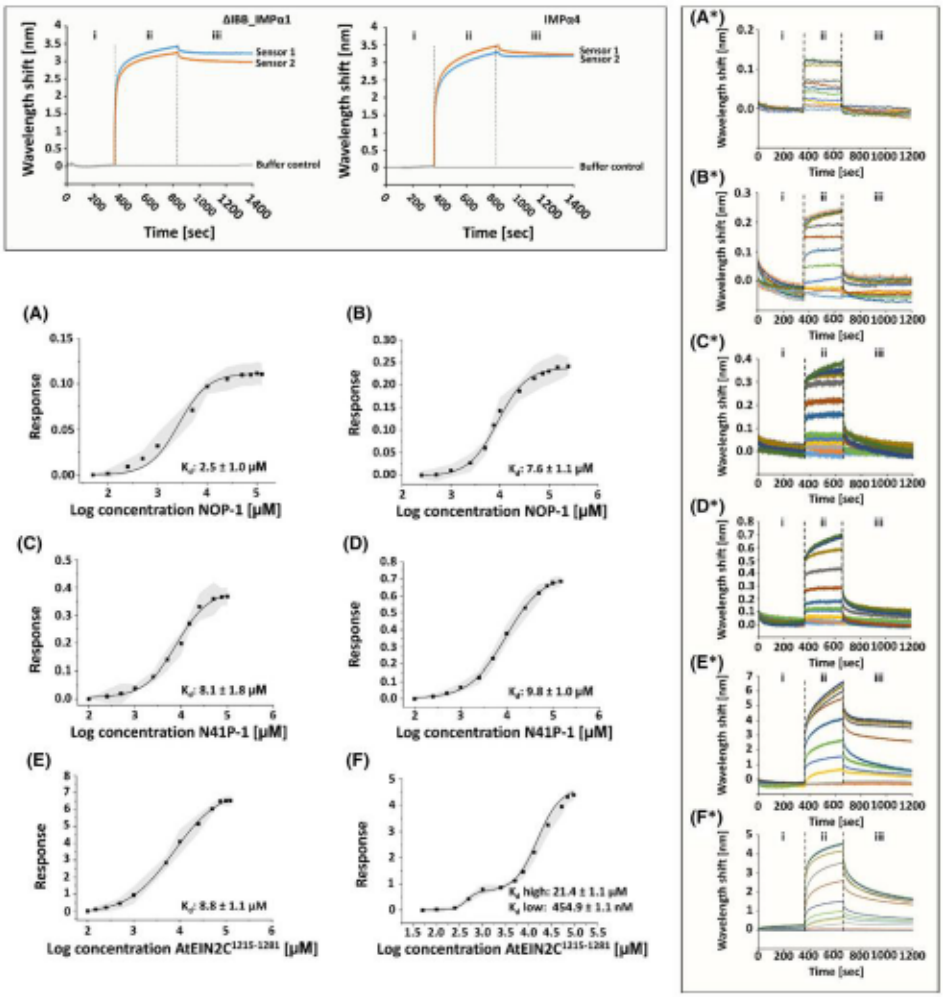

Fig. 5. Binding studies and dissociation constant (K_d) determination of different ligands to ΔIBB_IMPα1 and IMPα4 using BLI sensorgrams. The box on the top of the figure shows real-time sensorgram traces of the Biolayer Interferometry (BLI) protocol that uses streptavidin-coated biosensors. (i) baseline, (ii) loading with biotinylated ΔIBB_IMPα1 and IMPα4 (IBB, importin β binding domain; IMP, importin), (iii) running buffer baseline step after loading. A*–F* show real-time sensorgram traces of the BLI experiments that use streptavidin-coated biosensors, which were loaded with biotinylated ΔIBB_IMPα1 and IMPα4. Raw traces are shown for ΔIBB_IMPα1-NOP-1 (A*), -N41P-1 (C*), -AtEIN2C1215–1281 (E*), for IMPα4-NOP-1 (B*), -N41P-1 (D*), and -AtEIN2C1215–1281 (F*). A BLI protocol was used as follows: (i) running buffer baseline step, (ii) association, and (iii) dissociation. (Related to Table 1). Based on the BLI real-time sensorgram traces, the dissociation constant (K_d) of different ligands to ΔIBB_IMPα1 and IMPα4 was determined. The data are shown as dose response curves. The K_d values are implemented in the corresponding graphs. K_d values were determined for ΔIBB_IMPα1-NOP-1 (A), -N41P-1 (C), -AtEIN2C$^{1215–1281}$ (E), and for IMPα4-NOP-1 (B), -N41P-1 (D), and -AtEIN2C$^{1215–1281}$ (F). Data points represent mean values with 95% confidence intervals based on three independent BLI experiments (n = 3). (Related to Table 1).

Table 1. Binding parameters for the interaction of IMPα representatives ΔIBB_IMPα1 and IMPα4 with EIN2-NLS CEND probes NOP-1, N41P-1, and GB1-*At*EIN2C$^{1215–1281}$.

	ΔIBB_IMPα1	
Ligand	K_d + SD	Hill coefficient
GB1-*At*EIN2C$^{1215–1281}$	8.8 ± 1.1 μM	0.94 ± 0.06
N41P-1	8.1 ± 1.8 μM	1.25 ± 0.11
NOP-1	2.5 ± 1.0 μM	1.03 ± 0.09
	IMPα4	
Ligand	K_d + SD	Hill coefficient
GB1-*At*EIN2C$^{1215–1281}$	K_d high: 21.4 ± 1.1 μM K_d low: 454.9 ± 1.1 nM	0.15 ± 0.02
N41P-1	9.8 ± 1.0 μM	1.09 ± 0.05
NOP-1	7.6 ± 1.1 μM	1.15 ± 0.04

investigate whether any of these pivotal interactions could account for the differences in the EIN2-NLS binding affinities observed in our *in vitro* binding studies among the various IMPα isoforms, a multiple sequence alignment using T-COFFEE [79] with all nine *A. thaliana* IMPα isoforms was done.

As illustrated in Fig. 6C, the alignment reveals that IMPα1-6 show no variation at these pivotal interactions, IMPα7 and IMPα9 display one alteration each (IMPα7: D264Y; IMPα9: D264E), while IMPα8 has two distinct changes (IMPα8: T154P and D264N). In conclusion, it is unlikely that these changes cause the observed differences in binding affinities. However, based on the assumption that the auto-inhibitory N-terminal IBB domain competes for NLS binding at the major rather than at the minor NLS binding site [59,80,81] and given the incomplete match of the NOP-1 NLS-sequence (LKRYKRRL) with any of the six NLS classes defined by Kosugi *et al.* [82], it is reasonable to assume that NOP-1 may in fact bind at the minor site of IMPα proteins. Pang and Zhou demonstrated that residues G323, D325, W357, N361, E396, W399, and N403 are involved in the binding of non-canonical monopartite NLS at the minor site of mouse IMPα lacking the IBB domain [83]. Based on the sequence alignment and comparison of the various IMPα isoforms of *A. thaliana* with respect to the aforementioned residues involved in the minor site-specific binding, these isoforms can be classified into four distinct groups: IMPα1-4 and IMPα6-7 (no alternation with regard to the NLS-minor binding site), IMPα5 (D319S), IMPα8 (D319H), and IMPα9 (G317V; D319P and W394Y) (Fig. S2). This classification aligns well with the results of our *in vitro* binding studies and the overall phylogenetic clustering of the nine isoforms [70,84]. The only exception of this classification is IMPα6, which shows lower binding affinity than the other isoforms of the same category. The highest affinity was observed for IMPα1 (Fig. 3B) and IMPα7 lacking the IBB domain (Fig. 3A), with affinities of 3.2 ± 0.4 μM and 3.0 ± 0.3 μM, respectively. However, these affinities differ only slightly from those of full-length IMPαs showing low micromolar affinities. Accordingly, the results from our binding and computational studies can be interpreted in two ways. First, NOP-1 may bind preferentially at the minor binding site, regardless of whether the IBB domain is present or absent. Secondly, the small EIN2-NLS probe NOP-1 may bind preferentially at the major binding site, preventing auto-inhibition of the IBB domain with respect to NOP-1 binding. This hypothesis is further supported by the fact that reduced or absent auto-inhibition was observed for IMPα3 and IMPα4 in binding and genetic studies, respectively [76,85]. Further experiments are required to clearly identify the EIN2 CEND-NLS binding site in the IMPα superfamily. This may entail co-crystallization of IMPαs with NOP-1 or chemical crosslinking of IMPαs with photoactivable NOP-1.

The IMPα superfamily interacts with EIN2 CEND *in planta* and mediates its nucleocytoplasmic transport

To further investigate the interaction between members of the IMPα superfamily and EIN2 *in planta*, we used *in vivo* fluorescence lifetime microscopy and Förster's resonance energy transfer (FLIM-FRET). Accordingly, the C-terminal part of EIN2 (EIN2C$^{479–1294}$) [17] was fused to the fluorescent protein Cerulean (CER), serving as a donor, and the IMPα isoforms (IMPα1-7) were fused to YELLOW FLUORESCENCE PROTEIN (YFP), serving as acceptors. Transcriptome analysis on different *A. thaliana* tissues and aging plants demonstrated that IMPα8-9 are expressed in low amounts compared with IMPα1-7, especially during senescence of *A. thaliana* [86–88].

Consequently, IMPα8 and 9 were excluded from these experiments. The other constructs were transiently expressed in *N. benthamiana* epidermal leaf cells. EIN2C$^{479–1294}$ localized in the nucleus, ER, and cytoplasm as previously shown by Bisson and Groth [25], whereas the EIN2C$^{479–1294}$ΔNLS variant was only visible in the cytoplasm and ER and absent from the nucleus (Fig. 7). Co-expression of EIN2C$^{479–1294}$ and the IMPa isoforms revealed co-localization of both proteins in the cytoplasm and the nucleus (Fig. 7A,B), which was further confirmed by imaging over 16.5 μM

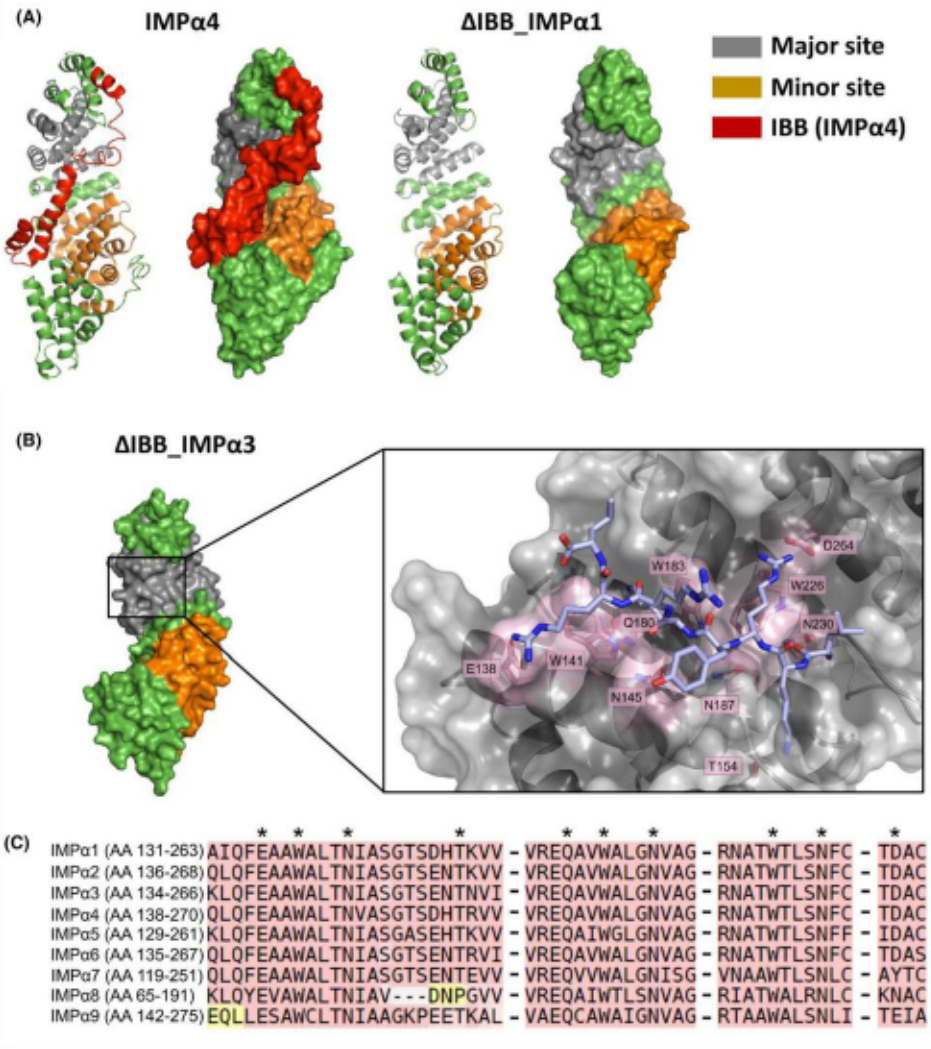

Fig. 6. Structural modeling of IMPα isoforms and predicted NOP-1 interaction with ΔIBB_IMPα3. (A) The structural models of ΔIBB_IMPα1 and IMPα4 (IBB, importin β binding domain; IMP, importin) were generated using the I-tasser online server. Structures are depicted in both ribbon and surface views. The major nuclear localization sequence (NLS) binding site, the minor NLS binding site, and the IBB domain are highlighted in gray, orange, and red, respectively. (B) Predicted binding mode of NOP-1 with IMPα3 lacking the IBB domain at the major NLS site. Binding position of the EIN2-NLS probe NOP-1 (light blue and in sticks) in the IMPα3 armadillo repeat (ARM) domains (gray; PDB code: 4TNM) as revealed by AlphaFold2 [78] modeling. Residues involved in the interaction are highlighted in pink and labeled with their one-letter amino acid code and position. Oxygen and nitrogen atoms are marked in red and blue, respectively. (C) Alignment of amino acid sequences of the nine IMPα isoforms predicted to be involved in NOP-1 binding, using T-COFFEE [79]. Residues depicted in A are marked with asterisks. T-COFFEE highlights residues with a good alignment in pink and residues with an averaged alignment in yellow.

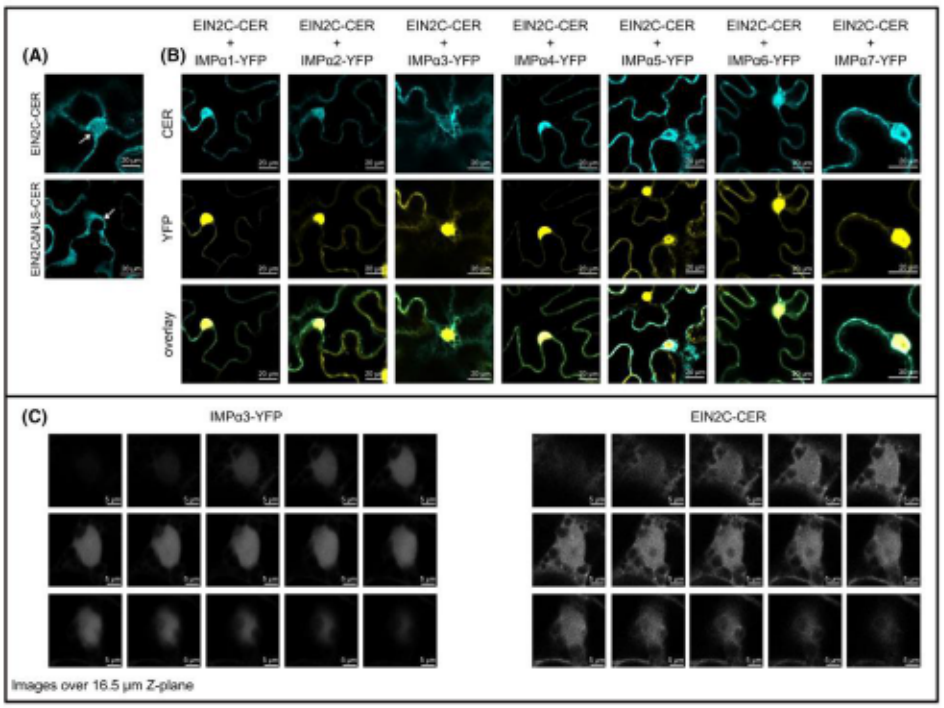

Fig. 7. Confocal fluorescence microscopy of the C-terminal end of the ethylene key regulator EIN2 and *Arabidopsis thaliana* IMPα superfamily members IMPα1-7 in transiently transformed *N. benthamiana* epidermal leaf cells. (A) Confocal images of EIN2C$^{479–1294}$ (Ethylene-insensitive protein 2 C-terminal cytosolic part$^{479–1294}$) and EIN2$^{479–1294}$ΔNLS (Ethylene-insensitive protein 2$^{479–1294}$Δnuclear localization signal) fused to Cerulean (Cer). White arrows indicate the nucleus. All scale bars equal 20 µm. (B) Confocal images of co-expressed EIN2C$^{479–1294}$-CER and *At*IMPα1-7 (*Arabidopsis thaliana* importinα1-7) fused to yellow fluorescence protein (YFP). Images show the emission channel for Cerulean (upper panell), YFP (middle panel), and an overlay of both fluorescence signals (lower panel). All scale bars equal 20 µm. (C) Representative images over 16.5 µm Z-axis with IMPα3-YFP and EIN2C-CER. All scale bars equal 5 µm.

in the Z-plane with IMPα3-YFP as a representative (Fig. 7C). Nucleoli are clearly visible and do not display signal from EIN2 CEND-CER. The EIN2 CEND-CER signal is evenly distributed around the nucleolus, overlapping with the signal from IMPα3-YFP, suggesting the signal is coming from the nucleus and not from the ER that is attached to the nucleus.

While EIN2C$^{479–1294}$ was predominantly localized in the cytoplasm, the IMPα isoforms were mainly found in the nucleus. The presence of IMPα1-4-YFP, IMPα6-FP, and IMPα7-YFP resulted in a significant reduction in the average fluorescence lifetime of the EIN2C$^{479–1294}$-CER donor, indicating interaction between EIN2 and the respective IMPα protein. When IMPα5-YFP served as the acceptor, the average donor lifetime was only slightly, but not significantly reduced (Fig. 8A–C).

FRET efficiencies ranged between 2.8–4.6%. Samples containing IMPα4 demonstrated the highest FRET efficiency (4.6%), while samples with IMPα5 exhibited a FRET efficiency of only 1% (Fig. 8D). Given that nuclear import of the EIN2C$^{479–1294}$ΔNLS variant is abolished [25], we then tested whether this is due to an impaired interaction with IMPα proteins. Co-expression of the IMPα3-YFP acceptor did not result in a reduction of the fluorescence lifetime of EIN2$^{479–1294}$ΔNLS-CER, indicating that no interaction occurred and suggesting that the EIN2$^{479–1294}$ΔNLS variant is not imported into the nucleus (Fig. 8). These findings strongly support a physiological role of the

293, 894–917 © 2025 The Author(s). *The FEBS Journal* published by John Wiley & Sons Ltd on behalf of Federation of European Biochemical Societies.

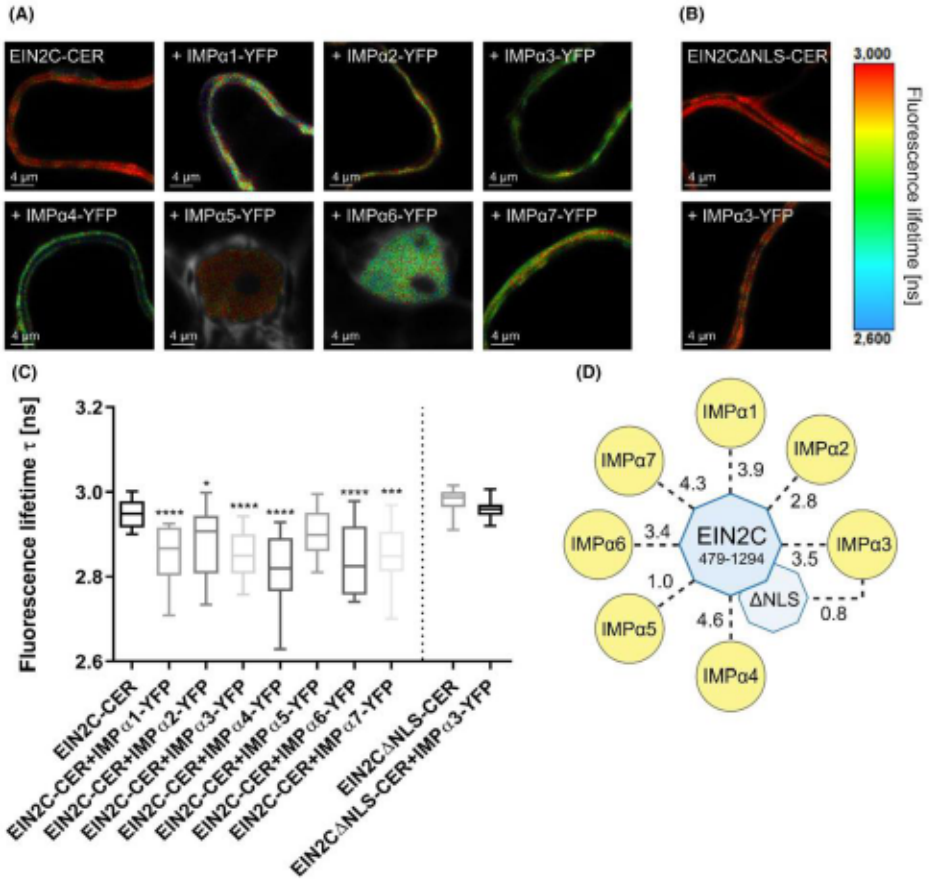

Fig. 8. *In planta* FLIM-FRET experiments using EIN2C$^{479–1294}$ fused to Cerulean and seven IMPα isoforms fused to YFP. The *in planta* experiments were carried out in *N. benthamiana* epidermal leaf cells. EIN2C$^{479–1294}$ fused to Cerulean (CER) was used as donor and the importin (IMP) α isoforms fused to yellow fluorescent protein (YFP) were used as acceptor. (A) Confocal images showing average fluorescence lifetime of the donor in the absence and presence of the different acceptor proteins IMPα1-IMPα7-YFP either in the cytoplasm or the nucleus. (B) Average fluorescence lifetime in the cytoplasm of EIN2C$^{479–1294}$ΔNLS (Ethylene-insensitive protein 2479–1294Δnuclear localization signal) in the absence and presence of the acceptor protein IMPα3-YFP served as negative control. Scale bars indicate 4 µm. (C) Boxplots show the median (line), 25-75th percentile (box) and 10-90th percentile (whiskers) of pooled data from at least 18–20 measurements for the indicated protein (col-expressions. Values outside the 10-90th percentile are not shown. Statistical analysis: Kruskal-Wallis and Dunn's multiple comparisons test. **P*-value <0.05; ****P*-value <0.001; *****P*-value <0.0001 (donor only vs. donor + acceptor). The statistical analysis of the EIN2C$^{479–1294}$ΔNLS-CER variant with IMPα3-YFP was performed by using a t-test. (D) Graphical visualization of mean förster resonance energy transfer (FRET) efficiencies calculated for each donor-acceptor pair which are indicated by dashed lines. Numbers next to the dashed lines reflect FRET efficiencies. The EIN2C$^{479–1294}$ΔNLS-CER fusion protein was only measured with IMPα3-YFP and served as a negative control. Created in BioRender (2024) https://BioRender.com/l78k942.

IMPα superfamily in nucleocytoplasmic transport of EIN2, which is essential for mediating ethylene responses. Additionally, there is a notable redundancy in terms of IMPα isoforms that interact with EIN2, possibly to guarantee efficient nuclear import of this key regulator of ethylene-mediated plant responses.

Discussion

The mechanisms, pathways, and processes by which EIN2, the central switch of the ethylene response pathway, integrates and bridges signaling of the plant hormone from the ER membrane to the nucleus have been studied in-depth and led to important insights in plant hormone signal transduction. While the generally accepted EIN2 'cleave and shuttle' model plausibly explains how the ethylene signal is transmitted from the ER to the nucleus, the specific elements and structures of the nuclear import pathway of the processed EIN2 C-terminus were entirely unknown. Based on the canonical NLS-sequence found in the EIN2 C-terminus and the impact of this sequence on nuclear import of CEND [31,32], our study hypothesized that transport of the released EIN2 CEND from the cytoplasm into the nucleus is mediated by the IMPα-IMPβ transport machinery. A study from Lu *et al.* [60] elucidated that the nuclear trafficking of *A. thaliana* EIN2 CEND can be induced by importin β1 (IMPβ1), either by ethylene treatment or by green peach aphid infestation. During the NLS-dependent protein trafficking from the cytoplasm into the nucleus, mediated by the IMPα-IMPβ transport machinery, the NLS on the cargo proteins is recognized by the IMPα subunit, which in turn is recognized by the IMPβ subunit [89]. An AlphaFold model of the *A. thaliana* IMPα1-IMPβ1-NOP-1 demonstrates that the NLS sequence interacts with IMPα1 and that IMPβ1 may interact with regions of bigger cargo proteins like EIN2 CEND (Fig. S3). The identification of the binding region between IMPβ1 and EIN2 CEND is so far unknown and needs further investigations.

To ascertain whether the cargo recognition adapter module of this machinery (IMPα) is implicated in the recognition and binding of EIN2 CEND, we initially studied the well-documented triple response, a set of morphological changes to dark-grown seedlings in response to ethylene, in a range of single and triple *impα* loss-of-function *Arabidopsis* mutants. Our results show that all studied *impα* single and triple mutants show the characteristic triple response phenotype when grown in the presence of the ethylene precursor ACC. This excludes the possibility that a single or a combination of three of the nine IMPα isoforms in *Arabidopsis* is specifically or exclusively responsible for EIN2 CEND nucleocytoplasmic transport, indicating a high level of functional redundancy of the IMPα isoforms for EIN2 CEND recognition and binding. Given the crucial role of the IMPα superfamily in the recognition and nucleocytoplasmic transport of a vast array of cargo proteins, as evidenced by the dwarf growth type of the *impα1;impα2;impα3* triple mutant [74], we reasoned that further deletion of additional members of the IMPα superfamily would result in severe developmental defects or plant lethality, thereby precluding triple response analysis as a means to study the impact of the IMPα superfamily on EIN2 CEND recognition and nucleocytoplasmic transport. Additionally, loss-of-function mutants of IMPβ1 and other IMPβ family proteins (e.g., HASTY and PAUSED) have shown strong effects on ethylene-enhanced expression of defense mechanisms, plant growth, and development [60,90–92]. This suggests that the IMPβ proteins may be involved in the nucleocytoplasmic transport of several pathways.

The outcome of our phenotypic studies led us to adopt a different approach to address the potential interactions of EIN2 CEND with members of the IMPα superfamily. We used purified recombinant IMPα1-9 proteins with defined EIN2-NLS probes for *in vitro* binding studies. The results of these studies demonstrated that EIN2-NLS is recognized by most members of the IMPα superfamily at low micromolar affinity. Prior studies on purified IMPα from yeast, mammals, and plants [65,93–96] have demonstrated that functional canonical NLS have binding affinities up to 1 μM [97]. In contrast, binding studies between IMPα3 from *A. thaliana* lacking the IBB domain and NLS peptides [76] showed affinities in the low micromolar range, which is comparable to the affinities observed in our binding studies of the various *Arabidopsis* IMPα isoforms. The discrepancy to the previously reported sub-micromolar affinities is likely due to the different techniques used to study biomolecular interactions. Affinities in the nanomolar range were determined by surface-bound assays, including plate binding assays [65,94,96] and surface plasmon resonance (SPR) [95]. Conversely, affinities in the low micromolar range were obtained by isothermal calorimetry (ITC) [76] or, as in our case, by fluorescence polarization (FP) measurements. The FP-based micromolar affinities for EIN2-NLS are further corroborated by BLI measurements on immobilized IMPα isoforms with EIN2 CEND-NLS probes of varying length and complexity, which revealed a decrease in affinity upon increasing sequence length of the NLS probe (K_d NOP-1 < N41P-1 < GB1_*At*EIN2$^{1215–1281}$). The BLI measurements on the N-terminal truncated IMPα1 further confirm the previously known competitive effect of the N-terminal IBB domain for NLS binding. For EIN2-NLS, this effect becomes more pronounced with increasing length, reduced flexibility of the NLS probe, and is most evident for

GB1-*At*EIN2C$^{1215–1281}$. The second, high-affinity binding observed in the sub-micromolar range for the EIN2 CEND GB1-fusion may be attributed to immobilization effects of the importin, as no such affinity was observed in the FP measurements with the various IMPαs in solution.

In order to predict how and where EIN2 CEND-NLS and related EIN2-NLS probes may bind to IMPα, we used Alphafold2 [78]. The results suggest that EIN2-NLS may potentially bind to the major binding groove situated between ARM repeats 2–4 (major NLS binding site). However, given the amino acid (aa) conservation at this site, binding would not align with the observed differences in binding affinity of the various isoforms. In accordance with this, previous structural and calorimetric studies by de Oliveira *et al*., demonstrated that NLS peptides do not bind exclusively to the major NLS binding site [98]. Rather, they also interact with the minor NLS binding site which is located at ARM 7–8. When the minor site is considered as the EIN2-NLS binding site, the observed differences in the experimentally determined K_d value align well with the aa substitutions observed in the various IMPα isoforms at this site. The only discrepancy was observed for IMPα6, which based on the aa composition at this site is expected to show similar affinities as IMPα1-4.

Given their high affinity, IMPα1-4 qualifies as the preferred EIN2-NLS interaction partner. Notably, the observed *in vitro* binding affinities are consistent with the expression pattern of the various IMPα isoforms in ethylene-dependent developmental processes at different stages of plant life (Fig. 9).

The hormone influences early developmental aspects such as the release of seed dormancy during germination, but also late events in plant life such as flower and leaf senescence. According to the TAIR database, IMPα1-4 show high expression during germination, in mature flowers, and senescent leaves. In contrast, low expression levels at these developmental stages are observed for IMPα5, IMPα6, IMPα8, and IMPα9, which is consistent with their lower affinity in our binding studies. Additionally, the analysis of deposited transcriptome data at the Expression Atlas database and protein expression levels at the ePlant database demonstrated that IMPαs and EIN2 show different expression levels in 17 tested *A. thaliana* tissues (Fig. 9C,D) [87,88,99]. Similar to the TAIR database, the strongest expression pattern could be observed for IMPα1-4. Based on deposited data of an expression analysis in senescent *A. thaliana* [86], we observed that most of the IMPαs, IMPβ1, and EIN2 show a similar expression profile during senescence, with an expression peak after 10 days and a second broad expression maximum between 12 and 14 days (Fig. 9A). We included six control genes that show different expression profiles compared to the IMPs and EIN2 (Fig. 9B) to demonstrate the significance of the expression profile. Interestingly, IMPα7-9 showed very low expression levels during these experiments, which may suggest that these proteins have a minor effect on the EIN2 CEND translocation. IMPα8 and 9 were excluded from the following *in planta* experiments. In contrast, the experiments were performed with IMPα7 because it showed one of the strongest K_d values against NOP-1 with 3 ± 0.3 μM.

The TAIR database includes the expression data of *A. thaliana* IMPα1-9 in the presence of ACC (1-Aminocyclopropane-1-carboxylic acid), an ethylene precursor [100]. The experiments were conducted for 3 h, during which a significant increase in expression was only observed for IMPα5 (Fig. S4). Importins are involved in the nuclear transport of several proteins and are permanently expressed in plants. Our triple response experiments have already demonstrated that none of the nine tested IMPα isoforms in *Arabidopsis* is exclusively responsible for EIN2 CEND nucleocytoplasmic transport. Consequently, the expression level following ACC treatment—equivalent to ethylene treatment—does not increase.

The *in planta* FLIM-FRET experiments corroborate the findings of the *in vitro* binding studies, demonstrating an interaction between EIN2$^{479–1294}$, the cytosolic part of EIN2 that is transported into the nucleus upon ethylene sensing, and at least six out of seven tested IMPα proteins. The localization of EIN2C$^{479–1294}$ in both the cytoplasm and the nucleus, even in the absence of co-expression of any of the *Arabidopsis* IMPα, is most likely due to the presence of endogenous importin proteins in *N. benthamiana*, given the high degree of conservation of the IMPα-IMPβ pathway [61,101]. The fusion of proteins to fluorophores has been shown to alter the biophysical properties of the fluorophore [102]. Thus, it is plausible that this phenomenon may occur *vice versa*. This will result in lower affinities of the IMPα-YFP constructs as compared to the endogenous importins, potentially due to alterations in their biophysical properties. Furthermore, the nucleocytoplasmic transport of EIN2 is a process that involves both IMPα and IMPβ proteins. Given that we only expressed IMPα proteins from *A. thaliana*, but not the related IMPβ proteins in the *N. benthamiana* leaf cells, it seems likely that the endogenous IMPα-IMPβ interaction is stronger than the interaction between *A. thaliana* IMPα and endogenous IMPβ. According to our *in planta* studies, all IMPα isoforms other than IMPα5 bind EIN2. Further analysis revealed that this

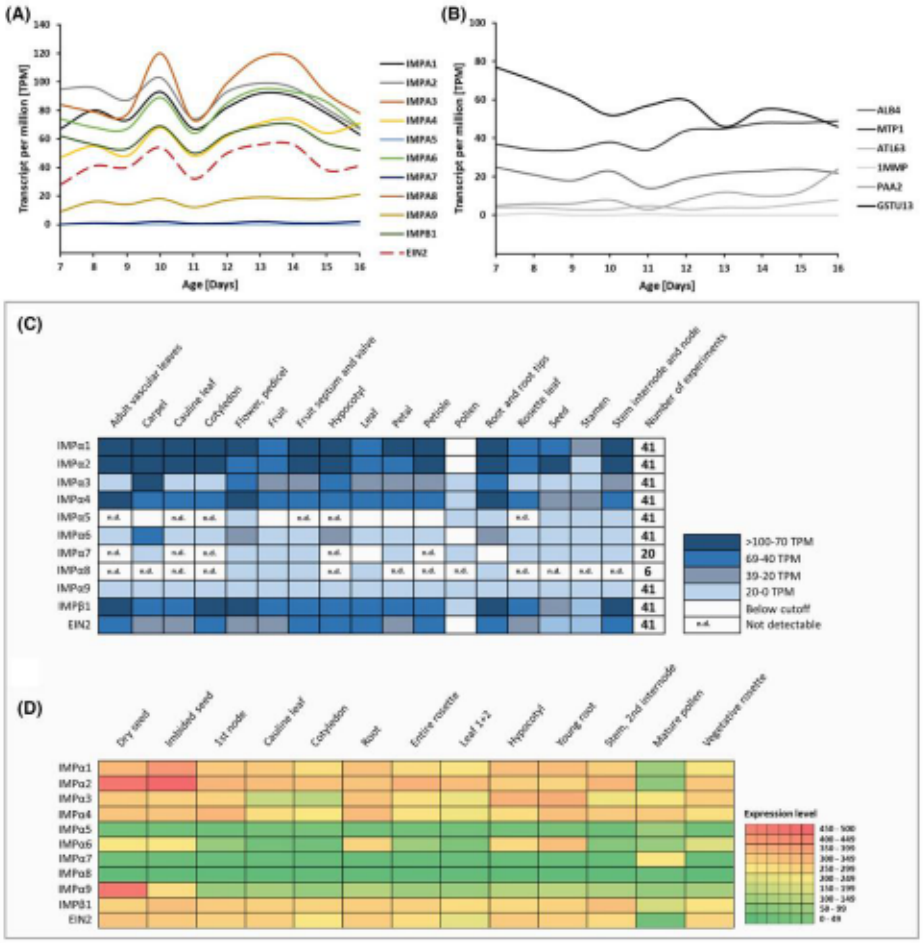

Fig. 9. Importin and EIN2 expression levels in *A. thaliana* tissues. A and B show expression profiles of importin (IMP)α, IMPβ1, ETHYLENE INSENSITIVE 2 (EIN2), and control proteins in senescent *A. thaliana*. Based on data that are deposited at the Expression Atlas webserver [107]. Expression profiles are shown for IMPα1-9, IMPβ1, and EIN2 (A). Expression maxima can be observed after 10 days and between 12 and 14 days. The expression of six random control proteins (*A. thaliana*) is shown (B), including ALB4 (ALBINO3-like protein 1), MTP1 (Metal tolerance protein 1), ATL63 (RING-H2 finger protein), 1MMP (Metalloendoproteinase), PAA2 (Copper-transporting ATPase), and GSTU13 (Glutathione S-transferase U13). The gray box shows the gene expression of importins and EIN2 in *A. thaliana* tissues at the RNA (C) and protein (D) levels. The results are based on data from the Expression Atlas webserver for RNA levels (IMPα1, 2, 3, 4, 6, and 9 based on 41 experiments, IMPα5 based on 12 experiments, IMPα7 based on 20, and IMPα8 based on 6 experiments) and the ePlant database for protein levels (results based on expression levels across 350 samples). The RNA levels are shown in TPM (Transcript per million), representing the number of transcripts for a given gene or isoform.

interaction is facilitated via the EIN2-NLS motif, as no lifetime reduction was detected in samples of IMPα3 and EIN2C$^{479–1294}$ΔNLS.

In conclusion, the results of our *in vitro* binding studies, *in planta* localization and interaction studies as well as our computational structure predictions

demonstrate that EIN2-NLS CEND can bind various members of the IMPα superfamily for mediating transport into the nucleus. Future studies aim at elucidating the precise binding site of EIN2-NLS with the IMPα superfamily.

Materials and methods

Sterilization and growth of *Arabidopsis thaliana* mutants

Around 10 mg of seeds was filled into a 2-mL reaction tube and put into a desiccator with the lid opened. Additionally, a beaker with 100 mL 37% perchloric acid was put into the desiccator. 3 mL of 37% hydrochloric acid was pipetted into the beaker to start the reaction, and the lid of the desiccator was closed immediately. The seeds were incubated for 1 h. After the incubation time, the lid of the desiccator was opened slightly, while the tubes were incubated for 20 more minutes to wait for the gas to evaporate. 1 mL of sterile water was added to the reaction tubes, and the seeds were stratified by storage at 4 °C for 3 days before planting (otherwise they can be planted directly after this procedure). Before starting to plant the seeds, any material (e.g., pots and tubs) was sterilized with 70% ethanol. A mixture of soil, vermiculite, and sand (ratio 8:1:1) was prepared, and water was added in the right proportion to make the soil mix soggy but not mushy. The soil mix was sterilized by heating it in the microwave at 800 W for about 10 min. Pots were filled with the sterilized soil mix afterwards. Around 100 µL of 1% agarose in tap water was added to the reaction tubes containing the sterilized seedlings for better pipetting precision, and the seeds were planted into the soil mix. The growth of *A. thaliana* was performed at 22 °C, 60% humidity, and 100–120 µEinstein light intensity. The plants were watered only from the bottom every 2–3 days. After 5 weeks, the plants were big enough to grow in their own pots instead of several plants being grown crowded in one pot.

Triple response assay

The triple response media for the agar plates was prepared by mixing 0.43% (w/v) of Murashige and Skoog (MS) salts and 1% (w/v) sucrose. The pH is adjusted to 6.0 before adding 0.7% (w/v) plant agar to the media and autoclaving it at 121 °C for 30 min. Before pouring the plates, the agar media was cooled down to about 45 °C and either ACC was added to the agar for plates containing ACC or the plates were poured directly after cooling down. The plates that were used for the triple response had the dimensions of 130 × 130 × 15 mm. Sterilization of the seeds had to take place directly before planting. The seeds were applied one by one in a straight horizontal line onto the agar plates. A maximum amount of two mutants, except the wild-type, was placed per plate. Afterwards, the plates were wrapped separately in aluminum foil and placed vertically (so that the seeds grow to the top) at 4 °C for 3 days (stratification). Subsequently, the plates were light-treated for 2 h at room temperature, which improves germination before being covered again and placed vertically at 22 °C for 5 days. The seedlings were documented, and the length of the hypocotyl was analyzed using a binocular microscope and the software Motion 3.0, respectively.

Transient transformation of *N. benthamiana*

A modified version of a previously described procedure was used for the transient transformation of *N. benthamiana* [17]. An overnight culture of agrobacteria was inoculated in DYT and incubated at 28°C one day before infiltration. Bacteria were then centrifuged at 4000 ***g*** and resuspended in infiltration medium (5% (w/v) Saccharose; 0.01% (w/v) $MgSO_4$; 0.01% (w/v) Glucose; Acetosyringone 450 µM) to an OD600 of 0.4–0.8. Resuspended bacteria were kept on ice for 1–2 h prior to infiltration. For co-infiltration, bacteria solutions were mixed in equal quantities, and Agrobacterium strain GV3101:p19 expressing the p19 silencing inhibitor was added to each mix. Infiltration of the bacteria solution was performed with a 1 mL syringe onto the abaxial side of 3- to 4-week-old plants. Plants were kept under continuous light before microscopy analysis. For ß-estradiol inducible constructs, plants were sprayed on the abaxial side of infiltrated leaves with an estradiol solution (ß-estradiol 20 µM; Tween-20 0.1% (w/v)) prior to imaging.

Fluorescence imaging

For fluorescence imaging, a Zeiss LSM 780 confocal microscope (40× water immersion objective, Zeiss C-PlanApo, NA 1.2) was used. YFP was excited at 514 nm and Cerulean at 458 nm. Signal recording of each fluorophore was done within its maximum emission peak while avoiding auto-fluorescence above 650 nm. Laser power and gain were adjusted differently for each image based on fluorophore signal intensity.

Fluorescence lifetime imaging

Fluorescence lifetime imaging was performed using a protocol described previously [103]. Fluorescence lifetime was measured at a Zeiss LSM 780 confocal microscope (40× water immersion objective, Zeiss C-PlanApo, NA 1.2). For TCSPC, a PicoQuant Hydra Harp 400 (PicoQuant, Berlin, Germany) was used. Photon counting was performed with a picosecond resolution. Cerulean was excited with a 440 nm (LDH-D-C-485, 32 MHz, PicoQuant, Berlin, Germany) pulsed polarized laser. Laser power at the objective

lens was adjusted to ~2.2 µW in *N. benthamiana* experiments. Light emitted from the sample was separated by a polarizing beam splitter before photons were selected with a band-pass filter. A 482/35 band-pass filter was used for Cerulean, and for YFP, a 534/30 band-pass filter was used. Photons were detected in both donor and acceptor channels simultaneously with Tau-SPADs (PicoQuant, Berlin, Germany). Images were acquired at zoom 8 with a resolution of 256 × 256 pixels, with a pixel size of 0.1 µm and a pixel dwell time of 12.54 µs, and a laser repetition rate of 32 MHz. Photons were collected over 40 frames. To avoid pileup effects, nuclei containing high donor concentrations were avoided. Before image acquisition, the system was calibrated for each donor. For this, the objective was adjusted to reach a maximal count rate. FCS curves of Atto425 dye and water were acquired to monitor the system function. Internal response functions for each laser were determined by measuring the fluorescence decay of quenched Atto425 in saturated KI, using the same hardware settings as for the FRET pair of interest. Fluorescence lifetime images were acquired in the cytosol, ER, or nucleus in donor-only samples and samples with IMPα1-4 and IMPα7. Signal intensity of IMPα5-YFP and IMPα6-YFP was considerably lower compared to the other IMPα-YFP fusions, likely due to lower protein concentrations. To ensure sufficient acceptor concentrations for FRET to occur, only FLIM images of nuclei were acquired for these samples. Micrographs display representative FLIM images for each sample.

Fitting of the fluorescence decays

The fluorescence decays were fitted using a previously reported method with minor modifications [104].

The fluorescence decays of selected ROIs in the FLIM image were analyzed with the SymPhoTime FLIM analysis software (SymPhoTime 64, version 2.4; PicoQuant, Berlin, Germany). TCSPC bins of Channels 1 and 2 (parallel and perpendicular light) were binned by 16, resulting in a bin width of 16 ps. Nuclei or cytoplasm/endoplasmic reticulum were selected by hand using the ROI tool. Chloroplasts and pixels above the pile-up limit (10% of the laser repetition rate) were manually removed. Decays from all samples were fitted with the FLIM analysis tool (Fitting model: n-exponential reconvolution) using two lifetimes (model parameter $n = 2$). FRET efficiency was calculated as the lifetime of the FRET sample over the arithmetic mean of the lifetimes of the donor-only samples measured on the same day.

Expression of importin alpha proteins and GB1-*At*EIN2C$^{1215–1281}$

Genes encoding several isoforms of the IMPα superfamily were either isolated from *Arabidopsis thaliana* (IMPα1, -2, -3, -4, -8) or synthetically produced by GenScript (IMPα5, -6, -7, -9) and cloned into the pETEV21a vector (modified version of the pET21a vector with an additional TEV cleavage site between the GOI and the His-tag), which contains a C-terminal hexa-His-tag. Only IMPα5 was additionally cloned into the pETEV16b vector (modified version of the pET16b vector with an additional TEV cleavage site between the GOI and the His-tag), which contains an N-terminal deca-His-tag (see Table S2 for primer list). The *At*EIN2C$^{1215–1281}$ gene was cloned into the pETEV16b vector and additionally contained a GB1-domain at the N terminus to enhance solubility. Most of the proteins were expressed in the *E. coli* BL21pRARE strain, while IMPα7, IMPα8, and ΔIBB_IMPα1 (lack of the IBB domain) were expressed using the *E. coli* BL21gold strain. The bacterial cultures were adjusted to an initial OD_{600} of 0.1 and grown in 2YT media at 37 °C until an OD_{600} between 0.6 and 0.8 was reached. Subsequently, the protein expression was induced with 0.5 mM IPTG. After two hours, the cells were harvested via centrifugation at 10,000 ***g*** for 10 min. IMPα5, IMPα6, IMPα7, IMPα8, ΔIBB_IMPα1, and GB1_*At*EIN2C$^{1215–1281}$ were expressed at 16 °C overnight with the addition of 2% (v/v) ethanol. The cell pellets were frozen in liquid nitrogen and stored at −20 °C.

Protein purification

The stored cell pellet was resuspended in 1× PBS, 5% (w/v) Glycerol and 0.1% (v/v) NP40 pH 7.4 (5 mL per g cell). A spatula tip of DNase and 4–6 drops of Antifoam were added to the resuspended cells, which were disrupted by using the cell disruptor afterwards. After cell disruption, cell debris and insoluble protein were separated by centrifugation at 100,000 ***g*** for one hour, and subsequently, the supernatant was loaded onto a pre-equilibrated Ni^{2+}-IMAC (immobilized metal affinity chromatography) column. The column was washed with 500 mM NaCl and 50 mM NaP_i buffer pH 7.4 until the baseline was reached again. Afterwards, unspecific proteins were washed off stepwise using 500 mM NaCl and 50 mM NaP_i buffer with increasing imidazole concentrations (50 mM and 100 mM imidazole), while the proteins of interest were eluted with 500 mM NaCl, 50 mM NaP_i buffer and 500 mM imidazole pH 7.4. The purified proteins were concentrated using ultrafiltration units (Amicon), frozen with liquid nitrogen, and stored at −80 °C.

Peptides

All NLS peptides were purchased from GenScript (NJ, USA) as a lyophilized powder with >95% purity. NOP-1 consists of 8 amino acid residues and N41P-1 consists of 41 amino acid residues. The C-termini of the D-ri-peptides are amidated, and the N-termini are acetylated. An analysis certificate from GenScript demonstrated the purity of each peptide (for details see Figs S5–S8).

Synthesis of fluorescently labeled NOP-1

The TAMRA-NOP-1 peptide was synthesized using solid-phase peptide synthesis (SPPS) with the Activotec P11 automated synthesizer (Activotec, Cambridge, UK) following the standard fluorenylmethoxycarbonyl (Fmoc) protocol. Depending on the NOP-1 sequence (LKRYKRRL), the following amino acids were used: Fmoc-Lys(Boc)-OH (99.5%), Fmoc-Tyr(tBu)-OH (98%) (BLD Pharmatech GmbH, Reinbek, Germany), Fmoc-Arg(Pbf)-OH (98%), and Fmoc-Leu-OH (98%) (Carbolution GmbH, Sankt Ingbert, Germany). Fmoc-protected amino acids were employed throughout the synthesis. The solid phase consisted of H-Leu-2-CT-polystyrene resin (loading 1.13 mmol·g^{-1}) (RAPP Polymere GmbH, Tübingen, Germany). The synthesis consisted of repetitive Fmoc deprotection and amino acid coupling steps. Fmoc cleavage was carried out by treating the resin three times with 25% (v/v) piperidine (Thermo Fisher Scientific) in dimethylformamide (DMF) (Biosolve, Valkenswaard, the Netherlands) for 10, 15, and 20 min, respectively. After each treatment, the resin was washed 10 times with DMF. Amino acid coupling was performed by treating the resin with a solution containing 5 eq. of Fmoc-amino acid, 5 eq. of benzotriazol-1-yloxytripyrrolidinophosphonium hexafluorophosphate (PyBOP) (Biosynth, Staad, Switzerland), and 10 eq. of diisopropylethylamine (DIPEA) (Carl Roth) in 2 mL of DMF for 1 h. After the coupling reaction, the resin was washed 10 times with dichloromethane (DCM) (Merck, Darmstadt, Germany) and DMF. For fluorophore conjugation, 1.3 eq. of 5-Carboxytetramethylrhodamine succinimidyl ester (TAMRA-NHS) (Biosynth, Staad, Switzerland) ester was dissolved in 4 mL of DMF, and 10 eq. of DIPEA were added to the solution. This mixture was incubated with the resin-bound peptide for 16 h in the absence of light. After conjugation, the resin was washed 10 times with DMF, followed by alternating washes with DCM and methanol until the washing solution became clear. Peptide cleavage from the resin was achieved by treatment with 2 mL of 70% (v/v) trifluoroacetic acid (TFA) (Fisher Chemical, Schwerte, Germany) and 30% (v/v) triisopropylsilane (TIPS) (Fluorochem, Hadfield, UK) for 1 h. The cleaved peptide was precipitated with diethyl ether (honey well). To remove TFA salts, an anionic exchange was performed using AG®1-X8 resin (Bio Rad, Hercules, USA). The resin was activated by sequential washes with 1.6 N acetic acid and 0.16 N acetic acid (Merck, Darmstadt, Germany). The peptide solution was incubated with the activated resin for 1 h and then lyophilized to yield the purified peptide.

Reversed phase- high pressure liquid chromatography (RP-HPLC) electron spray ionization- mass spectrometry (ESI-MS)

RP-HPLC-MS spectra were performed on an Agilent Technologies 1260 Infinity Instrument in combination with a 6120-quadrupole mass spectrometer (Figs S9, S10). The instrument has a wavelength detector (VWD1 A) that measures the absorbance at 214 nm. The mass spectrometer generates ions using the electrospray method, which is used at a Charge-to-mass ratio detected between 200 and 2000. The separation of the sample was performed on the MZ-AquaPerfect C18 column (3.0 × 50 mm, 3 µm) at 25 °C. As mobile Phase the following mixtures were used: (A) H_2O/acetonitrile (95:5 Vol.%) with 0.1 Vol.% Formic acid and (B) H_2O/acetonitrile (5:95 Vol.%) with 0.1 Vol.% formic acid. The flow rate was 0.4 mL·min$_{-2}$. A linear gradient from 100% A/0% B to 0% A/100% B with a total measurement time of 17 min.

Biolayer interferometry (BLI) measurements

An Octet K2 device (Fortè Bio, Dallas, USA) was used to obtain BLI binding data, which were processed using the system's built-in software. Experiments were conducted at room temperature with continuous shaking at 400 rpm in black 96-well plates, each well containing 200 µL. Biotinylated ΔIBB_IMPα1 and IMPα4 were loaded onto a streptavidin (SA) biosensor (Fortè Bio) at a concentration of 15 µM in 100 mM Tris (pH 7.0), 100 mM KCl, 0.01% (w/v) Tween 20 for 600 s. Therefore, ΔIBB_IMPα1 and IMPα4 were biotinylated using the Biotin-PEG_4-NHS ester Protein Labeling Kit from Jena Bioscience (Jena, Germany). Evaluation of successful biotinylation was performed with the Colorimetric Biotin Assay Kit from Sigma (St. Louis, USA). After establishing a baseline in the binding buffer, biosensors were dipped into peptide-containing wells at the indicated concentrations for 300 s to monitor association, followed by a 300 s dissociation phase in binding buffer. For reliable dissociation constant (K_d) measurements, BLI experiments were conducted with a range of peptide and protein concentrations tailored to their binding strengths. Stock solutions of peptides and proteins were diluted in binding buffer. The resulting raw data were corrected for background using reference sensors exposed only to buffer. All measurements were performed in quadruplicate. The raw data were evaluated with the octet data analysis software. Curve fitting was completed with ForteBio Biosystems using a heterogenous fitting algorithm and 1:2 binding model to obtain K_d values.

Fluorescence polarization (FP) measurements

The FP measurements were performed using the LS55 Fluorescence Spectrometer from PerkinElmer and a precision cuvette consisting of SUPRASIL® from Hellma. TAMRA-NOP-1 was used at a concentration of 250 nM and a detector voltage of 790 V, whereas Alexa488_GB1_*At*EIN2C$^{1215–1281}$ was used at a concentration of 200 nM and a detector voltage of 770 V. Samples

were prepared in a total volume of 50 µL with constant fluorophore but varying protein concentrations. The measurement was tracked for 100 s, and the polarization value was determined by averaging half of the recorded time period. The competition experiments were performed analogously with the exception that both the fluorophore and protein concentration were held constant, while the competitor concentration was varied. The protein concentration used in the competition experiments was identical to the determined K_d value resulting from the non-competition experiments.

In silico analysis

Importin α superfamily protein sequences were retrieved from the NCBI database, and sequence alignments were performed using T-COFFEE [79]. The I-TASSER server was used to construct 3-dimensional homology models of IMPα4 and ΔIBB_IMPα1 [105]. The IMPα homology models were calculated based on 10 proteins with highly similar structures in PDB, as identified by the TM-alignment algorithm. TM-align is a computer algorithm for protein structure alignment using dynamic programming and the TM-score rotation matrix. An optimal alignment between two proteins, as well as the TM-score, will be reported for each comparison. In general, a TM-score >0.5 means the structures share the same fold [105]. For all 10 structures used for the ΔIBB_IMPα1 model (PDB codes: 2YNS, 4RXH, 1WA5, 4UAE, 1IAL, 2JDQ, 4RV1, 5XJG, 4R0Z, and 7V7B), the TM-score shows values >0.75. For all 10 structures used for the IMPα4 model (PDB codes: 1WA5, 2YNS, 4RXH, 1IAL, 5XJG, 4UAE, 2JDQ, 4RV1, 5HB4, and 4R0Z), the TM-score shows values >0.65. The model of *A. thaliana* IMPα1-IMPβ1-NOP-1 was generated using the AlphaFold 3 web server [106]. All figures are made using the PyMOL Molecular Graphics System, Version 1.3, Schrödinger, LLC.

Statistical analysis

For statistical analysis, GraphPad Prism 6 was used. For the triple response assay and the *in planta* FLIM-FRET experiments, two-way ANOVA, Kruskal–Wallis test, Dunnett's multiple comparisons test, and t-test were performed.

Acknowledgements

We would like to acknowledge the Center for Advanced Imaging (CAi) at Heinrich-Heine-University Düsseldorf funded by the Deutsche Forschungsgemeinschaft (DFG, German Research Foundation)—Project-ID DFG- INST 208/551-1 FUGG for providing access to the Zeiss LSM 780 + 4-channel FLIM exten. (Picoquant). This work was supported by a grant from the Deutsche Forschungsgemeinschaft (DFG, German Research Foundation) to G.G. (project no. GR1616/14-1). Open Access funding enabled and organized by Projekt DEAL.

Conflict of interest

The authors declare that they have no known competing financial interests or personal relationships that could have appeared to influence the work reported in this paper.

Author contributions

Conceptualization, GG; Methodology, FW, GG, RJE; Investigation, FW, JEM, RJE, NJ, MW, and LH; Formal analysis, FW, JEM, RJE, NJ, MW, and LH; Validation, FW, JEM, RJE, NJ, RS and GG; Visualization, FW and RJE; Writing – Original draft, FW, JEM, RJE, and GG; Writing – Review and Editing, FW, RJE, MW, LH, RS, and GG. All authors read and edited the manuscript prior to publication.

Peer review

The peer review history for this article is available at https://www.webofscience.com/api/gateway/wos/peer-review/10.1111/febs.70285.

Data availability statement

All relevant data are included in this manuscript and its supporting information. Further inquiries or requests for materials can be directed to georg.groth@hhu.de.

References

1 Abeles FB, Morgan PW & Saltveit ME (1992) Ethylene in Plant Biology. Academic Press, San Diego, CA.
2 Ecker JR (1995) The ethylene signal transduction pathway in plants. *Science* **268**, 667–675.
3 Ju C, Van de Poel B, Cooper ED, Thierer JH, Gibbons TR, Delwiche CF & Chang C (2015) Conservation of ethylene as a plant hormone over 450 million years of evolution. *Nat Plants* **1**, 1–7.
4 Hamilton A, Lycett G & Grierson D (1990) Antisense gene that inhibits synthesis of the hormone ethylene in transgenic plants. *Nature* **346**, 284–287.
5 Wilkinson JQ, Lanahan MB, Yen H-C, Giovannoni JJ & Klee HJ (1995) An ethylene-inducible component of signal transduction encoded by never-ripe. *Science* **270**, 1807–1809.

6 Chen YF, Gao Z, Kerris RJ 3rd, Wang W, Binder BM & Schaller GE (2010) Ethylene receptors function as components of high-molecular-mass protein complexes in Arabidopsis. *PLoS One* **5**, e8640.

7 Grefen C, Stadele K, Ruzicka K, Obrdlik P, Harter K & Horak J (2008) Subcellular localization and in vivo interactions of the *Arabidopsis thaliana* ethylene receptor family members. *Mol Plant* **1**, 308–320.

8 Dong CH, Rivarola M, Resnick JS, Maggin BD & Chang C (2008) Subcellular co-localization of Arabidopsis RTE1 and ETR1 supports a regulatory role for RTE1 in ETR1 ethylene signaling. *Plant J* **53**, 275–286.

9 Bleecker AB, Estelle MA, Somerville C & Kende H (1988) Insensitivity to ethylene conferred by a dominant mutation in *Arabidopsis thaliana*. *Science* **241**, 1086–1089.

10 Chang C, Kwok SF, Bleecker AB & Meyerowitz EM (1993) Arabidopsis ethylene-response gene ETR1: similarity of product to two-component regulators. *Science* **262**, 539–544.

11 Hua J, Chang C, Sun Q & Meyerowitz EM (1995) Ethylene insensitivity conferred by Arabidopsis ERS gene. *Science* **269**, 1712–1714.

12 Hua J, Sakai H, Nourizadeh S, Chen QG, Bleecker AB, Ecker JR & Meyerowitz EM (1998) EIN4 and ERS2 are members of the putative ethylene receptor gene family in Arabidopsis. *Plant Cell* **10**, 1321–1332.

13 Hua J & Meyerowitz EM (1998) Ethylene responses are negatively regulated by a receptor gene family in *Arabidopsis thaliana*. *Cell* **94**, 261–271.

14 Guo H & Ecker JR (2004) The ethylene signaling pathway: new insights. *Curr Opin Plant Biol* **7**, 40–49.

15 Kieber JJ, Rothenberg M, Roman G, Feldmann KA & Ecker JR (1993) CTR1, a negative regulator of the ethylene response pathway in Arabidopsis, encodes a member of the raf family of protein kinases. *Cell* **72**, 427–441.

16 Alonso JM, Hirayama T, Roman G, Nourizadeh S & Ecker JR (1999) EIN2, a bifunctional transducer of ethylene and stress responses in Arabidopsis. *Science* **284**, 2148–2152.

17 Bisson MM, Bleckmann A, Allekotte S & Groth G (2009) EIN2, the central regulator of ethylene signalling, is localized at the ER membrane where it interacts with the ethylene receptor ETR1. *Biochem J* **424**, 1–6.

18 Bisson MM & Groth G (2010) New insight in ethylene signaling: autokinase activity of ETR1 modulates the interaction of receptors and EIN2. *Mol Plant* **3**, 882–889.

19 Huang Y, Li H, Hutchison CE, Laskey J & Kieber JJ (2003) Biochemical and functional analysis of CTR1, a protein kinase that negatively regulates ethylene signaling in Arabidopsis. *Plant J* **33**, 221–233.

20 Bisson MM & Groth G (2011) New paradigm in ethylene signaling: EIN2, the central regulator of the signaling pathway, interacts directly with the upstream receptors. *Plant Signaling & Behavior* **6**, 164–166.

21 Merchante C, Brumos J, Yun J, Hu Q, Spencer KR, Enríquez P, Binder BM, Heber S, Stepanova AN & Alonso JM (2015) Gene-specific translation regulation mediated by the hormone-signaling molecule EIN2. *Cell* **163**, 684–697.

22 Li W, Ma M, Feng Y, Li H, Wang Y, Ma Y, Li M, An F & Guo H (2015) EIN2-directed translational regulation of ethylene signaling in Arabidopsis. *Cell* **163**, 670–683.

23 Johnson PR & Ecker JR (1998) The ethylene gas signal transduction pathway: a molecular perspective. *Annu Rev Genet* **32**, 227–254.

24 Wang F, Cui X, Sun Y & Dong C-H (2013) Ethylene signaling and regulation in plant growth and stress responses. *Plant Cell Rep* **32**, 1099–1109.

25 Bisson MM & Groth G (2015) Targeting plant ethylene responses by controlling essential protein-protein interactions in the ethylene pathway. *Mol Plant* **8**, 1165–1174.

26 Milic D, Dick M, Mulnaes D, Pfleger C, Kinnen A, Gohlke H & Groth G (2018) Recognition motif and mechanism of ripening inhibitory peptides in plant hormone receptor ETR1. *Sci Rep* **8**, 3890.

27 Bisson MM, Kessenbrock M, Muller L, Hofmann A, Schmitz F, Cristescu SM & Groth G (2016) Peptides interfering with protein-protein interactions in the ethylene signaling pathway delay tomato fruit ripening. *Sci Rep* **6**, 30634.

28 Klein S, Fiebig A, Neuwald D, Dluhosch D, Muller L, Groth G, Noga G & Hunsche M (2019) Influence of the ethylene-related signal-inhibiting octapeptide NOP-1 on postharvest ripening and quality of 'Golden delicious' apples. *J Sci Food Agric* **99**, 3903–3909.

29 Kessenbrock M, Klein SM, Muller L, Hunsche M, Noga G & Groth G (2017) Novel protein-protein inhibitor based approach to control plant ethylene responses: synthetic peptides for ripening control. *Front Plant Sci* **8**, 1528.

30 Hoppen C, Muller L, Albrecht AC & Groth G (2019) The NOP-1 peptide derived from the central regulator of ethylene signaling EIN2 delays floral senescence in cut flowers. *Sci Rep* **9**, 1287.

31 Qiao H, Shen Z, Huang S-s C, Schmitz RJ, Urich MA, Briggs SP & Ecker JR (2012) Processing and subcellular trafficking of ER-tethered EIN2 control response to ethylene gas. *Science* **338**, 390–393.

32 Wen X, Zhang C, Ji Y, Zhao Q, He W, An F, Jiang L & Guo H (2012) Activation of ethylene signaling is mediated by nuclear translocation of the cleaved EIN2 carboxyl terminus. *Cell Res* **22**, 1613–1616.

33 Ju C, Yoon GM, Shemansky JM, Lin DY, Ying ZI, Chang J, Garrett WM, Kessenbrock M, Groth G, Tucker ML *et al.* (2012) CTR1 phosphorylates the central regulator EIN2 to control ethylene hormone signaling from the ER membrane to the nucleus in Arabidopsis. *Proc Natl Acad Sci U S A* **109**, 19486–19491.

34 Zhang F, Qi B, Wang L, Zhao B, Rode S, Riggan ND, Ecker JR & Qiao H (2016) EIN2-dependent regulation of acetylation of histone H3K14 and non-canonical histone H3K23 in ethylene signalling. *Nat Commun* **7**, 13018.

35 Chao Q, Rothenberg M, Solano R, Roman G, Terzaghi W & Ecker JR (1997) Activation of the ethylene gas response pathway in Arabidopsis by the nuclear protein ETHYLENE-INSENSITIVE3 and related proteins. *Cell* **89**, 1133–1144.

36 Solano R, Stepanova A, Chao Q & Ecker JR (1998) Nuclear events in ethylene signaling: a transcriptional cascade mediated by ETHYLENE-INSENSITIVE3 and ETHYLENE-RESPONSE-FACTOR1. *Genes Dev* **12**, 3703–3714.

37 Li Q, Fu H, Yu X, Wen X, Guo H, Guo Y & Li J (2024) The SALT OVERLY SENSITIVE 2–CONSTITUTIVE TRIPLE RESPONSE1 module coordinates plant growth and salt tolerance in Arabidopsis. *J Exp Bot* **75**, 391–404.

38 Zhang J, Chen Y, Lu J, Zhang Y & Wen C-K (2020) Uncertainty of EIN2Ser645/Ser924 inactivation by CTR1-mediated phosphorylation reveals the complexity of ethylene signaling. *Plant Communications* **1**, 100046.

39 Frey S, Richter RP & Görlich D (2006) FG-rich repeats of nuclear pore proteins form a three-dimensional meshwork with hydrogel-like properties. *Science* **314**, 815–817.

40 Lüdke D, Rohmann PF & Wiermer M (2021) Nucleocytoplasmic communication in healthy and diseased plant tissues. *Front Plant Sci* **12**, 719453.

41 Frey S & Görlich D (2009) FG/FxFG as well as GLFG repeats form a selective permeability barrier with self-healing properties. *EMBO J* **28**, 2554–2567.

42 Stewart M (2007) Molecular mechanism of the nuclear protein import cycle. *Nat Rev Mol Cell Biol* **8**, 195–208.

43 Tran EJ, Bolger TA & Wente SR (2007) SnapShot: nuclear transport. *Cell* **131**, 420.

44 Tang Y, Yang X, Huang A, Seong K, Ye M, Li M, Zhao Q, Krasileva K & Gu Y (2024) Proxiome assembly of the plant nuclear pore reveals an essential hub for gene expression regulation. *Nat Plants* **10**, 1–13.

45 Chang C-W, Couñago RM, Williams SJ, Boden M & Kobe B (2013) The distribution of different classes of nuclear localization signals (NLSs) in diverse organisms and the utilization of the minor NLS-binding site inplantnuclear import factor importin-α. *Plant Signal Behav* **8**, 5074–5088.

46 Corbett AH & Silver PA (1997) Nucleocytoplasmic transport of macromolecules. *Microbiol Mol Biol Rev* **61**, 193–211.

47 Nigg EA (1997) Nucleocytoplasmic transport: signals, mechanisms and regulation. *Nature* **386**, 779–787.

48 Fried H & Kutay U (2003) Nucleocytoplasmic transport: taking an inventory. *Cell Molec Life Sci* **60**, 1659–1688.

49 Yang Y, Guo L, Chen L, Gong B, Jia D & Sun Q (2023) Nuclear transport proteins: structure, function, and disease relevance. *Signal Transduct Target Ther* **8**, 425.

50 Görlich D, Vogel F, Mills AD, Hartmann E & Laskey RA (1995) Distinct functions for the two importin subunits in nuclear protein import. *Nature* **377**, 246–248.

51 Radu A, Blobel G & Moore MS (1995) Identification of a protein complex that is required for nuclear protein import and mediates docking of import substrate to distinct nucleoporins. *Proc Natl Acad Sci* **92**, 1769–1773.

52 Izaurralde E, Kutay U, Von Kobbe C, Mattaj IW & Görlich D (1997) The asymmetric distribution of the constituents of the ran system is essential for transport into and out of the nucleus. *EMBO J* **16**, 6535–6547.

53 Nielsen E (2020) The small GTPase superfamily in plants: a conserved regulatory module with novel functions. *Annu Rev Plant Biol* **71**, 247–272.

54 Terry LJ, Shows EB & Wente SR (2007) Crossing the nuclear envelope: hierarchical regulation of nucleocytoplasmic transport. *Science* **318**, 1412–1416.

55 Görlich D, Panté N, Kutay U, Aebi U & Bischoff FR (1996) Identification of different roles for RanGDP and RanGTP in nuclear protein import. *EMBO J* **15**, 5584–5594.

56 Moroianu J, Blobel G & Radu A (1996) Nuclear protein import: ran-GTP dissociates the karyopherin alphabeta heterodimer by displacing alpha from an overlapping binding site on beta. *Proc Natl Acad Sci* **93**, 7059–7062.

57 Christie M, Chang C-W, Róna G, Smith KM, Stewart AG, Takeda AA, Fontes MR, Stewart M, Vértessy BG & Forwood JK (2016) Structural biology and regulation of protein import into the nucleus. *J Mol Biol* **428**, 2060–2090.

58 Görlich D & Kutay U (1999) Transport between the cell nucleus and the cytoplasm. *Annu Rev Cell Dev Biol* **15**, 607–660.

59 Matsuura Y, Lange A, Harreman MT, Corbett AH & Stewart M (2003) Structural basis for Nup2p function in cargo release and karyopherin recycling in nuclear import. *EMBO J* **22**, 5358–5369.

60 Lu K, Zhang L, Qin L, Chen X, Wang X, Zhang M & Dong H (2023) Importin β1 mediates nuclear entry of EIN2C to confer the phloem-based defense against aphids. *Int J Mol Sci* **24**, 8545.

61 Goldfarb DS, Corbett AH, Mason DA, Harreman MT & Adam SA (2004) Importin α: a multipurpose nuclear-transport receptor. *Trends Cell Biol* **14**, 505–514.

62 Marfori M, Mynott A, Ellis JJ, Mehdi AM, Saunders NF, Curmi PM, Forwood JK, Bodén M & Kobe B (2011) Molecular basis for specificity of nuclear import and prediction of nuclear localization. *Biochim Biophys Acta* **1813**, 1562–1577.

63 Conti E, Uy M, Leighton L, Blobel G & Kuriyan J (1998) Crystallographic analysis of the recognition of a nuclear localization signal by the nuclear import factor karyopherin alpha. *Cell* **94**, 193–204.

64 Dias SM, Wilson KF, Rojas KS, Ambrosio AL & Cerione RA (2009) The molecular basis for the regulation of the cap-binding complex by the importins. *Nat Struct Mol Biol* **16**, 930–937.

65 Chang C-W, Couñago RLM, Williams SJ, Bodén M & Kobe B (2012) Crystal structure of rice importin-α and structural basis of its interaction with plant-specific nuclear localization signals. *Plant Cell* **24**, 5074–5088.

66 Cingolani G, Petosa C, Weis K & Müller CW (1999) Structure of importin-β bound to the IBB domain of importin-α. *Nature* **399**, 221–229.

67 Roman N, Christie M, Swarbrick CM, Kobe B & Forwood JK (2013) Structural characterisation of the nuclear import receptor importin alpha in complex with the bipartite NLS of Prp20. *PLoS One* **8**, e82038.

68 Kobe B (1999) Autoinhibition by an internal nuclear localization signal revealed by the crystal structure of mammalian importin α. *Nat Struct Biol* **6**, 388–397.

69 Vetter IR, Arndt A, Kutay U, Görlich D & Wittinghofer A (1999) Structural view of the ran–importin β interaction at 2.3 Å resolution. *Cell* **97**, 635–646.

70 Tamura K & Hara-Nishimura I (2014) Functional insights of nucleocytoplasmic transport in plants. *Front Plant Sci* **5**, 118.

71 Wang W, Ye R, Xin Y, Fang X, Li C, Shi H, Zhou X & Qi Y (2011) An importin β protein negatively regulates microRNA activity in Arabidopsis. *Plant Cell* **23**, 3565–3576.

72 Guzman P & Ecker JR (1990) Exploiting the triple response of Arabidopsis to identify ethylene-related mutants. *Plant Cell* **2**, 513–523.

73 Van Der Straeten D, Djudzman A, Van Caeneghem W, Smalle J & Van Montagu M (1993) Genetic and physiological analysis of a new locus in Arabidopsis that confers resistance to 1-aminocyclopropane-1-carboxylic acid and ethylene and specifically affects the ethylene signal transduction pathway. *Plant Physiol* **102**, 401–408.

74 Lüdke D, Roth C, Kamrad SA, Messerschmidt J, Hartken D, Appel J, Hörnich BF, Yan Q, Kusch S & Klenke M (2021) Functional requirement of the Arabidopsis importin-α nuclear transport receptor family in autoimmunity mediated by the NLR protein SNC1. *Plant J* **105**, 994–1009.

75 Moerke NJ (2009) Fluorescence polarization (FP) assays for monitoring peptide-protein or nucleic acid-protein binding. *Curr Protocols Chem Biol* **1**, 1–15.

76 Wirthmueller L, Roth C, Fabro G, Caillaud MC, Rallapalli G, Asai S, Sklenar J, Jones AM, Wiermer M & Jones JD (2015) Probing formation of cargo/importin-α transport complexes in plant cells using a pathogen effector. *Plant J* **81**, 40–52.

77 Jug A, Bratkovič T & Ilaš J (2024) Biolayer interferometry and its applications in drug discovery and development. *TrAC Trends Anal Chem* **176**, 117741.

78 Jumper J, Evans R, Pritzel A, Green T, Figurnov M, Ronneberger O, Tunyasuvunakool K, Bates R, Žídek A & Potapenko A (2021) Highly accurate protein structure prediction with AlphaFold. *Nature* **596**, 583–589.

79 Notredame C, Higgins DG & Heringa J (2000) T-Coffee: a novel method for fast and accurate multiple sequence alignment. *J Mol Biol* **302**, 205–217.

80 Fanara P, Hodel MR, Corbett AH & Hodel AE (2000) Quantitative analysis of nuclear localization signal (NLS)-importin α interaction through fluorescence depolarization: evidence for auto-inhibitory regulation of NLS binding. *J Biol Chem* **275**, 21218–21223.

81 Harreman MT, Cohen PE, Hodel MR, Truscott GJ, Corbett AH & Hodel AE (2003) Characterization of the auto-inhibitory sequence within the N-terminal domain of importin α. *J Biol Chem* **278**, 21361–21369.

82 Kosugi S, Hasebe M, Matsumura N, Takashima H, Miyamoto-Sato E, Tomita M & Yanagawa H (2009) Six classes of nuclear localization signals specific to different binding grooves of importin α. *J Biol Chem* **284**, 478–485.

83 Pang X & Zhou H-X (2014) Design rules for selective binding of nuclear localization signals to minor site of importin α. *PLoS One* **9**, e91025.

84 Park MY, Wu G, Gonzalez-Sulser A, Vaucheret H & Poethig RS (2005) Nuclear processing and export of microRNAs in Arabidopsis. *Proc Natl Acad Sci* **102**, 3691–3696.

85 Dey V & Patankar S (2018) Molecular basis for the lack of auto-inhibition of plasmodium falciparum importin α. *Biochem Biophys Res Commun* **503**, 1792–1797.

86 Klepikova AV, Logacheva MD, Dmitriev SE & Penin AA (2015) RNA-seq analysis of an apical meristem time series reveals a critical point in *Arabidopsis thaliana* flower initiation. *BMC Genomics* **16**, 1–16.

87 Mergner J, Frejno M, List M, Papacek M, Chen X, Chaudhary A, Samaras P, Richter S, Shikata H & Messerer M (2020) Mass-spectrometry-based draft of the Arabidopsis proteome. *Nature* **579**, 409–414.

88 Papatheodorou I, Moreno P, Manning J, Fuentes AM-P, George N, Fexova S, Fonseca NA, Füllgrabe A, Green M & Huang N (2020) Expression atlas update: from tissues to single cells. *Nucleic Acids Res* **48**, D77–D83.

89 Lu J, Wu T, Zhang B, Liu S, Song W, Qiao J & Ruan H (2021) Types of nuclear localization signals and mechanisms of protein import into the nucleus. *Cell Commun Signal* **19**, 60.

90 Bollman KM, Aukerman MJ, Park M-Y, Hunter C, Berardini TZ & Poethig RS (2003) HASTY, the Arabidopsis ortholog of exportin 5/MSN5, regulates phase change and morphogenesis. *Development* **130**, 1493.

91 Li J & Chen X (2003) PAUSED, a putative exportin-t, acts pleiotropically in Arabidopsis development but is dispensable for viability. *Plant Physiol* **132**, 1913–1924.

92 Luo Y, Wang Z, Ji H, Fang H, Wang S, Tian L & Li X (2013) An a rabidopsis homolog of importin β1 is required for ABA response and drought tolerance. *Plant J* **75**, 377–389.

93 Hodel AE, Harreman MT, Pulliam KF, Harben ME, Holmes JS, Hodel MR, Berland KM & Corbett AH (2006) Nuclear localization signal receptor affinity correlates with in vivo localization in *Saccharomyces cerevisiae*. *J Biol Chem* **281**, 23545–23556.

94 Hübner S, Smith HM, Hu W, Chan CK, Rihs H-P, Paschal BM, Raikhel NV & Jans DA (1999) Plant importin α binds nuclear localization sequences with high affinity and can mediate nuclear import independent of importin β. *J Biol Chem* **274**, 22610–22617.

95 Kosugi S, Hasebe M, Entani T, Takayama S, Tomita M & Yanagawa H (2008) Design of peptide inhibitors for the importin α/β nuclear import pathway by activity-based profiling. *Chem Biol* **15**, 940–949.

96 Timney BL, Tetenbaum-Novatt J, Agate DS, Williams R, Zhang W, Chait BT & Rout MP (2006) Simple kinetic relationships and nonspecific competition govern nuclear import rates in vivo. *J Cell Biol* **175**, 579–593.

97 Marfori M, Lonhienne TG, Forwood JK & Kobe B (2012) Structural basis of high-affinity nuclear localization signal interactions with importin-α. *Traffic* **13**, 532–548.

98 de Oliveira HC, da Silva TD, Salvador GH, Moraes IR, Fukuda CA, de Barros AC & Fontes MR (2021) Structural and calorimetric studies reveal specific determinants for the binding of a high-affinity NLS to mammalian importin-alpha. *Biochem J* **478**, 2715–2732.

99 Waese J, Fan J, Pasha A, Yu H, Fucile G, Shi R, Cumming M, Kelley LA, Sternberg MJ & Krishnakumar V (2017) ePlant: visualizing and exploring multiple levels of data for hypothesis generation in plant biology, the plant cell. *Plant Cell* **29**, 1806–1821.

100 Rhee SY, Beavis W, Berardini TZ, Chen G, Dixon D, Doyle A, Garcia-Hernandez M, Huala E, Lander G & Montoya M (2003) The Arabidopsis information resource (TAIR): a model organism database providing a centralized, curated gateway to Arabidopsis biology, research materials and community. *Nucleic Acids Res* **31**, 224–228.

101 Ström A-C & Weis K (2001) Importin-beta-like nuclear transport receptors. *Genome Biol* **2**, 1–9.

102 Duncan RR (2006) Fluorescence lifetime imaging microscopy (FLIM) to quantify protein–protein interactions inside cells. *Biochem Soc Trans* **34**, 679–682.

103 Gonçalves Dias M, Dharmasena T, Gonzalez-Ferrer C, Maika JE, Miguel VN, Dou R, Rodriguez Gallo MC, Bredow M, Siegel KR & Uhrig RG (2025) Catalytically inactive subgroup VIII receptor-like cytoplasmic kinases regulate the immune-triggered oxidative burst in *Arabidopsis thaliana*. *J Exp Bot* **76**, 1553–1568.

104 Maika JE, Krämer B, Strotmann VI, Wellmer F, Weidtkamp-Peters S, Stahl Y & Simon R (2023) One pattern analysis (OPA) for the quantitative determination of protein interactions in plant cells. *Plant Methods* **19**, 73.

105 Roy A, Kucukural A & Zhang Y (2010) I-TASSER: a unified platform for automated protein structure and function prediction. *Nat Protoc* **5**, 725–738.

106 Abramson J, Adler J, Dunger J, Evans R, Green T, Pritzel A, Ronneberger O, Willmore L, Ballard AJ & Bambrick J (2024) Accurate structure prediction of biomolecular interactions with AlphaFold 3. *Nature* **630**, 493–500.

107 Moreno P, Fexova S, George N, Manning JR, Miao Z, Mohammed S, Muñoz-Pomer A, Fullgrabe A, Bi Y & Bush N (2022) Expression atlas update: gene and protein expression in multiple species. *Nucleic Acids Res* **50**, D129–D140.

Supporting information

Additional supporting information may be found online in the Supporting Information section at the end of the article.

Fig. S1. Sequence alignment of *A. thaliana* IMPα1-9.

21808658, 2026, 1, Downloaded from https://onlinelibrary.wiley.com/doi/10.1111/febs.70203 by Universitat Autonoma de Barcelona, Wiley Online Library on [19/03/2026]. See the Terms and Conditions (https://onlinelibrary.wiley.com/terms-and-conditions) on Wiley Online Library for rules of use; OA articles are governed by the applicable Creative Commons License

Fig. S2. Alignment of amino acid sequences of the nine IMPα isoforms at the minor binding site.
Fig. S3. Alphafold model of the IMPα1-IMPβ1-NOP-1 complex.
Fig. S4. IMPα protein family expression levels in *A. thaliana* after ACC treatment.
Fig. S5. HPLC chromatogram of NOP-1.
Fig. S6. Mass spectrometry of NOP-1.
Fig. S7. HPLC chromatogram of N41P-1.
Fig. S8. Mass spectrometry of N41P-1.
Fig. S9. Reversed phase (RP) HPLC chromatogram of TAMRA-NOP-1.
Fig. S10. Mass spectrometry analysis of TAMRA-NOP-1.
Table S1. EIN2-NLS peptide/protein sequences investigated in this study.
Table S2. List of primers used for PCR amplification and cloning of IMPα genes.

17424658, 2026, 1, Downloaded from https://onlinelibrary.wiley.com/doi/10.1111/febs.70293 by Universiteit Gent Universiteitsbibliotheek, Wiley Online Library on [29/03/2026]. See the Terms and Conditions (https://onlinelibrary.wiley.com/terms-and-conditions) on Wiley Online Library for rules of use; OA articles are governed by the applicable Creative Commons License

Supporting Information

Linking ER to Nucleus in Ethylene Signaling: Role of the IMPα superfamily in nucleocytoplasmic transport of central regulator EIN2

Fabian Wynen, Jan Eric Maika, Raphael Josef Eberle, Nina Jahnke, Marcel Wiermer, Laura Hartmann, Rüdiger Simon and Georg Groth

Table of contents

Fig. S1. Sequence alignment of *A. thaliana* IMPα1-9.
Fig. S2. Alignment of amino acid sequences of the nine IMPα isoforms at the minor binding site using T-COFFEE.
Fig. S3. Alphafold model of the IMPα1-IMPβ1-NOP-1 complex.
Fig. S4. HPLC chromatogram of NOP-1.
Fig. S5. Mass spectrometry of NOP-1.
Fig. S6. HPLC chromatogram of N41P-1.
Fig. S7. Mass spectrometry of N41P-1.
Fig. S8. Reversed phase (RP) HPLC chromatogram of TAMRA-NOP-1.
Fig. S9. Mass spectrometry analysis of TAMRA-NOP-1.
Table S1. EIN2-NLS peptide/protein sequences investigated in this study.
Table S2. List of primers used for PCR amplification and cloning of IMPα genes.

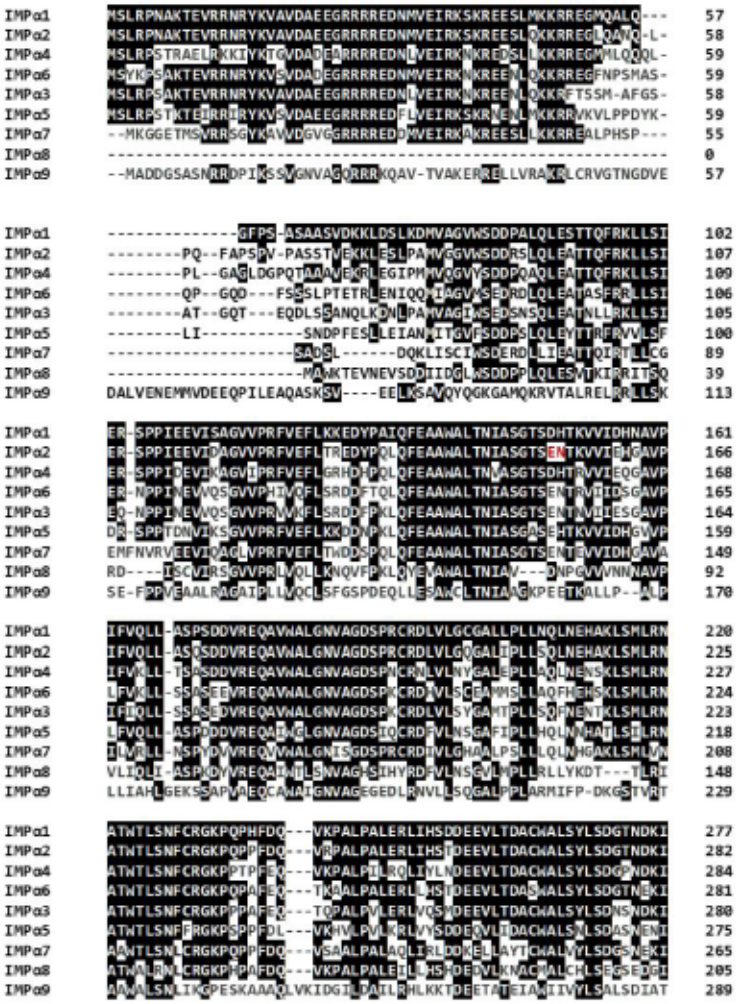

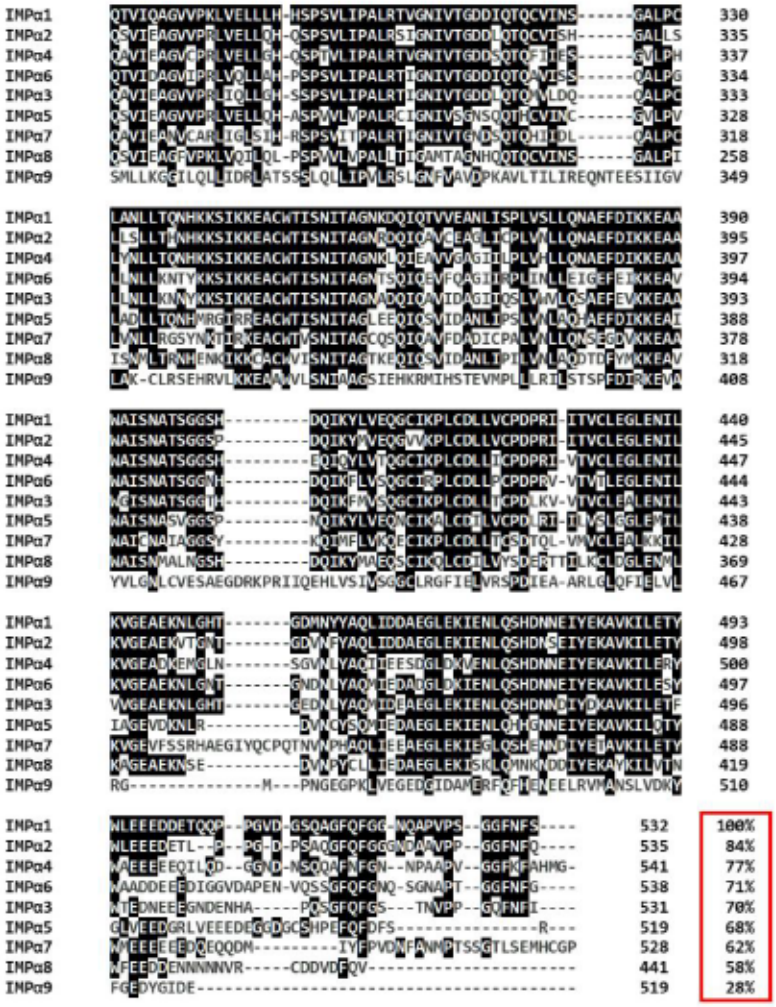

Fig. S1. Sequence alignment of *A. thaliana* IMPα1-9. Sequence identity to IMPα1 is shown in %. IMPα2-8 possess a sequence identity to IMPα1 >50%, in contrast the sequence identity of IMPα9 is <30%. IMPα1 (UniProt: Q96321), IMPα2 (UniProt: F4JL11), IMPα3 (UniProt: O04294), IMPα4 (UniProt: O80480), IMPα5 (UniProt: Q9FJ09), IMPα6 (UniProt: Q9FWY7), IMPα7 (UniProt: Q9M9X7), IMPα8 (UniProt: Q9FJ92), IMPα9 (UniProt: F4KF65). Alignments were made using the MUSCLE tool from EMBL-EBI.

```
                    * *             *   *           *  *  *
IMPα1 (AA 311-398) IVTGDDIQTQCVIN - EACWTISNITA - EFDIKKEAAWAISNATS
IMPα2 (AA 316-403) IVTGDDLQTQCVIS - EACWTISNITA - EFDIKKEAAWAISNATS
IMPα3 (AA 314-401) IVTGDDLQTQMVLD - EACWTISNITA - EFEVKKEAAWGISNATS
IMPα4 (AA 318-405) IVTGDDSQTQFIIE - EACWTISNITA - EFDIKKEAAWAISNATS
IMPα5 (AA 309-396) IVSGNSQQTHCVIN - EACWTISNITA - EFDIKKEAIWAISNASV
IMPα6 (AA 315-402) IVTGDDIQTQAVIS - EACWTISNITA - EFEIKKEAVWAISNATS
IMPα7 (AA 299-386) IVTGNDSQTQHIID - EACWTVSNITA - EGDVKKEAAWAICNAIA
IMPα8 (AA 239-326) MTAGNHQQTQCVIN - CACWVISNITA - DFYMKKEAVWAISNMAL
IMPα9 (AA 324-416) FVAVDPKAVLTILI - EAAWVLSNIAA - PFDIRKEVAYVLGNLCV
```

Fig. S2. Alignment of amino acid sequences of the nine IMPα isoforms at the minor binding site using T-COFFEE. Potential residues involved in NOP-1 binding are marked with asterisks (Related to Fig. 3). Pink yellow IMPα1 (UniProt: Q96321), IMPα2 (UniProt: F4JL11), IMPα3 (UniProt: O04294), IMPα4 (UniProt: O80480), IMPα5 (UniProt: Q9FJ09), IMPα6 (UniProt: Q9FWY7), IMPα7 (UniProt: Q9M9X7), IMPα8 (UniProt: Q9FJ92), IMPα9 (UniProt: F4KF65). Alignments were made using the MUSCLE tool from EMBL-EBI.

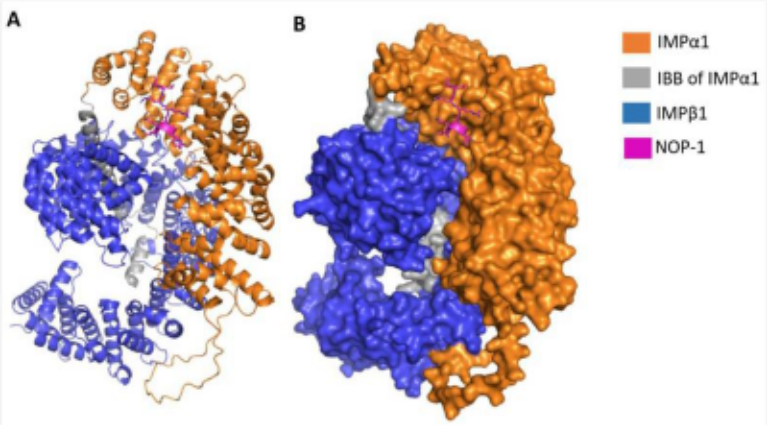

Fig. S3. Alphafold model of the IMPα1-IMPβ1-NOP-1 complex. The structural model was generated using the Alphafold 3 web server. The complex is shown in ribbon view (A) and surface view (B).

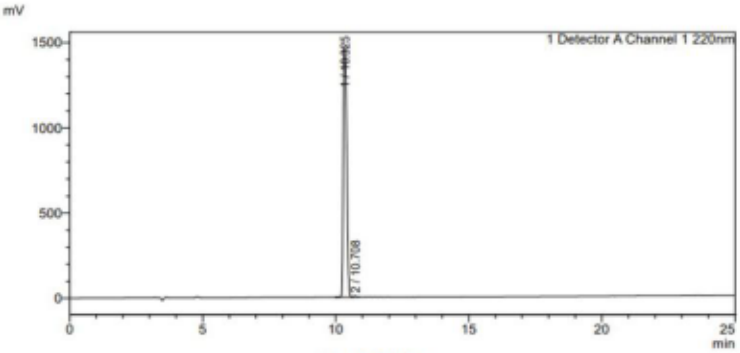

<Peak Table>

Detector A Channel 1 220nm

Peak#	Ret. Time	Area	Height	Area%
1	10.325	13660621	1470725	99.595
2	10.708	55578	7105	0.405
Total		13716199	1477829	100.000

Fig. S4. HPLC chromatogram of NOP-1. Information obtained from the purity and quality certificate from GenScript (New Jersey, USA).

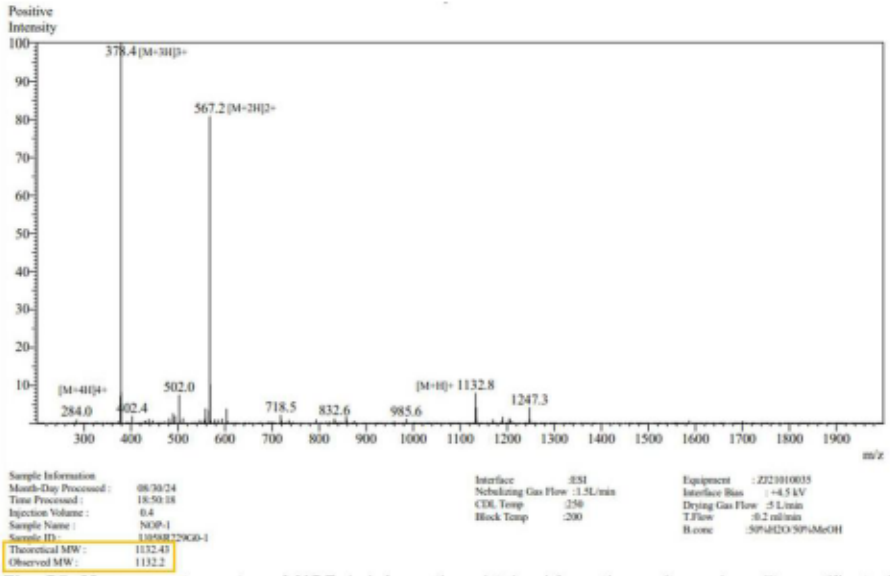

Fig. S5. Mass spectrometry of NOP-1. Information obtained from the purity and quality certificate from GenScript (New Jersey, USA).

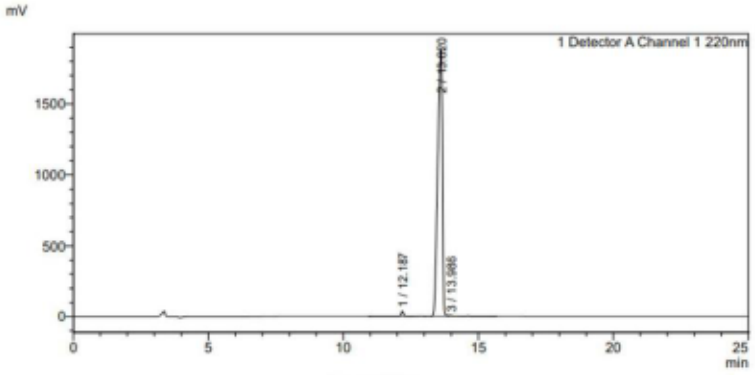

<Peak Table>

Detector A Channel 1 220nm

Peak#	Ret. Time	Area	Height	Area%
1	12.187	313557	37124	1.353
2	13.620	22694476	1884833	97.921
3	13.986	168213	7556	0.726
Total		23176246	1929512	100.000

Fig. S6. HPLC chromatogram of N41P-1. Information obtained from the purity and quality certificate from GenScript (New Jersey, USA).

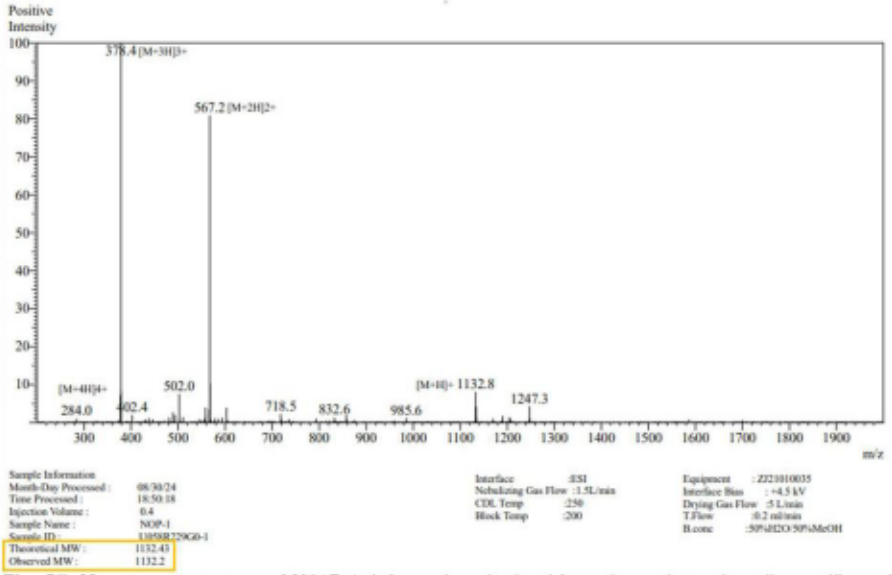

Fig. S7. Mass spectrometry of N41P-1. Information obtained from the purity and quality certificate from GenScript (New Jersey, USA).

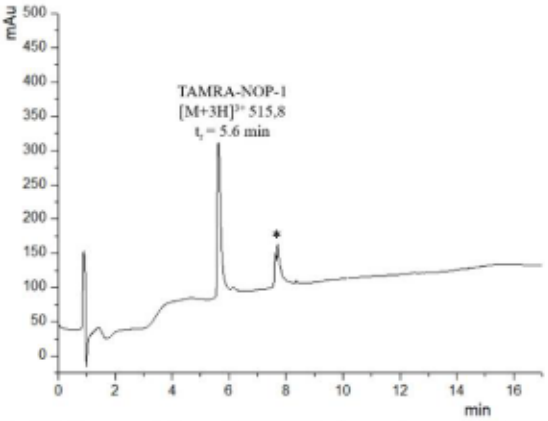

Fig. S8. Reversed phase (RP) HPLC chromatogram of TAMRA-NOP-1. *Byproduct in which the arginine Pbf protecting group was not fully removed during deprotection (TAMRA-NOP-1 +Pbf).

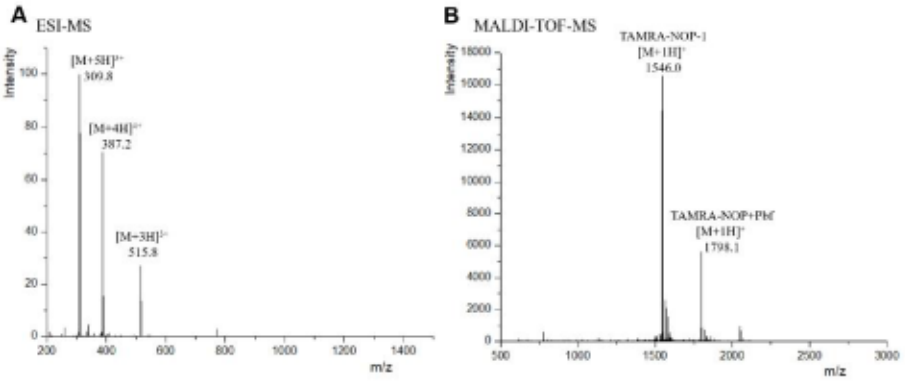

Fig. S9. Mass spectrometry analysis of TAMRA-NOP-1. (A) ESI-MS and (B) MALDI-TOF-MS.

Table S1. EIN2-NLS peptide/protein sequences investigated in this study. The NLS is highlighted in red, while basic amino acids within the NLS are marked in bold. The GB1-domain is highlighted in blue.

Name	Sequence
NOP-1	LKRYKRRL
TAMRA-NOP-1	TAMRA-LKRYKRRL
N41P-1	KDVEMAISSRKGRTGTAAGDVAFPKGKENLASVLKRYKRRL
GB1-*At*EIN2C_1215-1281	MQYKLILNGKTLKGETTTEAVDAATAEKVFKQYANDNGVDGEWTYDDA TKTYTVTESGSENLYFQGHKGKCTTAVTLLDLIKDVEMAISCRKGRTGT AAGDVAFPKGKENLASVLKRYKRRLSNKPVGMNQDGP

Table S2. List of primers used for PCR amplification and cloning of *IMPα* genes. Genes were either cloned into pETEV21a (*IMPα1-4/6-9*) or pETEV16b (*IMPα5*).

Primername	Primersequence (5'->3')
IMPα1_for	ctttaagaaggagatatacaATGTCACTGAGACCCAAC
IMPα1_rev	caggttttcggatcccatatgGCTGAAGTTGAATCCTCC
ΔIBB_IMPα1_for	ctttaagaaggagatatacaATGCTGAAGGATATGGTCGC
ΔIBB_IMPα1_rev	caggttttcggatcccatatgGCTGAAGTTGAATCCTCC
IMPα2_for	ctttaagaaggagatatacaATGTCTTTGAGACCTAAC
IMPα2_rev	caggttttcggatcccatatgCTGGAAGTTGAATCCACC
IMPα3_for	ctttaagaaggagatatacaATGTCTCTCAGACCTAGC
IMPα3_rev	caggttttcggatcccatatgAATAAAGTTGAATTGACC
IMPα4_for	ctttaagaaggagatatacaATGTCGCTGAGGCCGAGC
IMPα4_rev	caggttttcggatcccatatgGGCAAATTTGAATCCACC
IMPα5_for	ctttaagaaggagatatacaATGTCCTTGCGACCGAGC
IMPα5_rev	caggttttcggatcccatatgACGAGAAAAATCAAACTGGAATTCCG
IMPα6_for	ctttaagaaggagatatacaATGTCTTACAAACCAAGCG
IMPα6_rev	caggttttcggatcccatatgACCAAAGTTGAATCCAC
ΔIBB_IMPα7_for	ctttaagaaggagatatacaATGAGGGATCTGTTGATTG
ΔIBB_IMPα7_rev	caggttttcggatcccatatgAGGTCCGCAGTGCATCTC
IMPα8_for	ctttaagaaggagatatacaATGGCTTGGAAAACAGAG
IMPα8_rev	caggttttcggatcccatatgCACCTGAAAGTCCACATC
IMPα9_for	ctttaagaaggagatatacaATGGCGGATGATGGCTC
IMPα9_rev	caggttttcggatcccatatgTTCATCGATTCCATAATC

3.2 Molecular events upon EIN2 nuclear entry

Title	Structural mapping of the EIN2-EIN3 interaction core and its integration with ENAP1 in ethylene signaling
Authors	**Fabian Wynen**, Meik Henrik Thiele, Maya Hettesheimer, Raphael Josef Eberle, Jan Eric Maika, Rüdiger Simon, Georg Groth
Published in	To be submitted
Impact Factor	-
DOI	10.64898/2026.07.10.737652 (Manuscript deposited on bioRxiv)
Own contribution	**Methodology** Development and optimization of MST and Y2H data **Investigation** Performance of MST and Y2H binding experiments as well as cloning of all used protein constructs **Formal analysis** Analysis and interpretation of MST and Y2H data **Validation** Verification of experimental results and reproducibility **Visualization** Preparation of figures and graphical representations **Writing - Original draft** Preparation of the manuscript

bioRxiv preprint doi: https://doi.org/10.64898/2026.07.10.737652; this version posted July 10, 2026. The copyright holder for this preprint (which was not certified by peer review) is the author/funder. All rights reserved. No reuse allowed without permission.

Structural Mapping of the EIN2–EIN3 Interaction Core and Its Integration with ENAP1 in Ethylene Signaling

Fabian Wynen[1], Meik Thiele[2,3], Maya Hettesheimer[1], Raphael Josef Eberle[1], Jan Eric Maika[2], Rüdiger Simon[2,3] and Georg Groth[1]*

[1]Institute of Biochemical Plant Physiology, Heinrich-Heine-Universität Düsseldorf, 40225 Düsseldorf, Germany.

[2]Institute of Development Genetics, Heinrich-Heine-Universität Düsseldorf, 40225 Düsseldorf, Germany.

[3]Institute of Developmental Genetics, CEPLAS Cluster of Excellence on Plant Sciences, Heinrich-Heine-Universität Düsseldorf, Düsseldorf, Germany

*Corresponding author:
Georg Groth, Biochemical Plant Physiology, Heinrich-Heine-Universität Düsseldorf, Universitätsstraße 1, 40225 Düsseldorf, Tel. 0049 211 81-12822,
E-mail: georg.groth@hhu.de

Running Title: The EIN2-EIN3 interaction core as a central module in ethylene signaling

bioRxiv preprint doi: https://doi.org/10.64898/2026.07.10.737652; this version posted July 10, 2026. The copyright holder for this preprint (which was not certified by peer review) is the author/funder. All rights reserved. No reuse allowed without permission.

ABBREVIATIONS

AD, Activation domain;

At, *Arabidopsis thaliana*;

BD, Binding domain;

CTR1, CONSTITUTIVE TRIPLE RESPONSE1;

DBD, DNA-binding domain;

EBF1/2, EIN3 BINDING F-BOX PROTEINS ½

EBS, EIN3 binding site;

ER, endoplasmic reticulum;

EIN2-5, ETHYLENE INSENSITIVE2-5;

EIN2-C, C-terminal domain of EIN2;

EIL1-5, EIN3-like 1-5;

ENAP1/2; EIN2 NUCLEAR ASSOCIATED PROTEIN 1/2

ETR, ethylene receptor;

FLIM-FRET, fluorescence lifetime microscopy and Förster's resonance energy transfer;

GAL4, galactose-responsive transcription factor

NLS, Nuclear localization sequence

NRMAP, natural resistance-associated macrophage protein

SD-agar, synthetic defined agar

UPFs, up-frameshift proteins or nonsense-mediated decay proteins

Y2H, Yeast Two Hybrid

Key words: ethylene signaling, EIN2, nuclear events, NLS-motif, EIN3

bioRxiv preprint doi: https://doi.org/10.64898/2026.07.10.737652; this version posted July 10, 2026. The copyright holder for this preprint (which was not certified by peer review) is the author/funder. All rights reserved. No reuse allowed without permission.

ABSTRACT

Ethylene regulates diverse developmental processes, yet the molecular function of its central regulator, ETHYLENE INSENSITIVE 2 (EIN2), has remained unclear. Although EIN2 nuclear import is mediated by the Importin-α/β pathway, the molecular events initiated by EIN2 after nuclear entry were unknown. Here we show that EIN2 directly engages the transcription factor EIN3, establishing a mechanistic link between EIN2 nuclear accumulation and transcriptional activity. Microscale thermophoresis, yeast two-hybrid analysis and *in planta* FLIM-FRET consistently support this interaction. Domain mapping identifies EIN3 residues 86-173 as the core EIN2-binding region, and structural modeling refines the interface to a conserved segment within residues 86-120 that contacts a conserved region near the N-terminus of the EIN2-CEND fragment. *In planta*, EIN2 residues 1042-1214 are sufficient for EIN3 binding, revealing multiple interaction-competent surfaces with distinct affinities. The chromatin-associated protein ENAP1 also binds EIN2 and competes with EIN3, indicating a dynamic, concentration-dependent regulatory mechanism rather than a stable ternary complex. These findings define the molecular basis of the EIN2-EIN3 interaction and provide a mechanistic framework for EIN2-dependent transcriptional control in ethylene signaling.

bioRxiv preprint doi: https://doi.org/10.64898/2026.07.10.737652; this version posted July 10, 2026. The copyright holder for this preprint (which was not certified by peer review) is the author/funder. All rights reserved. No reuse allowed without permission.

INTRODUCTION

Ethylene is a gaseous plant hormone that regulates a broad spectrum of developmental, and stress-related processes, including inhibition of cell elongation, seed germination, apical hook formation, senescence, fruit ripening, abscission, and responses to biotic and abiotic stresses[1,2]. Ethylene perception and signaling occur through a largely linear pathway that transmits information from the endoplasmic reticulum (ER) membrane to the nucleus. In *Arabidopsis* five ER-localized ethylene receptors (ETR1, ETR2, ERS1, ERS2 and EIN4) act as negative regulators of the pathway[3,4]. In the absence of ethylene, these receptors activate the Raf-like kinase CONSTITUTIVE TRIPLE RESPONSE1 (CTR1), which suppresses downstream signaling. Ethylene binding inactivates receptor-CTR1 signaling, thereby relieving repression of the central regulator ETHYLENE INSENSITIVE2 (EIN2)[5,6]. EIN2 is the pivotal conduit between ER-localized ethylene perception and nuclear transcriptional responses. It is an ER-anchored protein comprising an N-terminal NRAMP-like (Natural Resistance-Associated Macrophage Proteins) domain and a large C-terminal cytosolic region. Upon ethylene perception, CTR1 inactivation prevents EIN2 phosphorylation, enabling proteolytic cleavage and nuclear translocation of the EIN2 C-terminal fragment (EIN2-C)[7-9]. EIN2-C regulates ethylene responses through both indirect and direct mechanisms. Indirectly, EIN2-C stabilizes the transcription factors ETHYLENE INSENSITIVE3 (EIN3) and EIN3-LIKE1 (EIL1) by inhibiting their ubiquitin-mediated degradation via the F-box proteins EBF1 and EBF2[10,11]. This mechanism includes the formation of processing bodies (P-bodies), where EIN2-C interacts with EIN5, nonsense-mediated decay proteins (UPFs) and the EBF1/2 mRNAs to suppress of EBF1/2 translation[12,13].

In addition to these cytosolic functions, nuclear-localized EIN2-C interacts with EIN2 NUCLEAR-ASSOCIATED PROTEIN1 (ENAP1), a histone-binding protein implicated in chromatin remodeling. This interaction has been proposed to promote association with ethylene-responsive loci and to modulate H3K14 and H3K23 acetylation, thereby facilitating EIN3-dependent transcriptional regulation[14,15]. Among the six members of the EIN3 family (EIN3 and EIL1-5) in *A. thaliana*, EIN3 and EIL1 constitute the key regulatory hub of ethylene signaling as *ein-3 eil-1* double mutants abolish ethylene responses[16]. EIN3/EIL proteins share a conserved N-terminal DNA-binding domain (DBD) that recognizes EIN3-binding sites (EBS) in target promoters[17]. EIN3 functions as a homodimer, a state detectable even in the absence of DNA [17,18]. The N-terminal region contains several critical structural components, including an acidic domain (AD), a proline-rich region (PR), and five clustered basic domains (BD I-V)[19,20], whereas the C-terminal region is more divergent among species and may contribute to functional diversification.

Although previous studies proposed a model in which ethylene responses may involve a ternary EIN2-EIN3-ENAP1 complex[15], the molecular basis of these interactions and the

bioRxiv preprint doi: https://doi.org/10.64898/2026.07.10.737652; this version posted July 10, 2026. The copyright holder for this preprint (which was not certified by peer review) is the author/funder. All rights reserved. No reuse allowed without permission.

existence of such complex remain unresolved. Moreover, the EIN2 nuclear localization signal (NLS) has been reported to interact with ETR1 and Importin-α/β family members[9,21,22], raising the question of whether the NLS contributes additional regulatory functions beyond nuclear import.

Here, we demonstrate direct EIN2-EIN3 binding across multiple experimental contexts and define the interface that mediates this interaction. We further refine the structural organization of EIN3 by delineating its homodimerization domain, nuclear localization requirements and functional regions. Competitive binding assays with ENAP1 reveal that EIN2 engages multiple nuclear partners, pointing to a more complex interaction landscape than previously recognized and providing new mechanistic insight into the nuclear events following EIN2 activation.

bioRxiv preprint doi: https://doi.org/10.64898/2026.07.10.737652; this version posted July 10, 2026. The copyright holder for this preprint (which was not certified by peer review) is the author/funder. All rights reserved. No reuse allowed without permission.

RESULTS

Protein-protein interaction (PPI) network analysis of EIN2

EIN2 is a central regulator of ethylene signaling and integrates multiple layers of control at both the protein and transcriptional levels. Previous studies have shown that EIN2 directly interacts with ethylene receptor ETR1, positioning it as a key mediator that transmits signals from receptor complexes to downstream components[5,21]. In addition, EIN2 promotes the formation of cytoplasmic processing bodies (P-bodies), linking it to post-transcriptional regulation through effects on mRNA stability[12]. EIN2 is further functionally connected to the transcription factor EIN3, thereby bridging upstream ethylene perception with nuclear transcription responses[7,12] (Figure 1A).

Figure 1

Co-expression analyses support this functional relationship. EIN2 and EIN3 transcripts show tightly coordinated expression patterns (Figure 1B, Expression atlas[23]), consistent with their sequential roles in ethylene signal transduction[5,20]. Quantitative expression data from FunCoup6[24] indicate that EIN2 and EIN3 are expressed at comparable levels, suggesting balanced regulation within the pathway (Figure 1B). ENAP1 (EIN2 NUCLEAR ASSOCIATED PROTEIN 1) also displays co-expression with EIN3, in line with its proposed role as chromatin-associated co-regulator of ethylene-responsive transcription. Phylogenetic profile similarity analyses further reveal that EIN2, EIN3, and ENAP1 are deeply conserved across plant species (FunCoup6[24]). Such conservation typically reflects essential biological functions and evolutionary constraints. The strong similarity in their phylogenetic distribution suggests that these proteins may have co-evolved as components of a conserved regulatory module in ethylene signaling.

Temporal expression profiling across a 16-day developmental series in *Arabidopsis thaliana* (Expression Atlas[23]) show that EIN2 maintains relatively constant transcript levels, whereas EIN3 expression increases markedly after day 12, indicating potential age-dependent regulation. ENAP1 expression remains stable throughout the time course, consistent with a sustained role in transcriptional regulation, while ENAP2 expression remains low (Figure 1C).

Previous ChIP-seq studies demonstrated that acetylation of histones H3K23 and H3K14 increases upon ethylene treatment in an EIN2-dependent manner. EIN2 interacts with ENAP1, and ENAP1 can bind EIN3, leading to the hypothesis that ENAP1 and EIN2 jointly stabilize EIN3 and promote chromatin acetylation at ethylene-responsive loci[14,15]. Despite these insights, the molecular architecture of this regulatory module remains unresolved. In particular, it is unclear whether EIN2 directly interacts with EIN3 or whether ENAP1 serves as a bridging factor to form a ternary complex.

bioRxiv preprint doi: https://doi.org/10.64898/2026.07.10.737652; this version posted July 10, 2026. The copyright holder for this preprint (which was not certified by peer review) is the author/funder. All rights reserved. No reuse allowed without permission.

To address these open questions, we employed a combined set of biophysical and cell-based assays across multiple biological contexts to determine whether EIN2 directly interacts with EIN3 and to dissect the interaction interfaces among EIN2, EIN3 and ENAP1. These analyses provide critical mechanistic insight into the protein interaction network that governs nuclear ethylene signaling.

Microscale thermophoresis (MST)-based characterization of EIN2–EIN3 and EIN2/EIN3-ENAP1 interactions

To dissect the molecular interfaces underlying the nuclear interactions of EIN2, we recombinantly expressed and purified a series of EIN2 C-terminal truncations (residues 479-1294, 663-1294, and 1078-1294), EIN3 N-terminal truncations (residues 1-85, 1-173, 1-306 and 1-471), and full-length ENAP1 (Figure 2A, Figure 3A). Microscale thermophoresis (MST) measurements revealed that EIN2 directly binds EIN3 with high affinity (K_D = 0.27 - 4.8 µM; Figure 2B).

Figure 2

$EIN3^{1-85}$ displayed only weak binding to all EIN2 truncations, whereas longer EIN3 constructs showed markedly increased affinity, particularly towards $EIN2^{479-1294}$ and $EIN2^{663-1294}$. $EIN3^{1-173}$ exhibited the highest affinity and further extension of the EIN3 C-terminus did not substantially enhance binding. These data identify EIN3 residues 86-173 as the core region required for EIN2 interaction. Consistent with this, affinities decreased progressively with shorter EIN2 constructs. Negative controls using BSA or Alexa488 dye showed no detectable interaction confirming the specificity of the EIN2-EIN3 association (Figure S1).

Figure 3

We next examined ENAP1 binding. MST analysis confirmed that ENAP1 interacts with both EIN2 and EIN3 (Figure 3B). As observed for EIN2-EIN3 binding, ENAP1 affinity toward EIN2 decreased with shorter EIN2 constructs: a modest two-fold reduction for $EIN2^{663-1294}$ (0.4 µM ± 0.04) and a six-fold reduction for $EIN2^{1078-1294}$ (1.24 µM ± 0.22) relative to $EIN2^{479-1294}$ (0.22 µM ± 0.02).

ENAP1 also bound all EIN3 truncations with low-to-mid micromolar affinity. Extension of the EIN3 86-173 region increased affinity four-fold, and further extension to residues 307-471 produced an additional three-fold increase, suggesting that ENAP1 engages multiple regions within EIN3 (Figure 3B). To test whether ENAP1 modulates EIN2-EIN3 complex formation, we performed competition assays using $EIN2^{479-1294}$ and $EIN3^{1-173}$, the constructs with the highest intrinsic affinity (Figure 4). At ENAP1 concentrations approximating its K_D (~ 0.2 µM) EIN2-EIN3

bioRxiv preprint doi: https://doi.org/10.64898/2026.07.10.737652; this version posted July 10, 2026. The copyright holder for this preprint (which was not certified by peer review) is the author/funder. All rights reserved. No reuse allowed without permission.

binding increased approximately two-fold. In contrast, a 5-fold excess of ENAP1 (~ 1 μM) markedly reduced MST response amplitude, revealing a dynamic interaction landscape among these nuclear ethylene signaling components.

Figure 4

Yeast two-hybrid (Y2H) analysis confirms the EIN2-EIN3 interaction in a cellular context

To validate the direct EIN2-EIN3 interaction observed *in vitro* in a cellular context, we next performed yeast two-hybrid (Y2H) studies using the *Saccharomyces cerevisiae* strain AH109 (Figure 5A-B). $EIN2^{479-1294}$ was fused to the GAL4 DNA-binding domain (BD), whereas EIN3 truncations were fused to the GAL4 activation domain (AD) to avoid the known auto-activation abilities of EIN3-BD[25,26]. Successful co-transformation was confirmed on SD-LW medium, and protein-protein interactions were assessed on SD-LWH agar plates supplemented with 0.5 mM 3-AT (3-amino-1,2,4-triazole). Empty vectors served as negative controls, and the bHLH039-Fit-C interaction was used as a positive control[27]. Consistent with MST measurements, BD-$EIN2^{479-1294}$ and full-length AD-EIN3 supported growth on SD-LWH, demonstrating a direct interaction *in vivo*. BD-$EIN2^{479-1294}$ alone exhibited moderate auto-activation, but co-expression with AD-EIN3 resulted in visible stronger growth, confirming a genuine interaction despite the background activity. Interaction was retained with $EIN3^{1-173}$ but not with $EIN3^{1-85}$ supporting the conclusion that EIN3 residues 86-173 constitute the core EIN2 binding region, in agreement with MST data. Notably, $EIN3^{1-85}$ suppressed the auto-activation of BD–$EIN2^{479-1294}$, indicating that this short EIN3 fragment interferes with the reporter activity of the BD-fusion. This effect is unlikely to reflect productive EIN2 binding and may instead arise from non-specific interference with BD–EIN2 function in yeast, for example through partial misfolding, aggregation, or steric hindrance. Further truncation of EIN2 eliminated both auto-activation and interaction with EIN3 (Figure 5B). In particular, BD-$EIN2^{663-1294}$ failed to interact with EIN3 despite only minor affinity differences between $EIN2^{663-1294}$ and $EIN2^{479-1294}$ *in vitro*, suggesting that the EIN2 region between residues 479-663 is required for productive interaction in the cellular context. The lack of $EIN2^{663-1294}$ interaction in yeast likely reflects folding or localization constraints rather than absence of binding.

Because EIN3 is a transcription factor, BD-EIN3 auto-activation was also examined (Figure 5C). Full-length EIN3 showed strong reporter activation that was not suppressed by 3-AT, whereas BD-$EIN3^{1-306}$ lacked auto-activation, consistent with previous reports[26]. Extension to BD-$EIN3^{1-471}$ restored moderate reporter activity, which was fully suppressed by 3-AT, indicating that residues 307-471 contribute to transcriptional activation, but additional C-terminal regions are required for full activity. To refine the EIN3 dimerization domain, BD-$EIN3^{1-306}$ was tested against a panel of AD-EIN3 truncations (Figure 5D). Interaction was detected with AD-$EIN3^{1-306}$ and AD-$EIN3^{1-173}$, but not with AD-$EIN3^{1-85}$. These results narrow

bioRxiv preprint doi: https://doi.org/10.64898/2026.07.10.737652; this version posted July 10, 2026. The copyright holder for this preprint (which was not certified by peer review) is the author/funder. All rights reserved. No reuse allowed without permission.

the EIN3 dimerization domain to residues 113-173, consistent with earlier studies but providing a more precise boundary.

Figure 5

***In planta* FLIM-FRET analysis reveals the EIN2-EIN3 interaction and defines the nuclear localization requirements of both proteins**

To assess the EIN2-EIN3 interaction in a physiological context, we turned to *in planta* FLIM-FRET measurements following transient expression of fluorescently tagged protein truncations in *N. benthamiana*. Because EIN2-EIN3 binding must occur in the nucleus, we first examined the subcellular localization of all constructs. EIN2 truncations fused to GFP localized to both cytoplasm and nucleus consistent with previous reports for $EIN2^{479-1294}$ [7,9,21]. Shorter EIN2 variants, $EIN2^{1042-1294}$ and $EIN2^{1215-1294}$, showed progressively stronger nuclear accumulation, reflecting the position of the EIN2 nuclear localization signal (NLS) at residues 1262-1269. $EIN2^{1215-1294}$ also showed pronounced nucleolar enrichment, likely due to size-dependent trafficking rather than physiological relevance. In contrast, full-length EIN3 and $EIN3^{1-471}$ localized exclusively in the nucleus, whereas shorter EIN3 truncations ($EIN3^{1-306}$, $EIN3^{1-173}$ and $EIN3^{1-85}$) showed markedly reduced nuclear accumulation. Sequence analysis and PredictNLS [28] identified two putative NLS motifs at residues 59-66 (N-terminal NLS) and 377-384 (C-terminal NLS). Deletion analysis demonstrated that the C-terminal NLS (residues 377-384) is essential for the nuclear import, while the N-terminal NLS contributes little or not at all.

Figure 6

To enable FLIM-FRET measurements, we restored nuclear localization of EIN3 truncations by fusing the identified C-terminal NLS (MRKRKPNR) to their C-termini, which substantially increased nuclear-localized fluorescence signal and confirmed the functional relevance of this motif. FLIM-FRET measurements were performed using EIN2 truncations fused to GFP (donor) and EIN3 constructs fused to mCherry (acceptor). Donor only controls were included for lifetime normalization and mCherry fused to an NLS (mCherry-NLS) served as a negative control for bystander FRET. All EIN2-EIN3 combinations showed reduced donor lifetimes relative to donor-only controls. However, only $EIN2^{479-1294}$-GFP and $EIN2^{1042-1294}$-GFP exhibited significantly shorter lifetimes than their respective negative controls. $EIN2^{1215-1294}$-GFP did not differ from the negative control, indicating absence of specific interaction. Negative controls displayed fluorescence lifetimes ranging from 2.47 ± 0.02 ns for $EIN2^{1215-1294}$-GFP to 2.49 and

bioRxiv preprint doi: https://doi.org/10.64898/2026.07.10.737652; this version posted July 10, 2026. The copyright holder for this preprint (which was not certified by peer review) is the author/funder. All rights reserved. No reuse allowed without permission.

2.50 ± 0.02 ns for the other two EIN2-GFP truncations. $EIN2^{479-1294}$-GFP and $EIN2^{1042-1294}$-GFP co-expressed with EIN3-mCherry showed lifetimes of 2.46 ± 0.04 ns and 2.38 ± 0.07 ns, respectively, whereas $EIN2^{1215-1294}$-GFP exhibited a fluorescence lifetime of 2.46 ± 0.03 ns. These data demonstrate that EIN2 residues 1042-1214 are sufficient to mediate EIN3 binding *in planta*, while residues beyond 1214, including the EIN2 NLS, are not required. To further define the EIN3 interaction surface, we tested $EIN3^{1-85}$-mCherry and $EIN3^{1-173}$-mCherry as acceptors. Co-expression of $EIN2^{479-1294}$-GFP with $EIN3^{1-173}$-mCherry significantly reduced donor lifetimes relative to the negative control, whereas $EIN3^{1-85}$-mCherry did not. Fluorescence lifetimes of $EIN2^{479-1294}$-GFP were 2.52 ± 0.01 ns with the negative control, 2.52 ± 0.01 ns with $EIN3^{1-85}$-mCherry and 2.50 ± 0.02 ns when co-expressed with $EIN3^{1-173}$-mCherry. When $EIN2^{1042-1294}$-GFP served as the donor, neither EIN3 truncation produced significant lifetime reductions, indicating that the distal EIN2 region interacts with the C-terminal portion of EIN3 beyond residue 173. These results confirm that EIN3 residues 86-173 constitute the core EIN2 binding domain and that the distal EIN2 region engages a separate C-terminal surface of EIN3.

Together, the FLIM-FRET results corroborate the *in vitro* MST and Y2H data and define the minimal EIN2 region capable of engaging EIN3 in a physiological environment.

Figure 7

Structural modeling, docking and sequence conservation analysis identify a putative EIN3 and EIN2 binding interface

To further refine the molecular interface underlying the EIN2-EIN3 interaction, we generated homology models of *Arabidopsis thaliana* EIN2 (residues 479–995) and EIN3 (full length) and performed protein-protein docking using HADDOCK[29] (Figure 8A-D). Docking results were ranked according to the HADDOCK score (Cluster size, Van der Waals forces, electrostatic and desolvation energy for each docking cluster are shown in supplementary tables S1-S3), where positive values indicate unfavorable binding and negative values reflect favorable interactions. The EIN2 model was systematically docked against the experimentally defined EIN3 interaction region (residues 86–173). Among all tested regions, $EIN2^{646–674}$ produced the most favorable HADDOCK score (−40), indicating a preferred interaction surface (Figure 8A). To validate this result, we performed reciprocal docking using $EIN2^{646–674}$ against sequential EIN3 regions. A stepwise evaluation from the N- to the C-terminus revealed that the N-terminal portion of EIN3 (up to residue 200), contributes most strongly to the binding. The most favorable docking scores were obtained for $EIN3^{75–100}$ with (−90) and $EIN3^{100–150}$ (−75) (Figure 8B). Fine-mapping, using overlapping EIN3 segments spanning residues 86 to 215 narrowed the predicted interaction interface to EIN3 residues 86 to 100 (Figure 8C), consistent with the

bioRxiv preprint doi: https://doi.org/10.64898/2026.07.10.737652; this version posted July 10, 2026. The copyright holder for this preprint (which was not certified by peer review) is the author/funder. All rights reserved. No reuse allowed without permission.

MST, FLIM-FRET and Y2H data identifying residues 86-173 as essential for binding. This putative EIN2 binding surface is in close proximity to the DNA binding domain (DBD) (residues 174-306) of EIN3 (Figure 8D-E).

To assess the evolutionary conservation of the predicted interface, we performed multiple sequence alignments of EIN2 and EIN3 orthologs from *A. thaliana*, *C. arabica*, *A. chinensis*, *S. tuberosum*, *S. lycopersicum*, *C. papaya*, *M. acuminata*, *V. vinifera*, *H. annuus* and *N. attenuata* using T-Coffee[30] (see Figure 8F-G). The selected species represent a wide evolutionary spectrum of angiosperms. This diversity enables robust assessment of evolutionary conservation and divergence of EIN2 and EIN3 across distinct plant lineages. EIN2 displayed strong conservation across species, with the N-terminal transmembrane region being most conserved (Figure 8F). The EIN2 constructs used in this study derived from the soluble C-terminal domain (residues 479–1294). Notably, the docking-identified region $EIN2^{646–674}$ corresponding to the N-terminus of the EIN2-C fragment after cleavage at Ser645/Phe646 [8] is highly conserved across species, with the exception of *Musa acuminata* (Figure 8F). The C-terminal NLS (1262-LKRYKRRL-1269) is also strongly conserved.

Figure 8

EIN3 exhibited high conservation in its N-terminal region, which contains several functional elements, including the acidic domain (AD), proline-rich domain (PRD), four basic domains (BD I–IV), and the DNA-binding domain (DBD). In contrast, the C-terminal region showed substantial divergence (Figure 8G). The EIN3 constructs analyzed here predominantly encompass the conserved N-terminal portion. Within the experimentally identified interaction region, residues 86–153 were strongly conserved, whereas residues 154–173 showed greater variability (Figure 8G). Sequence analysis also revealed that the N-terminal NLS (residues 59-66, KMRLKRLK) is highly conserved, while the C-terminal NLS (residues 377-384, MRKRKPNR) is conserved mainly in its core RKRK motif (Figure 8G). Given that only the C-terminal NLS is required for nuclear localization, the strong conservation of the N-terminal NLS suggests a potential auxiliary or backup role.

Together, structural modeling, docking and evolutionary analysis converge on a conserved EIN2-EIN3 interaction interface involving EIN2 residues 646-674 and EIN3 residues 86-120, providing mechanistic support for the experimentally defined binding regions.

bioRxiv preprint doi: https://doi.org/10.64898/2026.07.10.737652; this version posted July 10, 2026. The copyright holder for this preprint (which was not certified by peer review) is the author/funder. All rights reserved. No reuse allowed without permission.

DISCUSSION

Despite substantial progress in elucidating ethylene signaling, the molecular events linking EIN2 nuclear translocation to transcriptional activation remain incompletely defined. By integrating quantitative biophysics, yeast genetics, *in planta* imaging, and structural modeling, we demonstrate that EIN2 directly engages EIN3 and delineate the minimal regions required for this interaction. Together, these complementary approaches reveal a modular interaction landscape in which distinct EIN2 surfaces contribute differentially to EIN3 binding depending on affinity and cellular context. Our MST and docking analyses converge on EIN2 residues 479-662 as the primary high-affinity interaction hotspot. This region is evolutionarily conserved, yields the most favorable docking scores, and dominates binding in controlled biophysical assays. Correspondingly, EIN3 constructs containing residues 86-173 display the highest affinity for EIN2, and further C-terminal extension does not enhance binding, identifying $EIN3^{86-173}$ as the core interaction region. MST experiments also revealed pronounced changes in initial fluorescence (IF) when EIN2 truncations served as fluorophores. Control experiments exclude dye artifacts (Figure S1), suggesting that EIN3 binding induces conformational rearrangements within the intrinsically disordered EIN2 C-terminus. ENAP1, previously proposed to stabilize an EIN2-EIN3 complex, bound both proteins with appreciable affinity (Figure 3B), consistent with its proposed chromatin-associated role[15], yet MST-based competition assays (Figure 3B) show that ENAP1 and EIN3 compete for the same EIN2 region at elevated ENAP1 concentrations. Thus, ENAP1 does not universally stabilize an EIN2-EIN3 complex but instead acts in a dynamic, concentration-dependent manner that can either facilitate or antagonize EIN3 recruitment. The fact that ENAP1 and $EIN3^{1-173}$ engage the same EIN2 segment further supports this interpretation and argues against a constitutive ternary complex.

Yeast two-hybrid (Y2H) assays provided additional support for a direct EIN2-EIN3 interaction, and aligned well with the intrinsic affinity landscape defined by MST despite overall weaker reporter activation in yeast due to crowding and folding constraints of the system[31]. Co-expression of EIN3 constructs consistently enhanced reporter activity above the auto-activation background of BD- $EIN2^{479-1294}$, and the observation that $EIN3^{1-173}$ but not $EIN3^{1-85}$ supported interaction reinforces the MST-derived conclusion that residues 86-173 constitute the core EIN2-interaction region. Y2H analysis also clarified the functional organization of EIN3, showing that full-length EIN3 displayed strong auto-activation consistent with earlier studies[26]. $EIN3^{1-471}$ showed intermediate activity, and only constructs containing the C-terminal region beyond residue 471 retained full transcriptional activation capacity, indicating that activation, DNA binding, and dimerization reside in distinct domains. The failure of BD-$EIN2^{663-1294}$ to interact with EIN3 in yeast, despite comparable affinities *in vitro*, likely reflects differences in folding, stability or nuclear accessibility rather than absence of binding.

bioRxiv preprint doi: https://doi.org/10.64898/2026.07.10.737652; this version posted July 10, 2026. The copyright holder for this preprint (which was not certified by peer review) is the author/funder. All rights reserved. No reuse allowed without permission.

To assess interaction under more physiological conditions, we performed *in planta* FLIM-FRET measurements, ensuring nuclear accumulation of EIN3 by fusing its essential C-terminal NLS (residues 377-384) to truncations lacking it. EIN2 fragments showed progressively stronger nuclear localization with decreasing size, consistent with passive diffusion of proteins <60 kDa through the nuclear pore complex [32], and the pronounced nucleolar accumulation of $EIN2^{1215-1294}$ likely reflects this size-dependent trafficking rather than physiological relevance, as this fragment is not known to occur *in vivo*. FLIM-FRET analyses revealed robust lifetime reductions for $EIN2^{479-1294}$ and $EIN2^{1042-1294}$ when co-expressed with EIN3, whereas $EIN2^{1215-1294}$ showed no interaction, demonstrating that residues 1042-1214 are sufficient to mediate EIN3 binding *in planta*. These findings align with MST data showing that $EIN2^{1078-1294}$ retains measurable, albeit lower affinity for EIN3 (low µM affinity instead of nM affinity), and explain why Y2H assays fail to detect interaction with shorter EIN2 fragments whose binding strength likely falls below the detection threshold of the yeast system.

Complementary FLIM-FRET experiments with $EIN2^{1042-1294}$ and EIN3 truncations ruled out involvement of the EIN3 core binding domain (amino acids 86-173) in this distal interaction. Importantly, the ability of $EIN2^{1042–1294}$ to interact with EIN3 *in planta* reflects the transient overexpression context of agroinfiltration, where elevated nuclear protein concentrations, and molecular crowding stabilize weak or transient contacts. Under such non-physiological conditions, the contribution of the high-affinity region is masked by mass-action effects, and detectable interaction does not necessarily indicate sufficiency under endogenous expression levels. This distinction is underscored by the classical rescue experiments in *ein2* mutants. Only EIN2 fragments that include the high-affinity region such as 454/459/479-1294 or 645-1294 fully restore ethylene responses[5,8,9,33]. These fragments retain either the complete or the C-terminal portion of the primary hotspot together with the distal interaction region, ensuring sufficient binding capacity at endogenous nuclear concentrations. In contrast, the distal region alone is unlikely to support robust EIN3 engagement under physiological expression levels.

In silico docking identified a highly conserved interaction hotspot within *A. thaliana* EIN2 residues 646-674 and placed the corresponding EIN3 contact surface within residues 86-100, providing a structural rationale for the high-affinity interaction detected by MST and the Y2H-defined requirement for $EIN3^{1-173}$. This docking-derived interface aligns with the intrinsic affinity landscape revealed by MST, which consistently identified $EIN2^{479-662}$ as the dominant high-affinity region, and it complements Y2H results showing that only EIN3 constructs containing residues 86–173 support interaction. At the same time, FLIM-FRET demonstrated that a more distal $EIN2^{1042-1214}$ segment is sufficient to mediate detectable interaction under

bioRxiv preprint doi: https://doi.org/10.64898/2026.07.10.737652; this version posted July 10, 2026. The copyright holder for this preprint (which was not certified by peer review) is the author/funder. All rights reserved. No reuse allowed without permission.

399 transient overexpression, indicating that EIN2 harbors multiple interaction-competent surfaces
400 whose contribution depends on affinity and cellular context.

401 Together, these biochemical, cellular, and structural analyses support a two-tiered model in
402 which a conserved, specificity-defining high-affinity interface ($EIN2^{479-662}$ / $EIN3^{86-173}$) underpins
403 physiological signaling, while a secondary, lower-affinity surface downstream of residue ~1042
404 can contribute under conditions of elevated local concentration or in the presence of stabilizing
405 cofactors. This framework reconciles the intrinsic affinity landscape with the context-dependent
406 behavior observed *in planta* and provides a mechanistic basis how EIN2 engages EIN3 to
407 initiate ethylene transcriptional responses.

408

bioRxiv preprint doi: https://doi.org/10.64898/2026.07.10.737652; this version posted July 10, 2026. The copyright holder for this preprint (which was not certified by peer review) is the author/funder. All rights reserved. No reuse allowed without permission.

MATERIAL AND METHODS

Prediction of EIN2 and EIN3 protein-protein interactions (PPI) and functional networks in *A. thaliana*

Protein–protein and gene interaction analyses for EIN2 and EIN3 were performed using the STRING database, which integrates experimentally validated interactions, computational prediction, and text mined associations[34]. A PPI network was constructed to visualize their roles within the ethylene response pathway. A high-confidence threshold (interaction score ≥ 0.7) was applied and analysis was restricted to *Arabidopsis thaliana*, to ensure species-specific relevance. Gene co-expression information available within STRING was also incorporated. Complementary network analyses were conducted using FunCoup 6, which integrates additional evidence types such as mRNA co-expression and phylogenetic profile similarity, where conservation across species indicates functional association[24]. Default parameters were used unless otherwise stated.

Age dependent expression patterns of EIN2 and EIN3 and related proteins in *A. thaliana*

The expression dynamics of ETR1, CTR1, EIN2, EBF1, EBF2, EIN5, UPF1, EIN3, EIL1, ENAP1, and ENAP2 were examined across a 16-day developmental time course in *Arabidopsis thaliana*. Publicly available transcriptomic datasets from the Expression Atlas repository were used for this analysis[23]. Transcript abundancies reported as transcripts per million (TPM), a normalization metric that reflects the relative abundance of transcripts for each gene or isoform, enabling quantitative comparison across samples.

Multiple interspecies sequence alignment for EIN2 and EIN3

EIN2 and EIN3 protein sequences were retrieved from the Uniprot database (see Table S4), and multiple sequence alignments were performed using T-COFFEE[30,35] and COBALT (Constraint-based Multiple Alignment Tool)[36]. For EIN2, the alignment focused on the major interaction region identified in this study (residues 479 to 663). For EIN3, both the full-length proteins and the multi-functional interaction region comprising residues 86 to 173 were aligned to assess conservation across species.

Homology modelling of EIN2 and EIN3 core regions and docking experiments

Three-dimensional homology models of EIN2$^{479\text{-}995}$ and EIN3 full length were generated using the I-TASSER protein structure prediction server[37]. Both proteins contain extensive intrinsically disordered and flexible regions, which limited the reliability of structure prediction using AlphaFold and Chai. Therefore, I-TASSER was selected as an alternative approach capable of producing homology models suitable for downstream structural and functional investigations. Model construction was based on the 10 closest homologs identified by

bioRxiv preprint doi: https://doi.org/10.64898/2026.07.10.737652; this version posted July 10, 2026. The copyright holder for this preprint (which was not certified by peer review) is the author/funder. All rights reserved. No reuse allowed without permission.

TM-alignment. For each comparison, I-TASSER reports the optimal structural alignment between two proteins and the corresponding TM-score, where values >0.5 indicate that two proteins share the same overall fold. Model quality was further evaluated using the C-score, a confidence metric that estimates the reliability of predicted protein structures and typically ranges from −5 to 2. Higher C-scores correspond to increased confidence and improved model quality, while values greater than −1.5 are generally indicative of correct global topology. Model quality evaluation revealed high confidence, with TM-scores above 0.6, consistent with correct fold prediction (TM-score > 0.5). The C-scores were −1.31 for $EIN2^{479–995}$ and −1.03 for EIN3, falling within the typical range of −5 to 2, indicating reliable model quality. Model construction was performed using multiple template structures. The $EIN2^{479–995}$ model was generated based on PDB templates 5A1U, 7BII, 4A0C, 7JQ9, 2QNA, 6YEJ, 6EZ8, 6N1Z, 3EA5, and 6AHO. In parallel, the EIN3 model was built using the following PDB entries: 3CHN, 7CUN, 5U1S, 6Z2W, 7ABI, 6UM1, 2NYY, 2UVC, 6EGO, and 3CMX. Protein-protein docking simulations between EIN3-EIN2 were carried out using HADDOCK[29]. Docking poses were ranked according to the HADDOCK scoring function (corresponding binding energies and cluster size are shown in supplementary tables S1-S3), where positive scores denote unfavorable interactions and negative scores indicate energetically favorable binding. The full-length EIN3 model was used and residues in different regions were activated in the docking approach to be involved in the interaction with EIN2 (e.g., $EIN3^{86-173}$, $EIN3^{75-100}$, $EIN3^{100-150}$). For EIN2, multiple truncated variants were screened including $EIN2^{479-995}$, $EIN2^{479-663}$, $EIN2^{640-663}$, $EIN2^{640-645}$, $EIN2^{646-663}$, $EIN2^{646-674}$, $EIN2^{654-674}$, $EIN2^{658-674}$, $EIN2^{640-652}$ and $EIN2^{653-663}$. All figures were made using the PyMOL Molecular Graphics System, Version 1.3, Schrödinger, LLC.

Expression of EIN2 truncations

The following EIN2 constructs were successfully expressed and purified: $EIN2^{479-1294}$, $EIN2^{663-1294}$ and $EIN2^{1078-1294}$. $EIN2^{479-1294}$ was expressed from the pET15b vector containing an N-terminal deca-His-tag, whereas all other constructs were expressed from the pET21a vector which provides a C-terminal hexa-His-tag. Protein expression was carried out in the *E. coli* ArcticExpress cells grown in LB media according to the manufacturer's instructions. Briefly, Ampicillin (100 µg/mL working concentration) and Gentamycin (20 µg/mL working concentration) were added to the pre-culture, while no antibiotic was used for the main culture. After overnight incubation of the pre-culture at 37 °C, the main culture was inoculated to an initial OD_{600} of 0.1 and grown for 3 hours at 30 °C. The temperature was then reduced to 12 °C, cultures were equilibrated for 15 minutes, and protein expression was induced with 1 mM IPTG., Cells were harvested the following day by centrifugation (7.000 x g, 10 minutes), flash-frozen in liquid nitrogen and stored at -20 °C until usage.

bioRxiv preprint doi: https://doi.org/10.64898/2026.07.10.737652; this version posted July 10, 2026. The copyright holder for this preprint (which was not certified by peer review) is the author/funder. All rights reserved. No reuse allowed without permission.

Expression of EIN3 truncations

$EIN3^{1-85}$, $EIN3^{1-173}$, $EIN3^{1-306}$ and $EIN3^{1-471}$ were cloned into the pETEV16b (a modified pET16b backbone containing a TEV cleavage site between the GOI and the His-tag). $EIN3^{1-85}$ and $EIN3^{1-173}$ were expressed in *E. coli* BL21pRARE cells using 2YT-media, whereas $EIN3^{1-306}$ and $EIN3^{1-471}$ were expressed in ArcticExpress cells following the protocol described for EIN2. The pre-culture was mixed with ampicillin (100 µg/mL working concentration) and chloramphenicol (30 µg/mL working concentration) and grown overnight at 37 °C. For main cultures, 2 % ethanol and ampicillin were added prior to inoculation to an OD_{600} of 0.1. The main culture was grown at 37 °C until an OD_{600} of 0.4 was reached. Afterwards, the temperature was decreased to 16 °C and the induction with 0.5 mM IPTG was performed between an OD_{600} of 0.6 – 0.8. Cells were harvested the next day by centrifugation (7.000 x g, 10 minutes), flash-frozen in liquid nitrogen and stored at -20 °C until usage.

Expression of ENAP1

ENAP1 was cloned into the pETEV16b vector containing an N-terminal deca-His-tag. Expression was performed in *E. coli* BL21pRARE cells following the protocol used for EIN3 truncations, except that the expression was performed at 37 °C and cells were harvested 2 hours after IPTG induction.

Protein purification

All proteins were purified by immobilized affinity chromatography (IMAC) essentially as described in [22]. Briefly, the stored cell pellet was resuspended in 1× PBS, 5 % (w/v) glycerol and 0.1 % (v/v) Nonidet-P40 pH 7.4 (5 mL per g cell). DNase and antifoam were added, and cells were lysed using a high-pressure cell disruptor afterwards. After cell disruption, cell debris and insoluble protein were separated by centrifugation at 100.000 x g for 1 h, and the supernatant was applied to a pre-equilibrated Ni^{2+}-IMAC column. For proteins expressed in BL21pRARE, the column was washed with 500 mM NaCl and 50 mM sodium phosphate (pH 7.4) until baseline stabilization. Non-specific proteins were removed using stepwise washes containing 50 mM and 100 mM imidazole. Target proteins were eluted with 500 mM imidazole in 500 mM NaCl, 50 mM sodium phosphate buffer (pH 7.4). For proteins expressed in ArcticExpress cells, an additional wash with 20 mM TRIS and 2 M urea (pH 6.8) was included prior to imidazole elution. Purified proteins were concentrated using ultrafiltration devices, flash-frozen in liquid nitrogen, and stored at −80 °C.

bioRxiv preprint doi: https://doi.org/10.64898/2026.07.10.737652; this version posted July 10, 2026. The copyright holder for this preprint (which was not certified by peer review) is the author/funder. All rights reserved. No reuse allowed without permission.

Labeling of *At*EIN2 truncations with Alexa488-NHS ester

Purified and concentrated EIN2 proteins were first rebuffered into labeling buffer (300 mM NaCl and 50 mM NaP_i) using a PD-10 desalting column. Alexa488-NHS ester was added in a 2.5-fold molar excess and incubated with the protein for 45 minutes at room temperature under gentle rotation in the dark. To remove unreacted dye, the reaction mixture was rebuffered into labeling buffer supplemented with 5 % glycerol (w/v) using a PD-mini desalting column. The labeled protein was concentrated using an ultrafiltration unit and centrifuged at 229.600 x g (50.000 rpm) for 35 minutes to remove aggregates. Protein and fluorophore concentration were determined using a NanoDrop One spectrophotometer. Labeling efficiency was calculated by dividing the fluorophore concentration by the protein concentration and multiplying the result with 100 %.

Microscale Thermophoresis (MST) measurements

MST measurements were performed using a Monolith NT.115 (NanoTemper). LED power was adjusted according to labeling efficiency, while the MST power was kept constant at 40 %. For all measurements, MST Buffer (300 mM NaCl, 50 mM HEPES and 0.05 % Tween-20, pH 7.5) and standard capillaries were used. Fo assays involving *At*EIN3$^{1-306}$, the buffer was adjusted to 8.0 due to the pI of the protein. Unless stated otherwise, data were analyzed using the Initial Fluorescence method and fitted in Origin using a logistic model. Fluorophore-labelled proteins were used at 100 nM, and ligands were titrated up to 50 µM. To this end, a serial dilution of the ligand was prepared in PCR tubes and mixed in a 1:1 ratio with 200 nM of the respective fluorophore (resulting in 100 nM fluorophore final concentration). Samples were incubated on ice for 18 min, centrifuged at 13.400 x g for 2 min, loaded into the capillaries and measured. All MST data represent three independent replicates. Negative controls include BSA as a non-binding ligand or free dye without labelled protein.

Yeast Two-Hybrid Assay

Yeast Two-Hybrid (Y2H) Assays were performed using *S. cerevisiae* strain AH109 with pACT2 (AD-Gal4) and pGBKT7 (BD-Gal4) vectors. Constructs were cloned into either the pACT2 (Ampicillin resistance) or pGBKT7 (Kanamycin resistance) vector, the constructs were previously cloned into pDONR207 (Gentamycin resistance) which was used as the donor vector for the subsequent Gateway Cloning method (Invitrogen). The strain was kindly provided by Prof. Dr. Wilde (University of Freiburg), and empty vectors and the positive control were kindly provided by Prof. Dr. Bauer (Heinrich Heine University Düsseldorf). Co-transformations were performed via the lithium acetate (LiAc) method according to[38]. Tansformants were selected on synthetic defined (SD) medium containing adenine and all amino acids except Leu (pACT2) and Trp (pGBKT7) and incubated for 2-3 days at 30 °C. For

bioRxiv preprint doi: https://doi.org/10.64898/2026.07.10.737652; this version posted July 10, 2026. The copyright holder for this preprint (which was not certified by peer review) is the author/funder. All rights reserved. No reuse allowed without permission.

548 interaction assays, overnight liquid cultures grown in SD-LW medium (lacking Leu and Trp)
549 were adjusted to an OD_{600} of 0.1 (10^{-1}) and serial dilutions down to 10^{-4} were prepared. Ten
550 microliters of each dilution were spotted onto SD-LW plates (transformation control) and SD-
551 LWH plates (lacking Leu, Trp and His) to test for protein-protein interaction. To increase
552 selectivity and ensure reliable and valid interaction data, SD -LWH plates were supplemented
553 with 0.5 mM 3-amino-1,2,4-triazole.

554 **Transient transformation and expression in *N. benthamiana***

555 Transient transformation of *N. benthamiana* abaxial leaf epidermal cells was conducted as
556 described previously[22] with minor changes. OD_{600} was always set to 0.5 and since
557 agrobacterium strain GV3101:p19 was used for all expression vectors (except mCherry-NLS),
558 the strain did not need to be added in addition. Plants were kept under a natural day/night
559 cycle before microscopy analysis.

560 **Fluorescence lifetime imaging and fitting of fluorescence decays**

561 Fluorescence lifetime imaging was performed on a Leica Stellaris 8 FALCON microscope or a
562 ZEISS LSM780 with LSM Upgrade Kit from Picoquant. Imaging on the LSM 780 was done as
563 described in [39]. The fluorescence decays from data acquired using the LSM 780 were fitted
564 using a previously reported method with a minor modification[22].

565 On the Stellaris 8 FALCON (FALCON extension), a Leica HC PL APO 40x/1,1 W motCORR
566 CS2 objective was used. GFP(S65T) and mCherry were excited with a pulsed white-light laser
567 (40 MHz), filtered for 488 nm and 561 nm using an acousto-optical tunable filter (AOTF). For
568 emission detection, HyD X detectors were used, and the emitted light was filtered through an
569 acousto-optical beam splitter (AOBS) to detect a range of 493-534 nm (GFP) and 590-636 nm
570 (mCherry). Images were acquired at zoom 10 with a resolution of 256x256 pixels (each pixel
571 corresponding to an area of 0.01299 µm² (113.97 × 113.97 nm)), and a pixel dwell time of
572 15.24 µs. The number of frames was slightly adjusted to reach comparable photon counts per
573 pixel in each measurement. Nuclei containing high donor concentrations were avoided to
574 prevent pile-up effects.

575 Fluorescence decays of selected ROIs in the FLIM images were analyzed within Leica
576 Application Suite X (LAS X, version 4.8.2). Decays were fitted using the inbuilt FLIM fitting tool
577 (Fitting model: n-exponential reconvolution). For donor-only samples one lifetime was fitted
578 (model parameter n = 1). For all other samples, one lifetime was fixed to the arithmetic mean
579 of the lifetime of the donor-only samples, and a second lifetime was fitted within the limits of
580 10 % and 80 % of this value (model parameter n = 2). The intensity weighted lifetime was
581 regarded as the apparent lifetime of the sample. FRET efficiency was calculated from the

bioRxiv preprint doi: https://doi.org/10.64898/2026.07.10.737652; this version posted July 10, 2026. The copyright holder for this preprint (which was not certified by peer review) is the author/funder. All rights reserved. No reuse allowed without permission.

intensity weighted lifetime of the FRET sample over the arithmetic mean of the intensity weighted lifetimes of the donor-only samples.

Fluorescence imaging

Images showing protein localization in *N. benthamiana* were acquired with a ZEISS LSM 780 or a Leica Stellaris 8 microscope using the same objectives as described for FRET-FLIM experiments. GFP and mCherry were excited at 488 nm or 561 nm, respectively. Signal was acquired around the maximum emission peaks of the fluorophores. Laser power was adjusted differently based on signal intensity.

Statistical analysis

For statistical analysis, GraphPad Prism 8 was used. For the *in planta* FLIM-FRET experiments, Kruskal–Wallis test combined with Dunn's multiple comparisons test were performed.

Data availability statement

All relevant data are included in this manuscript and its supporting information. Imaging datasets supporting the findings of this study are available in the BioImage Archive under accession S-BIAD3653. Further inquiries or requests for materials can be directed to georg.groth@hhu.de.

bioRxiv preprint doi: https://doi.org/10.64898/2026.07.10.737652; this version posted July 10, 2026. The copyright holder for this preprint (which was not certified by peer review) is the author/funder. All rights reserved. No reuse allowed without permission.

REFERENCES

1 Abeles, F. B., Morgan, P. W. & Saltveit Jr, M. E. *Ethylene in plant biology*. (Academic press, 2012).

2 Wang, K. L.-C., Li, H. & Ecker, J. R. Ethylene biosynthesis and signaling networks. *The plant cell* **14**, S131–S151 (2002).

3 Chang, C., Kwok, S. F., Bleecker, A. B. & Meyerowitz, E. M. Arabidopsis ethylene-response gene ETR1: similarity of product to two-component regulators. *Science* **262**, 539–544 (1993).

4 Hua, J. *et al.* EIN4 and ERS2 are members of the putative ethylene receptor gene family in Arabidopsis. *The Plant Cell* **10**, 1321–1332 (1998).

5 Alonso, J. M., Hirayama, T., Roman, G., Nourizadeh, S. & Ecker, J. R. EIN2, a bifunctional transducer of ethylene and stress responses in Arabidopsis. *Science* **284**, 2148–2152 (1999).

6 Kieber, J. J., Rothenberg, M., Roman, G., Feldmann, K. A. & Ecker, J. R. CTR1, a negative regulator of the ethylene response pathway in Arabidopsis, encodes a member of the raf family of protein kinases. *Cell* **72**, 427–441 (1993).

7 Ju, C. *et al.* CTR1 phosphorylates the central regulator EIN2 to control ethylene hormone signaling from the ER membrane to the nucleus in Arabidopsis. *Proceedings of the National Academy of Sciences* **109**, 19486–19491 (2012).

8 Qiao, H. *et al.* Processing and subcellular trafficking of ER-tethered EIN2 control response to ethylene gas. *Science* **338**, 390–393 (2012).

9 Wen, X. *et al.* Activation of ethylene signaling is mediated by nuclear translocation of the cleaved EIN2 carboxyl terminus. *Cell research* **22**, 1613–1616 (2012).

10 Guo, H. & Ecker, J. R. Plant responses to ethylene gas are mediated by SCFEBF1/EBF2-dependent proteolysis of EIN3 transcription factor. *Cell* **115**, 667–677 (2003).

11 Potuschak, T. *et al.* EIN3-dependent regulation of plant ethylene hormone signaling by two Arabidopsis F box proteins: EBF1 and EBF2. *Cell* **115**, 679–689 (2003).

12 Li, W. *et al.* EIN2-directed translational regulation of ethylene signaling in Arabidopsis. *Cell* **163**, 670–683 (2015).

13 Merchante, C. *et al.* Gene-specific translation regulation mediated by the hormone-signaling molecule EIN2. *Cell* **163**, 684–697 (2015).

14 Zhang, F. *et al.* EIN2-dependent regulation of acetylation of histone H3K14 and non-canonical histone H3K23 in ethylene signalling. *Nature communications* **7**, 13018 (2016).

15 Zhang, F. *et al.* EIN2 mediates direct regulation of histone acetylation in the ethylene response. *Proceedings of the National Academy of Sciences* **114**, 10274–10279 (2017).

16 Guo, H. & Ecker, J. R. The ethylene signaling pathway: new insights. *Current opinion in plant biology* **7**, 40–49 (2004).

17 Song, J. *et al.* Biochemical and structural insights into the mechanism of DNA recognition by Arabidopsis ETHYLENE INSENSITIVE3. *PLoS One* **10**, e0137439 (2015).

18 Solano, R., Stepanova, A., Chao, Q. & Ecker, J. R. Nuclear events in ethylene signaling: a transcriptional cascade mediated by ETHYLENE-INSENSITIVE3 and ETHYLENE-RESPONSE-FACTOR1. *Genes & development* **12**, 3703–3714 (1998).

19 Dietzen, C. *et al.* The transcription factor EIL1 participates in the regulation of sulfur-deficiency response. *Plant Physiology* **184**, 2120–2136 (2020).

bioRxiv preprint doi: https://doi.org/10.64898/2026.07.10.737652; this version posted July 10, 2026. The copyright holder for this preprint (which was not certified by peer review) is the author/funder. All rights reserved. No reuse allowed without permission.

20 Dolgikh, V. A., Pukhovaya, E. M. & Zemlyanskaya, E. V. Shaping ethylene response: the role of EIN3/EIL1 transcription factors. *Frontiers in Plant Science* **10**, 1030 (2019).

21 Bisson, M. M. & Groth, G. New insight in ethylene signaling: autokinase activity of ETR1 modulates the interaction of receptors and EIN2. *Molecular Plant* **3**, 882–889 (2010).

22 Wynen, F. *et al.* The importin-alpha superfamily engages in ethylene signaling by shuttling ETHYLENE INSENSITIVE 2 from the endoplasmic reticulum to the nucleus. *The FEBS Journal* (2025).

23 Moreno, P. *et al.* Expression Atlas update: gene and protein expression in multiple species. *Nucleic acids research* **50**, D129–D140 (2022).

24 Buzzao, D., Persson, E., Guala, D. & Sonnhammer, E. L. FunCoup 6: advancing functional association networks across species with directed links and improved user experience. *Nucleic Acids Research* **53**, D658–D671 (2025).

25 He, X., Jiang, J., Wang, C. Q. & Dehesh, K. ORA59 and EIN3 interaction couples jasmonate-ethylene synergistic action to antagonistic salicylic acid regulation of PDF expression. *Journal of Integrative Plant Biology* **59**, 275–287 (2017).

26 Wawrzyńska, A. & Sirko, A. EIN3 interferes with the sulfur deficiency signaling in Arabidopsis thaliana through direct interaction with the SLIM1 transcription factor. *Plant Science* **253**, 50–57 (2016).

27 Gratz, R. *et al.* Phospho-mutant activity assays provide evidence for alternative phospho-regulation pathways of the transcription factor FER-LIKE IRON DEFICIENCY-INDUCED TRANSCRIPTION FACTOR. *New Phytologist* **225**, 250–267 (2020).

28 Cokol, M., Nair, R. & Rost, B. Finding nuclear localization signals. *The EMBO Reports* **1**, 411–415 (2000).

29 Honorato, R. V. *et al.* The HADDOCK2. 4 web server for integrative modeling of biomolecular complexes. *Nature protocols* **19**, 3219–3241 (2024).

30 Notredame, C., Higgins, D. G. & Heringa, J. T-Coffee: A novel method for fast and accurate multiple sequence alignment. *Journal of molecular biology* **302**, 205–217 (2000).

31 Minton, A. P. The influence of macromolecular crowding and macromolecular confinement on biochemical reactions in physiological media. *Journal of biological chemistry* **276**, 10577–10580 (2001).

32 Timney, B. L. *et al.* Simple rules for passive diffusion through the nuclear pore complex. *Journal of Cell Biology* **215**, 57–76 (2016).

33 Bisson, M. M., Bleckmann, A., Allekotte, S. & Groth, G. EIN2, the central regulator of ethylene signalling, is localized at the ER membrane where it interacts with the ethylene receptor ETR1. *Biochemical Journal* **424**, 1–6 (2009).

34 Szklarczyk, D. *et al.* The STRING database in 2023: protein–protein association networks and functional enrichment analyses for any sequenced genome of interest. *Nucleic acids research* **51**, D638–D646 (2023).

35 UniProt Consortium, T. UniProt: the universal protein knowledgebase. *Nucleic acids research* **46**, 2699–2699 (2018).

36 Papadopoulos, J. S. & Agarwala, R. COBALT: constraint-based alignment tool for multiple protein sequences. *Bioinformatics* **23**, 1073–1079 (2007).

37 Roy, A., Kucukural, A. & Zhang, Y. I-TASSER: a unified platform for automated protein structure and function prediction. *Nature protocols* **5**, 725–738 (2010).

38 Gietz, R. D. & Schiestl, R. H. High-efficiency yeast transformation using the LiAc/SS carrier DNA/PEG method. *Nature protocols* **2**, 31–34 (2007).

bioRxiv preprint doi: https://doi.org/10.64898/2026.07.10.737652; this version posted July 10, 2026. The copyright holder for this preprint (which was not certified by peer review) is the author/funder. All rights reserved. No reuse allowed without permission.

695 39 Gonçalves Dias, M. *et al.* Catalytically inactive subgroup VIII receptor-like cytoplasmic
696 kinases regulate the immune-triggered oxidative burst in Arabidopsis thaliana. *Journal of*
697 *Experimental Botany* **76**, 1553–1568 (2025). https://doi.org/10.1093/jxb/erae486

698 40 Discovery, C. *et al.* Chai-1: Decoding the molecular interactions of life. *bioRxiv*,
699 2024.2010.2010.615955 (2024). https://doi.org/10.1101/2024.10.10.615955

700 41 Abramson, J. *et al.* Accurate structure prediction of biomolecular interactions with
701 AlphaFold 3. *Nature* **630**, 493–500 (2024).

702

703

bioRxiv preprint doi: https://doi.org/10.64898/2026.07.10.737652; this version posted July 10, 2026. The copyright holder for this preprint (which was not certified by peer review) is the author/funder. All rights reserved. No reuse allowed without permission.

Acknowledgements

We would like to thank the Bauer's Lab (Heinrich-Heine-University, Institute of Botany) for kindly supplying the positive control used in the Y2H assay as well as the Wilde's Lab (University of Freiburg, Institute for Molecular Genetics of Prokaryotes) for providing the AH109 strain.

Funding

This work was supported by a grant of the Deutsche Forschungsgemeinschaft (DFG, German Research Foundation) to G.G. (project ID 504365166). We would like to acknowledge the Center for Advanced Imaging (CAi) at Heinrich-Heine-University Düsseldorf for providing access to to the Zeiss LSM 780 + 4-channel FLIM exten. (Picoquant), funded by the Deutsche Forschungsgemeinschaft (DFG, German Research Foundation) – Project-ID DFG- INST 208/551-1 FUGG as well as the Leica STELLARIS 8, funded by the Deutsche Forschungsgemeinschaft (DFG, German Research Foundation) – Project-ID INST 208/941-1 FUGG. Meik Thiele funded by the Deutsche Forschungsgemeinschaft (DFG, German Research Foundation) under Germany´s Excellence Strategy – EXC-2048 – project ID 390686111 and Jan Eric Maika was supported by the Deutsche Forschungsgemeinschaft (DFG, German Research Foundation) through CSCS (FOR5235).

Author contributions

Conceptualization, G.G and R.S; Methodology, F.W., M.H. and G.G.; Investigation, F.W., M.T. and J.E.M.; Formal analysis, F.W. and M.T.; Validation, F.W. and M.T.; Visualization, F.W. and R.J.E.; Writing – Original draft, F.W., M.T., R.J.E., R.S. and G.G.

All authors read and edited the manuscript prior to publication.

Competing Interests statement

The authors declare that they have no known competing financial interests or personal relationships that could have appeared to influence the work reported in this paper.

bioRxiv preprint doi: https://doi.org/10.64898/2026.07.10.737652; this version posted July 10, 2026. The copyright holder for this preprint (which was not certified by peer review) is the author/funder. All rights reserved. No reuse allowed without permission.

FIGURE LEGENDS

Figure 1: Bioinformatical analysis of ethylene-related proteins in *A. thaliana* including protein-protein interaction networks, co-expression patterns, and temporal gene expression.
Analyses were performed using data from STRING[34], FunCoup6[24] and Expression Atlas[23], restricted to *A. thaliana*. **(A)** Protein-protein-interaction (PPI) network, highlighting the central positions of EIN2 and EIN3 within the ethylene signaling pathway. Proteins associated with (1) ETR1-mediated receptor regulation, (2) P-body formation, and (3) transcriptional regulation are grouped to illustrate functional modules. **(B)** Heat map summarizing (top) gene co-expression of core ethylene signaling components (ETR1, CTR1, EIN2, EBF1, EBF2, EIN3 and EIL1), (middle) mRNA co-expression of proteins involved in post-transcriptional and translational regulation (ETR1, CTR1, EIN2, EIN5, UPF1, EIN3 and ENAP1), and (bottom) phylogenetic profile similarity of EIN2, EIN5, UFP1, EIN3 and EIN2, reflecting functional relationships across plant species. **(C)** Temporal expression heat map showing transcript abundance of ethylene-related genes (ETR1, CTR1, EIN2, EBF1, EBF2, EIN5, UPF1, EIN3, EIL1, ENAP1 and ENAP2) across a 16-day developmental time course in *A. thaliana*.

Figure 2: *In vitro* MST analysis of EIN2 and EIN3 truncation binding.
A) SDS-PAGE and Coomassie staining of purified EIN2 and EIN3 truncations. The corresponding protein bands for each construct are indicated by red boxes. **B)** Microscale Thermophoresis (MST) binding curves and dissociation constants (K_D, µM) for EIN2 and EIN3 truncations. EIN2 constructs were labeled with Alexa488 and used as fluorophores. Binding data were evaluated using initial fluorescence analysis, and curves were fitted with a logistic model in Origin. Data represent mean +/- standard deviation from three independent measurements (n = 3). **C)** Heat-map representation of KD values (µM) for all EIN2-EIN3 truncation combinations shown in B), with higher affinity depicted in red and lower affinity in blue. For visualization, structural models of EIN2 and EIN3 were generated using Chai Discovery[40] or AlphaFold3[41], respectively, and the amino acid regions corresponding to each truncation are highlighted in red (EIN2) or blue (EIN3).

Figure 3: MST-based analysis of ENAP1 binding to EIN2 and EIN3 truncations.
A) SDS-PAGE and Coomassie staining of purified ENAP1. The ENAP1 band is indicated by red boxes. **B)** Microscale Thermophoresis (MST) binding curves showing affinities (Kd, µM) between ENAP1 and EIN2 or EIN3 truncations. EIN2 truncations were labeled with Alexa488 for ENAP1 binding assays, whereas ENAP1 served as the fluorophore in EIN3 binding

bioRxiv preprint doi: https://doi.org/10.64898/2026.07.10.737652; this version posted July 10, 2026. The copyright holder for this preprint (which was not certified by peer review) is the author/funder. All rights reserved. No reuse allowed without permission.

765 experiments. Binding data were evaluated using Initial Fluorescence (ENAP1-EIN2) or MST
766 trace analysis (ENAP1-EIN3) and fitted with a logistic model in Origin. Data represent mean
767 +/- SD from three independent measurements (n = 3). **C)** Heatmap representation of (K_D)
768 values (µM) for ENAP1 binding to EIN2 and EIN3 truncations. Higher affinity is shown in red,
769 lower affinity in blue.

770

771 **Figure 4: Competitive MST analysis of EIN2-EIN3 binding in the presence of ENAP1.**
772 Microscale Thermophoresis (MST) binding curves showing the interaction between $EIN2^{479-1294}$
773 (Alexa488-labeled) and $EIN3^{1-173}$ in the absence or presence of ENAP1. ENAP1 was added
774 at concentrations corresponding to its observed binding affinity towards $EIN2^{479-1294}$ (1x K_D =
775 0.2 µM; 5 x K_D = 1 µM). Binding data were evaluated using Initial Fluorescence analysis and
776 fitted with a logistic model in Origin. Data represent mean +/- SD from three independent
777 measurements (n = 3).

778

779 **Figure 5: Yeast Two Hybrid (Y2H) analysis of EIN2-EIN3 interactions and EIN3**
780 **dimerization.**
781 **A)** Interaction between $EIN2^{479-1294}$ fused to the GAL4 binding domain (BD) and EIN3
782 truncations fused to the GAL4 activation domain (AD). AH109 yeast co-transformants were
783 spotted in 10-fold serial dilution ($OD_{600} = 10^{-1} – 10^{-4}$) on SD-LW medium (transformation control)
784 and SD-LWH medium (interaction selection) supplemented with 0.5 mM 3-AT. Images were
785 taken after 3 days (SD-LW), or 8 days (SD-LWH). The bHLH039-Fit-C pair served as positive
786 control as previously reported[27], while empty vectors served as negative controls. Arrows
787 indicate positive interactions. **B)** Interaction analysis of AD-EIN3 and BD-EIN2 truncations,
788 performed as described in panel A. **C)** Auto-activation assays of BD-EIN3 truncations. **D)** EIN3
789 dimerization analysis. $BD\text{-}EIN3^{1-306}$ was transformed with different AD-EIN3 truncations and
790 tested as described in panel A. Arrows indicate interactions.

791

792 **Figure 6: *In planta* nuclear localization of EIN2 as well as EIN3 truncations.**
793 **A)** Confocal fluorescence microscopy of EIN3 truncations fused to mCherry in transiently
794 transformed *N. benthamiana* epidermal cells. **B)** Localization of $EIN3^{1-471}$ and two NLS-deletion
795 variants fused to mCherry **C)** $EIN3^{1-85}$ and $EIN3^{1-173}$ fused to the C-terminal NLS (residues 377-
796 384) and mCherry **D)** Confocal fluorescence microscopy of EIN2 truncations fused to GFP. In
797 all panels, white arrows indicate nuclei and scale bars represent 20 µm.

bioRxiv preprint doi: https://doi.org/10.64898/2026.07.10.737652; this version posted July 10, 2026. The copyright holder for this preprint (which was not certified by peer review) is the author/funder. All rights reserved. No reuse allowed without permission.

Figure 7: *In planta* FLIM-FRET analysis of EIN2-EIN3 interactions in *N. benthamiana*. **A)** FLIM-FRET measurements using EIN2$^{479–1294}$, EIN2$^{1042-1294}$, and EIN2$^{1215-1294}$ fused to GFP as donors and full-length EIN3 fused to mCherry as acceptor. **B)** FLIM-FRET experiments using EIN2$^{479–1294}$-GFP as donor and EIN3$^{1-85}$-mCherry and EIN3$^{1-173}$-mCherry as acceptors. **C)** FLIM-FRET experiments using EIN2$^{1042–1294}$ fused to GFP and EIN3$^{1-85}$-mCherry or EIN3$^{1-173}$-mCherry as acceptors. In all experiments, EIN2 truncations fused to GFP served as donors and EIN3 constructs fused to mCherry as acceptors. Donor-only measurements (black) were included for lifetime normalization, and mCherry fused to an NLS (mCherry-NLS) served as a negative control (red) to account for bystander FRET. The tested EIN2-EIN3 FRET pairs are depicted in blue. Due to weak nuclear localization, EIN3$^{1-85}$ and EIN3$^{1-173}$ were fused to the internal EIN3-NLS identified in Figure 6. Boxplots show the median (line), 25-75th percentile (box) and 10-90th percentile (whiskers) from pooled datasets comprising at least 16 measurements per condition. Values outside the 10-90th percentile are omitted for clarity. Statistical analysis was performed using Kruskal-Wallis and Dunn's multiple comparisons test. *P-value <0.05; **P-value <0.01; ***P-value <0.001; ****P-value <0.0001 (donor only vs. interaction // donor only vs. negative control // negative control vs. interaction).

Figure 8: Structural modeling, docking, and sequence conservation of EIN2 and EIN3. **A)** Docking analysis of predicted interaction interfaces between EIN3$^{86-173}$ and EIN2 truncations. Structural models were generated using I-TASSER [37] and are shown in ribbon and surface representation. EIN3$^{86-173}$ is highlighted in blue, whereas EIN2$^{479-663}$ and its truncated variants are shown in orange. Docking results were ranked by HADDOCK score, with more negative values indicating more favorable interactions. **B)** Reciprocal docking of EIN2$^{464-674}$ against sequential EIN3 segments. **C)** Fine-mapping of the interaction surface using overlapping EIN3 fragments (residues 86-215) docked against EIN2$^{464-674}$. **D)** Representative structural models of *Arabidopsis thaliana* EIN3 and *At*EIN2$^{479-1294}$. The EIN3 core binding regions (residues 86-173 and 86-100) are highlighted in blue and pink, respectively, while the DNA binding domain (residues 174-206) is marked in green. EIN2 models are depicted in orange with the identified core binding region (residues 646-674) highlighted in yellow. **E)** Predicted EIN3-DNA complex (Haddock score of -37). DNA is shown in yellow, whereas EIN3 fragments follow the color scheme in panel D). **F) and G)** Multiple sequence alignment of EIN2 (B) and EIN3 (C) orthologs from ten angiosperm species (*A. thaliana*, *C. arabica*, *A. chinensis*, *S. tuberosum*, *S. lycopersicum*, *C. papaya*, *M. acuminata*, *V. vinifera*, *H. annuus* and *N. attenuate)*. Alignments include conservation plots, annotated functional domains, predicted binding regions, protein constructs used in this study, and nuclear localization signals (NLSs).

bioRxiv preprint doi: https://doi.org/10.64898/2026.07.10.737652; this version posted July 10, 2026. The copyright holder for this preprint (which was not certified by peer review) is the author/funder. All rights reserved. No reuse allowed without permission.

833 Conserved regions corresponding to the predicted EIN2-EIN3 interaction interface are
834 highlighted.

835

bioRxiv preprint doi: https://doi.org/10.64898/2026.07.10.737652; this version posted July 10, 2026. The copyright holder for this preprint (which was not certified by peer review) is the author/funder. All rights reserved. No reuse allowed without permission.

836 **FIGURE 1**

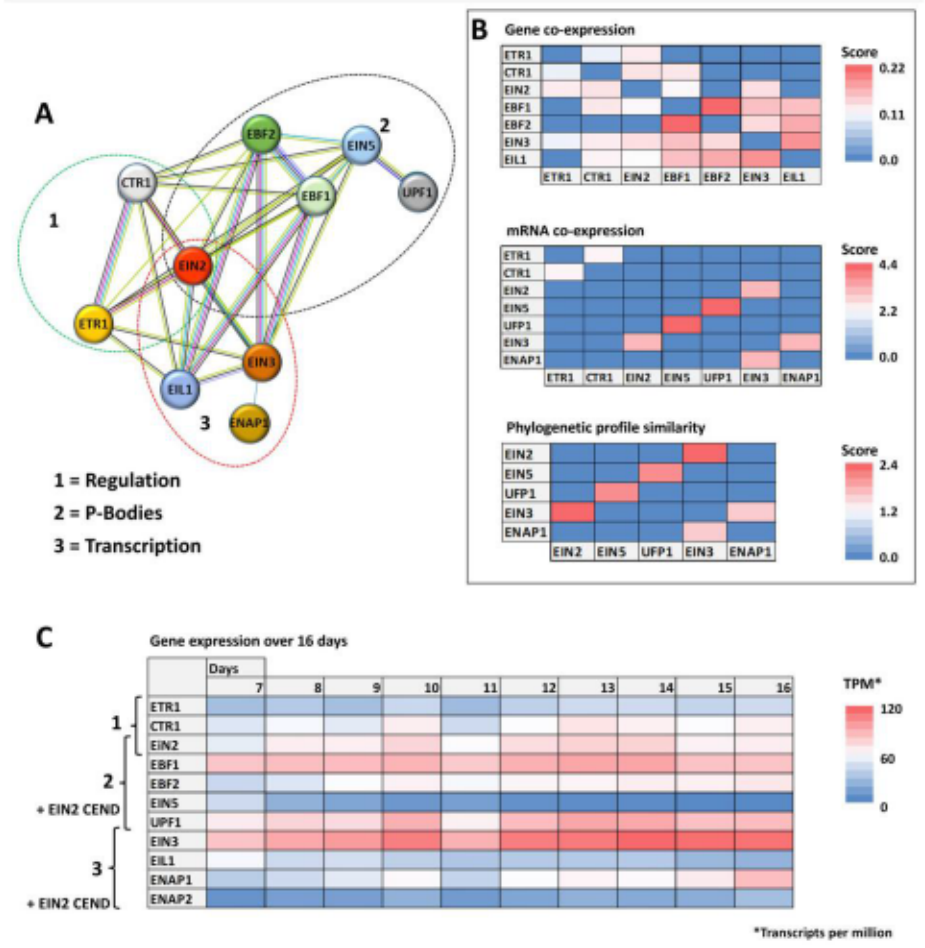

837

838

839

840

841

842

843

844

bioRxiv preprint doi: https://doi.org/10.64898/2026.07.10.737652; this version posted July 10, 2026. The copyright holder for this preprint (which was not certified by peer review) is the author/funder. All rights reserved. No reuse allowed without permission.

FIGURE 2

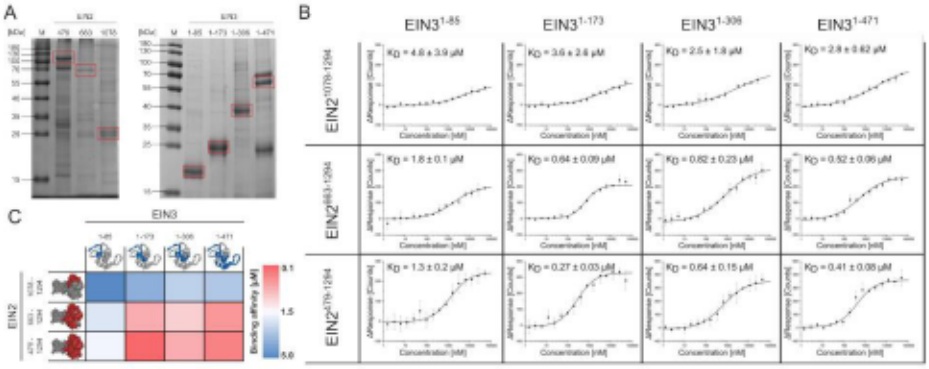

bioRxiv preprint doi: https://doi.org/10.64898/2026.07.10.737652; this version posted July 10, 2026. The copyright holder for this preprint (which was not certified by peer review) is the author/funder. All rights reserved. No reuse allowed without permission.

FIGURE 3

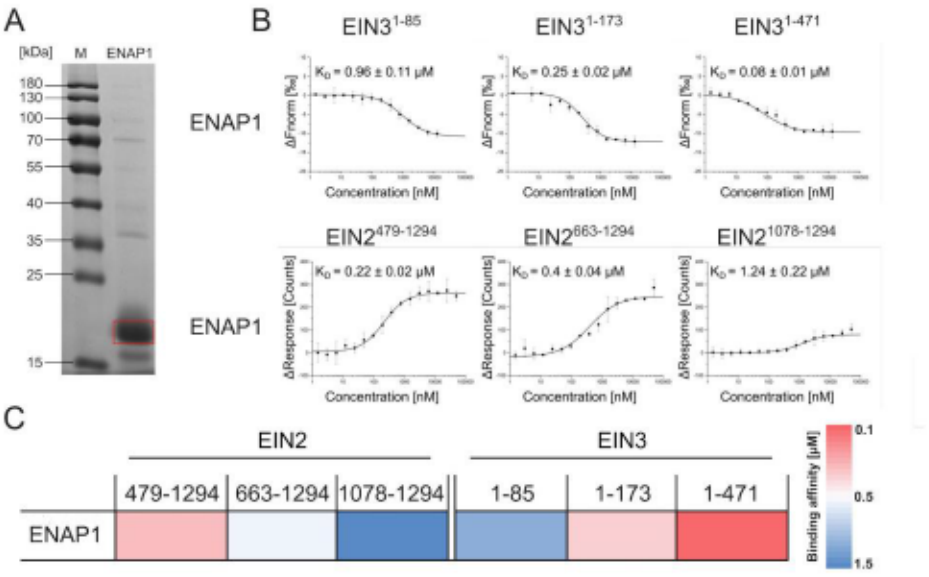

bioRxiv preprint doi: https://doi.org/10.64898/2026.07.10.737652; this version posted July 10, 2026. The copyright holder for this preprint (which was not certified by peer review) is the author/funder. All rights reserved. No reuse allowed without permission.

881 **FIGURE 4**

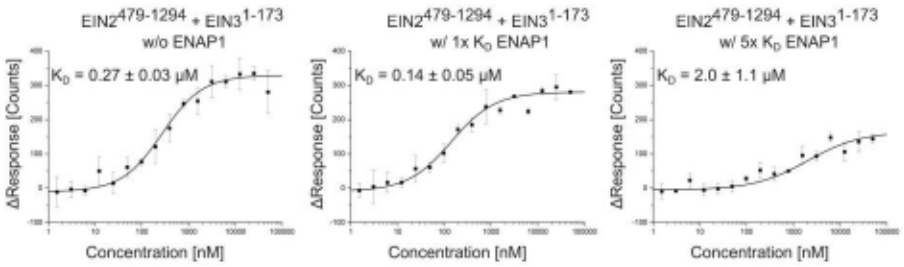

882

883

884

885

886

887

888

889

890

891

892

893

894

895

896

897

898

899

900

901

902

bioRxiv preprint doi: https://doi.org/10.64898/2026.07.10.737652; this version posted July 10, 2026. The copyright holder for this preprint (which was not certified by peer review) is the author/funder. All rights reserved. No reuse allowed without permission.

FIGURE 5

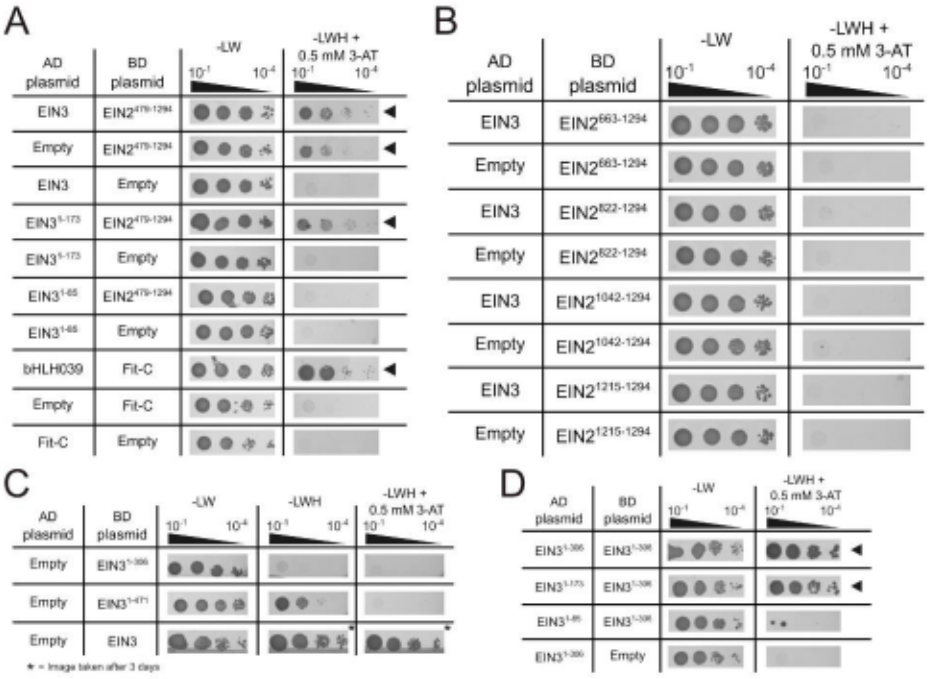

bioRxiv preprint doi: https://doi.org/10.64898/2026.07.10.737652; this version posted July 10, 2026. The copyright holder for this preprint (which was not certified by peer review) is the author/funder. All rights reserved. No reuse allowed without permission.

FIGURE 6

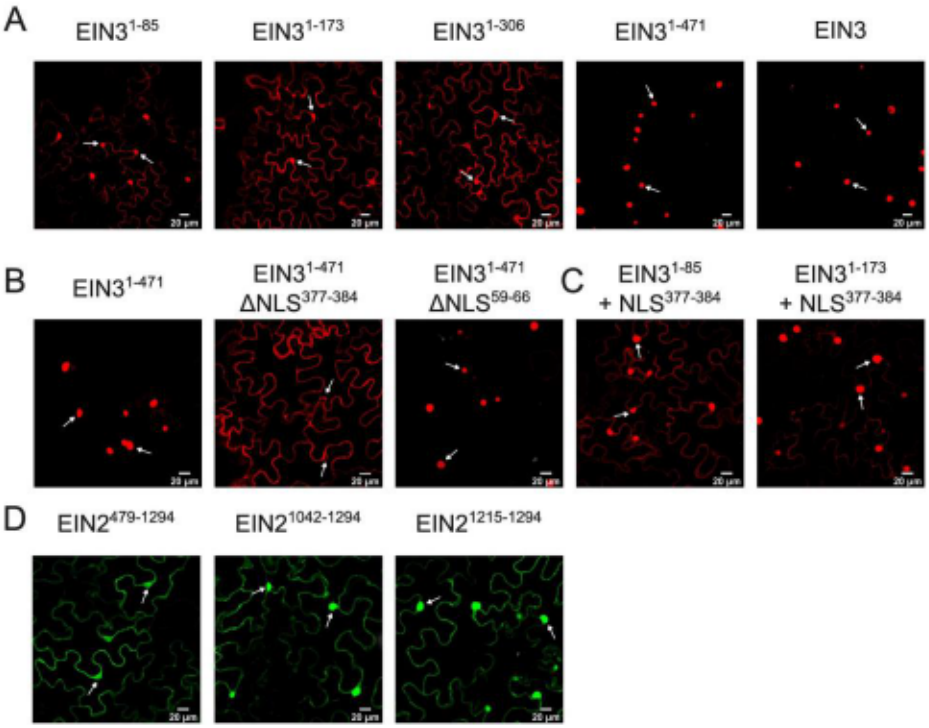

bioRxiv preprint doi: https://doi.org/10.64898/2026.07.10.737652; this version posted July 10, 2026. The copyright holder for this preprint (which was not certified by peer review) is the author/funder. All rights reserved. No reuse allowed without permission.

FIGURE 7

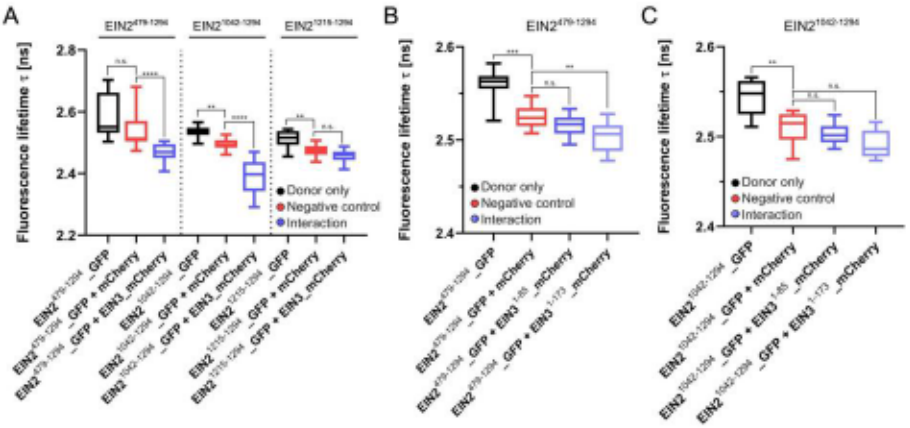

bioRxiv preprint doi: https://doi.org/10.64898/2026.07.10.737652; this version posted July 10, 2026. The copyright holder for this preprint (which was not certified by peer review) is the author/funder. All rights reserved. No reuse allowed without permission.

951 **FIGURE 8**

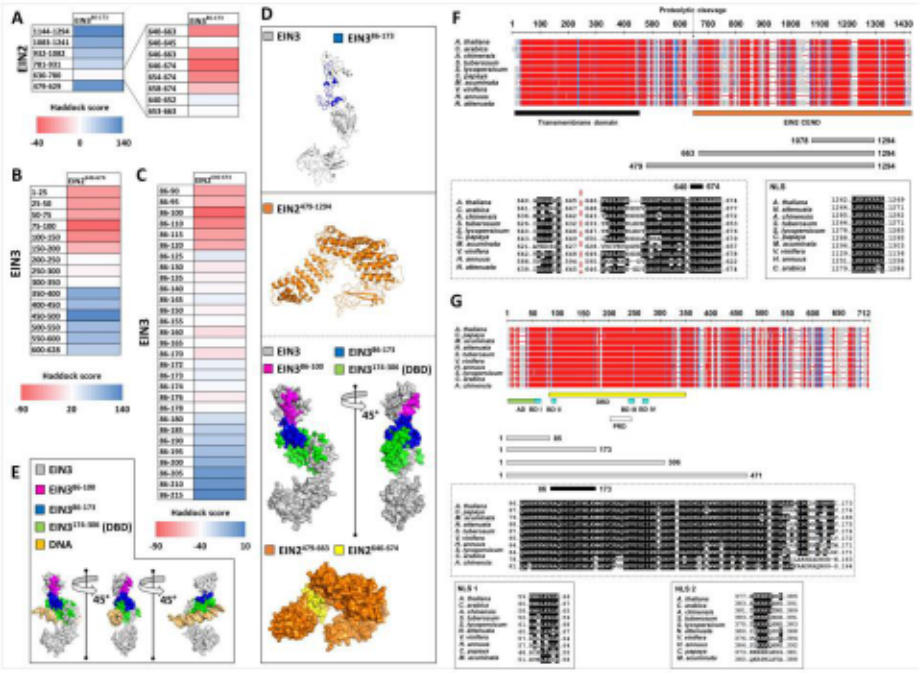

952

Supporting Information

Structural Mapping of the EIN2–EIN3 Interaction Core and Its Integration with ENAP1 in Ethylene Signaling

Fabian Wynen, Meik Thiele, Maya Hettesheimer, Raphael Josef Eberle, Jan Eric Maika, Rüdiger Simon and Georg Groth

Table of contents

Fig. S1. *In vitro* MST binding analysis of representative negative controls.
Fig. S2. Y2H assay with positive hits of the EIN2-EIN3 interaction with different 3-AT concentrations (1, 2, and 3 mM) after 10, 12 and 14 days.
Table S1. Binding Energies and size of the docking clusters analyzed in Figure 8A.
Table S2. Binding Energies and size of the docking clusters analyzed in Figure 8B.
Table S3. Binding Energies and size of the docking clusters analyzed in Figure 8C.
Table S4. Information of the EIN2 and EIN3 sequences used in the multiple sequence alignment.

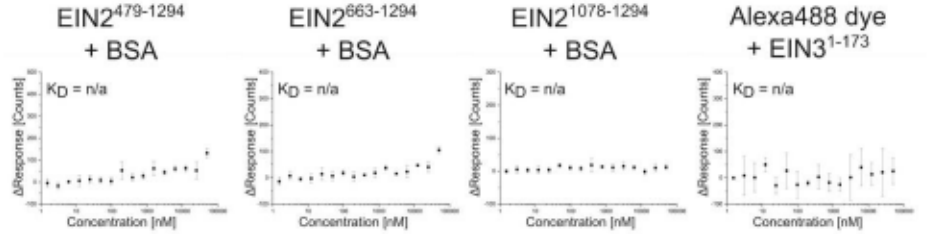

Figure S1: *In vitro* MST binding analysis of representative negative controls. Binding of labeled EIN2 truncations was tested against BSA to check for unspecific interaction. To eliminate unspecific dye interactions, $EIN3^{1-173}$ was used as a representative and titrated against the Alexa488 dye. MST binding data were analyzed via Initial Fluorescence analysis and curves were fitted using the Logistic Fit function in Origin. Data points represent mean values and standard deviation based on three independent measurements (n = 3).

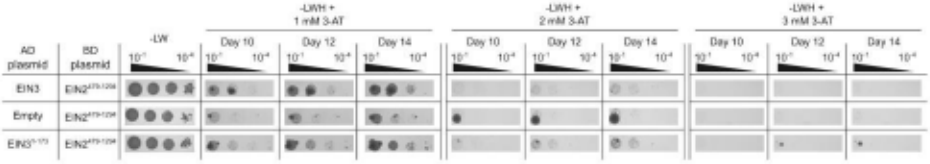

Figure S2: Y2H assay with positive hits of the EIN2-EIN3 interaction with different 3-AT concentrations (1, 2, and 3 mM) after 10, 12 and 14 days. $EIN2^{479-1294}$ was fused to the binding domain of GAL4 (BD plasmid), whereas EIN3 truncations were fused to the activation domain of GAL4 (AD plasmid). Yeast strain AH109 co-transformed with both plasmids was spotted in a 10-fold serial dilution (OD_{600} = 10^{-1} – 10^{-4}) on synthetic defined (SD) agar plates lacking leucine and tryptophane (-LW) (transformation control) as well as lacking leucine, tryptophane and histidine (-LWH) (selection for protein interaction). SD -LWH agar plates additionally contained either 1, 2 or 3 mM 3-amino-1,2,4-triazole (3-AT) for better selectivity. Images of SD -LW plates were taken after three days, while -LWH plates were imaged after 10,12, and 14 days.

Table S1. Binding Energies and size of the docking clusters analyzed in Figure 8A.

	Energy				
Complex	Van der walls [kcal/mol]	Electrostatic [kcal/mol]	Desolvation [kcal/mol]	Cluster size	Score
$EIN2^{479-629}$-$EIN3^{86-173}$	-29.7 ± 4.2	-373.8 ± 58.2	30.7 ± 7.0	8	110
$EIN2^{630-780}$-$EIN3^{86-173}$	-44.0 ± 18.0	-123.9 ± 37.9	-23.1 ± 1.5	10	9
$EIN2^{781-931}$-$EIN3^{86-173}$	-39.7 ± 3.9	-166.8 ± 54.8	-7.6 ± 3.4	11	47
$EIN2^{932-1082}$-$EIN3^{86-173}$	-32.7 ± 3.7	-393.7 ± 112.8	2.8 ± 1.7	7	63
$EIN2^{1083-1241}$-$EIN3^{86-173}$	-27.7 ± 3.3	-290.9 ± 48.9	17.1 ± 2.5	7	90
$EIN2^{1144-1294}$-$EIN3^{86-173}$	-21.6 ± 2.9	-389.4 ± 73.7	26.9 ± 3.4	6	120
$EIN2^{640-663}$-$EIN3^{86-173}$	-29.7 ± 4.8	-213.3 ± 28.2	-2.4 ± 0.9	26	-30
$EIN2^{640-645}$-$EIN3^{86-173}$	-20.5 ± 3.4	-91.7 ± 25.3	8.0 ± 1.4	17	10
$EIN2^{646-663}$-$EIN3^{86-173}$	-31.9 ± 4.6	-316.0 ± 48.3	1.7 ± 0.3	41	-30
$EIN2^{646-674}$-$EIN3^{86-173}$	-22.2 ± 9.7	-271.3 ± 21.7	-4.4 ± 0.9	14	-40
$EIN2^{654-674}$-$EIN3^{86-173}$	-28.0 ± 7.8	-142.3 ± 16.9	-3.3 ± 0.5	14	-30
$EIN2^{658-674}$-$EIN3^{86-173}$	-19.6 ± 7.1	-196.3 ± 37.4	-2.9 ± 0.9	25	-10
$EIN2^{640-652}$-$EIN3^{86-173}$	-13.1 ± 6.8	-132.7 ± 49.1	-2.6 ± 0.6	16	20
$EIN2^{653-663}$-$EIN3^{86-173}$	-18.5 ± 6.7	-108.7 ± 13.8	7.1 ± 1.2	19	10

Table S2. Binding Energies and size of the docking clusters analyzed in Figure 8B.

	Energy				
Complex	Van der Walls [kcal/mol]	Electrostatic [kcal/mol]	Desolvation [kcal/mol]	Cluster size	Score
$EIN3^{1-25}$-$EIN2^{646-674}$	-29.4 ± 3.5	-188.5 ± 9.5	-4.8 ± 1.0	15	-40
$EIN3^{25-50}$-$EIN2^{646-674}$	-25.9 ± 1.6	-230.4 ± 9.5	-5.5 ± 1.3	17	-40
$EIN3^{50-75}$-$EIN2^{646-674}$	-27.2 ± 2.7	-215.4 ± 20.4	-6.1 ± 2.9	11	-30
$EIN3^{75-100}$-$EIN2^{646-674}$	-38.1 ± 4.7	-239.0 ± 20.9	-9.2 ± 1.2	56	-90
$EIN3^{100-150}$-$EIN2^{646-674}$	-31.7 ± 3.0	-240.0 ± 15.7	-11.5 ± 2.1	12	-55
$EIN3^{150-200}$-$EIN2^{646-674}$	-37.3 ± 5.3	-187.1 ± 15.0	-6.2 ± 1.1	29	-10
$EIN3^{200-250}$-$EIN2^{646-674}$	-15.6 ± 3.4	-328.4 ± 44.5	6.9 ± 1.5	16	60
$EIN3^{250-300}$-$EIN2^{646-674}$	-19.2 ± 8.1	-81.9 ± 39.4	5.6 ± 1.7	22	50
$EIN3^{300-350}$-$EIN2^{646-674}$	-17.1 ± 4.6	-113.2 ± 28.6	8.4 ± 2.2	14	60
$EIN3^{350-400}$-$EIN2^{646-674}$	-27.3 ± 4.8	-117.5 ± 41.9	14.9 ± 1.8	11	110
$EIN3^{400-450}$-$EIN2^{646-674}$	-33.2 ± 2.6	-61.4 ± 14.7	16.6 ± 2.1	25	100
$EIN3^{450-500}$-$EIN2^{646-674}$	-24.3 ± 3.2	-119.5 ± 24.1	21.6 ± 2.5	15	130
$EIN3^{500-550}$-$EIN2^{646-674}$	-26.6 ± 2.4	-177.6 ± 31.8	15.3 ± 1.8	19	100
$EIN3^{550-600}$-$EIN2^{646-674}$	-22.6 ± 3.2	-129.8 ± 34.5	18.3 ± 1.1	15	100
$EIN3^{600-628}$-$EIN2^{646-674}$	-25.4 ± 4.4	-103.1 ± 33.1	17.5 ± 2.9	25	90

Table S3. Binding Energies and size of the docking clusters analyzed in Figure 8C.

	Energy				
Complex	Van der Walls [kcal/mol]	Electrostatic [kcal/mol]	Desolvation [kcal/mol]	Cluster size	Score
$EIN3^{86-90}$-$EIN2^{646-674}$	-28.4 ± 3.8	-246.4 ± 16.4	-12.6 ± 2.0	17	-70
$EIN3^{86-95}$-$EIN2^{646-674}$	-26.8 ± 5.0	-202.6 ± 36.7	-15.8 ± 1.2	13	-65
$EIN3^{86-100}$-$EIN2^{646-674}$	-31.2 ± 1.5	-255.9 ± 11.9	-16.2 ± 2.1	28	-90
$EIN3^{86-110}$-$EIN2^{646-674}$	-29.9 ± 6.5	-249.1 ± 15.0	-16.6 ± 1.3	22	-80
$EIN3^{86-115}$-$EIN2^{646-674}$	-35.2 ± 5.1	-124.4 ± 38.6	-14.2 ± 3.1	17	-71
$EIN3^{86-120}$-$EIN2^{646-674}$	-40.9 ± 6.6	-80.7 ± 16.9	-18.2 ± 0.7	19	-67
$EIN3^{86-125}$-$EIN2^{646-674}$	-29.5 ± 3.3	-204.2 ± 17.8	-6.0 ± 2.0	17	-32
$EIN3^{86-130}$-$EIN2^{646-674}$	-25.8 ± 1.7	-179.9 ± 44.5	-6.1 ± 1.1	16	-46
$EIN3^{86-135}$-$EIN2^{646-674}$	-30.3 ± 3.3	-276.6 ± 51.8	-3.2 ± 1.9	15	-43
$EIN3^{86-140}$-$EIN2^{646-674}$	-23.5 ± 6.6	-200.1 ± 45.7	-6.9 ± 1.4	12	-42
$EIN3^{86-145}$-$EIN2^{646-674}$	-25.4 ± 4.9	-195.7 ± 32.8	-7.6 ± 2.1	17	-35
$EIN3^{86-150}$-$EIN2^{646-674}$	-26.5 ± 5.5	-220.9 ± 41.3	-6.5 ± 2.0	12	-43
$EIN3^{86-155}$-$EIN2^{646-674}$	-15.7 ± 5.3	-240.1 ± 44.1	-8.3 ± 3.2	11	-40
$EIN3^{86-160}$-$EIN2^{646-674}$	-24.6 ± 4.5	194.6 ± 23.1	-10.3 ± 3.9	13	-50
$EIN3^{86-165}$-$EIN2^{646-674}$	-21.7 ± 3.4	-216.9 ± 17.9	-5.5 ± 2.2	12	-40
$EIN3^{86-170}$-$EIN2^{646-674}$	-25.8 ± 5;2	-190.8 ± 12.7	-10.3 ± 2.2	13	-50
$EIN3^{86-172}$-$EIN2^{646-674}$	-14.0 ± 4.2	-227.2 ± 27.3	-3.9 ± 1.5	10	-35
$EIN3^{86-173}$-$EIN2^{646-674}$	-14.1 ± 3.9	-226.2 ± 29.9	-4.0 ± 1.7	14	-35
$EIN3^{86-174}$-$EIN2^{646-674}$	-29.2 ± 7.1	-201.3 ± 34.7	-2.5 ± 0.8	12	-38
$EIN3^{86-176}$-$EIN2^{646-674}$	-30.6 ± 3.4	-287.8 ± 24.4	-4.7 ± 1.1	11	-45
$EIN3^{86-178}$-$EIN2^{646-674}$	-28.6 ± 6.3	-213.3 ± 6.3	-1.1 ± 0.4	14	-40
$EIN3^{86-180}$-$EIN2^{646-674}$	-35.1 ± 1.4	-288.5 ± 44.4	-1.6 ± 0.6	11	-27
$EIN3^{86-185}$-$EIN2^{646-674}$	-25.2 ± 4.3	-308.6 ± 75.5	-5.5 ± 2.4	11	-21
$EIN3^{86-190}$-$EIN2^{646-674}$	-30.4 ± 9.4	-143.0 ± 22.3	-9.3 ± 3.8	10	-19
$EIN3^{86-195}$-$EIN2^{646-674}$	-19.7 ± 5.7	-273.6 ± 41.8	15.0 ± 4.7	12	-13
$EIN3^{86-200}$-$EIN2^{646-674}$	-22.4 ± 4.3	-302.7 ± 81.7	14.1 ± 4.3	15	-8
$EIN3^{86-205}$-$EIN2^{646-674}$	-39.5 ± 6.7	309.9 ± 5.4	26.0 ± 0.5	6	3
$EIN3^{86-210}$-$EIN2^{646-674}$	-30.1 ± 6.1	-250.2 ± 17.6	15.0 ± 0.4	11	5
$EIN3^{86-215}$-$EIN2^{646-674}$	-46.3 ± 7.9	-300.2 ± 7.2	28.0 ± 2.0	12	10

Table S4. Information of the EIN2 and EIN3 sequences used in the multiple sequence alignment.

Protein	Species	Uniprot ID
EIN2	*Arabidopsis thaliana*	Q9S814
EIN3		O24606
EIN2	*Vitis vinifera*	F6HR32
EIN3		A0A438JCI9
EIN2	*Helianthus annuus*	A0A251UC58
EIN3		A0A251SIP3
EIN2	*Nicotiana attentuata*	A0A142IX47
EIN3		A0A1J6HTH5
EIN2	*Solanum tuberosum*	M1BY00
EIN3		M1A5I7
EIN2	*Solanum lycopersicum*	A0A3Q7HW43
EIN3		Q94FV4
EIN2	*Coffea arabica*	A0A6P6SYT8
EIN3		A0A6P6TVG4
EIN2	*Actinidia chinensis*	A0A2R6PWM2
EIN3		A0A075EAR5
EIN2	*Carica papaya*	AIO12155.1
EIN3		A0A0R5PE43
EIN2	*Musa acuminata*	065046552.1
EIN3		A1IIY3

4 Discussion

Ethylene is a small gaseous molecule and the chemically simplest plant hormone (Abeles, 1992; Bakshi *et al.*, 2015). Due to its pivotal role in a broad range of plant developmental processes, including senescence or fruit ripening (Bakshi et al., 2015), further understanding of the underlying molecular mechanism of the ethylene signaling pathway is of great relevance. This becomes even more evident considering the forecasted population growth of about 25 % within the next 25 years (Sadigov, 2022). Therefore, the ethylene signaling pathway represents a significant target both scientifically and agronomically. Ethylene functions as a negative regulator in the ethylene signaling pathway by inhibiting ER membrane-localized receptors responsible for ethylene perception. This, in turn, prevents proteasomal degradation of the key regulator EIN2, resulting in its nuclear localization and transcriptional activation in response to ethylene (Ju et al., 2012). The ethylene signaling pathway has been extensively studied for decades, leading to the identification of its core components, the elucidation of copper transport to ethylene receptors, and the determination of first crystal structures of soluble receptor domains (Binder, 2020; Dluhosch et al., 2024; Hoppen et al., 2019b; Mayerhofer et al., 2015; Müller-Dieckmann et al., 1999). However, several aspects remain unresolved, including the structures of full-length receptors, signal transduction from the ER to the nucleus, and nuclear events upon ethylene perception.

The thesis aimed to unravel the molecular mechanisms regarding EIN2-mediated signal transduction and the subsequent nuclear events leading to ethylene-responsive gene regulation. In this context, the investigation of EIN3 for a better understanding of its molecular characteristics and functional domains was indispensable.

Previous studies in our lab identified a nuclear localization sequence (NLS) located at the C-terminal region of EIN2 (amino acids 1262-1269) from which a peptide, called NOP-1, was derived (Bisson and Groth, 2011). Based on this NLS, it was hypothesized that the strongly conserved and well-known IMPα/IMPβ transport machinery, involved in the nucleocytoplasmic shuttling of proteins, is responsible for EIN2-mediated signal transduction upon ethylene perception. Triple response analyses of *impα* single and triple mutants provided evidence for the involvement of the IMPα superfamily in the

ethylene pathway, as the triple response is a well-established phenotypic marker to identify ethylene-related proteins (Chapter 3.1, Figure 2). However, no differences in ethylene sensitivity were observed among the individual triple mutants, indicating functional redundancy within the IMPα superfamily. Consequently, the contribution of individual IMPα isoforms to EIN2 nuclear trafficking could not be resolved. Ideally, mutant seedlings retaining only a single functional IMPα isoform would allow a clear assessment of the contribution of individual isoforms. Given the pivotal role of this shuttle pathway in translocation of numerous proteins and the observation of a dwarfed phenotype already present in the *impα1;impα2;impα3* triple mutant (Lüdke et al., 2021), mutants carrying additional *impα* mutations might have more severe growth defects, potentially complicating or even precluding their phenotypic characterization (Sang et al., 2020; Strasser et al., 2010; Wang et al., 2021). Nevertheless, as only one of the five triple mutants displayed a dwarfed phenotype, the generation and analysis of quadruple or quintuple mutants may still be feasible. Focusing on combinations other than the *impα1;impα2;impα3* mutant may avoid severe developmental defects while enabling a more detailed characterization of isoform-specific functions and functional redundancy. Furthermore, the triple mutants used in this thesis included only five of the nine IMPα genes in total. Hence, triple response approaches including the four remaining IMPα variants in different combinations might provide further insights.

As the triple response experiments did not resolve functional specificity among IMPα isoforms regarding EIN2 nucleocytoplasmic transport, *in vitro* binding studies using purified IMPα proteins and NOP-1 were performed (Chapter 3.1, Figure 3). The octa-peptide NOP-1, derived from the EIN2 nuclear localization sequence, served as a proxy for EIN2 binding. All nine IMPα proteins were found to bind NOP-1. Unlike the triple response experiments, FP measurements revealed differences in binding affinity towards NOP-1 among the isoforms, with IMPα1-4 and IMPα7 exhibiting the highest affinities. Notably, IMPα7 was only investigated without its IBB domain due to insolubility of the full-length IMPα7. Under physiological conditions, IMPβ interacts with the IBB domain of IMPα. Otherwise, the IBB domain is stated to possess an auto-inhibitory effect competing with the cargo NLS for the IMPα binding sites, which might alter the binding affinity depending on the presence of the IBB domain. However, the IBB domain of IMPα1 had no substantial effect on binding affinity. This is in line with previous reports indicating reduced or lack of auto-inhibition in individual isoforms,

also including higher organisms such as *Arabidopsis thaliana* and *Homo sapiens* (Dey and Patankar, 2018). The extent of auto-inhibition varies even among IMPα isoforms within the same species and is additionally cargo-dependent (Pumroy and Cingolani, 2015; Pumroy et al., 2015). Therefore, auto-inhibitory properties have to be evaluated individually for each IMPα isoform-cargo combination. Consequently, the *in vitro* results of the IBB-deficient IMPα7 isoform should be interpreted with caution, despite the lack of evidence for auto-inhibition of IMPα1 in the FP experiments. Additional competitive FP measurements, as well as BLI experiments with NOP-1 and some derivatives (N41P-1 and GB1_EIN2$^{1215-1281}$), confirmed the specificity of this interaction (Chapter 3.1, Figure 4 and 5). Interestingly, the affinity decreased with increasing EIN2 sequence as observed in both competitive FP measurements and BLI binding studies. This observation was unexpected but might be related to immobilization effects in the BLI experiments or steric hindrances, especially for the GB1 fusion construct. Furthermore, larger constructs might require more or tighter stabilization for stronger binding, which is physiologically mediated by IMPβ proteins. To address this, future studies could determine binding affinities in the presence of IMPβ proteins, particularly since IMPβ1 has been identified as a mediator of EIN2 trafficking (Lu et al., 2023). In contrast to the results presented in this thesis, Lu et al. (2023) observed binding only between IMPβ1 and EIN2, but no interaction between several IMPα isoforms and EIN2 in split-ubiquitin yeast two-hybrid (SUB-Y2H) experiments. Although the split-ubiquitin assay provides several advantages compared to the conventional Y2H setup, it is still very sensitive regarding correct folding and protein aggregation. Proper folding, especially in the split-ubiquitin system, might be hampered since one interaction partner requires fusion to partial ubiquitin and additionally to an external transcription factor. Thus, these limitations may account for the observed inconsistency. Furthermore, this discrepancy might be explained by the relatively high error susceptibility regarding false-positive and false-negative results of the Y2H system in general (Mehla et al., 2018).

The obtained binding results between the IMPα superfamily and NOP-1 as a proxy for EIN2 were further substantiated by *in planta* investigations using IMPα1-7 fused to YFP (YELLOW FLUORESCENT PROTEIN) and EIN2$^{479-1294}$ fused to CER (CERULEAN). Six of the seven IMPα isoforms interacted with EIN2 *in planta*, indicated by a decay in fluorescence lifetime of the donor, whereas IMPα5 exhibited signal reduction

comparable to the negative control (Chapter 3.1, Figure 8). This corroborates the observed binding affinities, with IMPα5 showing one of the weakest affinities towards NOP-1. The lowest FRET efficiency (2.8 %), and therefore weakest binding, of all interacting isoforms was observed for IMPα2, which was unexpected from the *in vitro* experiments, where IMPα2 exhibited strong binding towards NOP-1 (5.8 µM). Furthermore, localization studies with EIN2$^{479-1294}$-CER and its NLS-deficient variant confirmed the significance of the NLS for nuclear import (Wen et al., 2012), as nuclear accumulation of NLS-deficient EIN2 was completely abolished (Chapter 3.1, Figure 7). However, EIN2$^{479-1294}$-CER was found in the nucleus even in the absence of co-expressed IMPα proteins. This observation is likely explained by endogenous IMPα/β proteins mediating EIN2 trafficking, which is supported by the high sequence identity (approximately 57 %) and sequence similarity (approximately 69 %) between *A. thaliana* and *N. benthamiana* IMPα proteins. The closest orthologs display substantially higher conservation (Lüdke *et al.*, 2021). Moreover, endogenous IMPβ proteins likely account for the observed nuclear localization of *At*IMPα proteins, as IMPα isoforms function solely as adaptor molecules and have not been reported to mediate nuclear trafficking independently, unlike IMPβ proteins (Xiong et al., 2021). Nevertheless, even if endogenous IMPα/β proteins may interact with the transiently expressed proteins, they are unlikely to affect the FLIM-FRET measurements because only fluorescently labeled proteins contribute to the detected signal.

Collectively, the combination of phenotypic analysis, *in vitro* binding studies, and *in planta* experiments verified the involvement of the IMPα superfamily in nucleocytoplasmic transport of EIN2. Despite functional redundancy within this family, distinct binding characteristics suggest that IMPα1, IMPα3-4, and IMPα7 may contribute more strongly to EIN2 recognition than the remaining isoforms. Together, these findings close an important gap between ethylene perception at the ER membrane and downstream nuclear signaling.

Despite the functional insights obtained in this work, the molecular basis of IMPα-EIN2 recognition remains poorly understood. Therefore, structural predictions using AlphaFold2 (Jumper et al., 2021) based on the crystal structure of *At*IMPα3 lacking the IBB domain (PDB: 4TNM) (Wirthmueller et al., 2015) and NOP-1 were performed (Chapter 3.1, Figure 6). However, these predictions failed to reliably identify crucial amino acids involved in this interaction, resulting in a lack of further mechanistic

insights. Even without using crystal structures, several benchmarking studies demonstrated a great potential of structural prediction tools for precise protein-peptide complex prediction (Ko and Lee, 2021; Wang et al., 2025; Zhang et al., 2026). However, the prediction accuracy of peptides becomes more difficult as chemical complexity increases. Structures of chemically-modified peptides are therefore harder to predict than peptide conformations of short peptides such as antimicrobial peptides, anticancer peptides or signaling peptides (e.g. NOP-1) (Zhang *et al.*, 2026). Additionally, precise structure prediction of protein-peptide complexes is challenging as peptide conformation may depend on the protein binding surface or proteins may undergo small structural transitions upon binding (Zhang *et al.*, 2026). Although the accuracy of predicting protein-peptide complexes has significantly improved with new-generation tools such as AlphaFold3, Chai-1, Boltz-1, and Protenix, these methods can still suffer from overfitting, meaning that the use of advanced prediction tools does not necessarily guarantee a more accurate structure prediction (Zhou et al., 2025). As the data of this thesis did not allow reliable prediction of whether NOP-1 binds to the major or the minor NLS-binding site of IMPα, structural analysis of IMPα/EIN2(-NLS) complexes by X-ray crystallography or cryo-EM is indispensable to provide molecular and structural insights into the IMPα/EIN2 binding mode. Additionally, incorporation of IMPβ1 to reconstitute the physiological ternary complex may enhance the complex stability and thereby increase the likelihood of successful structure elucidation. Besides, complementary binding studies using IMPα proteins carrying site-directed mutations might provide further insights into the molecular basis for EIN2 binding. Especially, the aspartate residue at position 319 (D319) located in the minor binding site may represent a suitable target, as this residue is mutated in IMPα5 (D319S), IMPα8 (D319H), and IMPα9 (D319P), which exhibited the weakest binding affinities towards NOP-1. If the affinity decreases in IMPα isoforms carrying mutations at position D319, this supports the hypothesis of minor site-specific binding while simultaneously providing additional molecular insights. To determine whether NOP-1 preferentially binds to the major or the minor NLS-binding site, IMPα isoforms carrying mutations in all residues predicted to mediate NOP-1 binding at either site represent a suitable experimental approach. An isoform completely mutated in both binding sites simultaneously should be used as a negative control to exclude potential compensatory effects of the two binding clefts since NLS binding occurs mostly

preferential and not exclusively. Thus, while the work of this thesis provided evidence about the functional role of the IMPα superfamily in EIN2 nuclear trafficking, the molecular basis of cargo recognition remains an important objective for future studies.

After shedding light on the nucleocytoplasmic transport of EIN2, the focus was subsequently placed on downstream events upon nuclear entry of EIN2, including the characterization of EIN3, the key component of ethylene-responsive gene expression.

ENAP1 has been proposed to bridge EIN2 and EIN3 in a ternary complex that regulates histone modifications and transcriptional activation upon ethylene signaling (He and Lehming, 2003; Zhang et al., 2016). Therefore, these proteins were investigated to gain mechanistic insights into their functional relationship. The combined data from MST, Y2H, and FLIM-FRET studies demonstrated for the first time that EIN2 directly interacts with EIN3 (Chapter 3.2, Figure 2, 5A, and 7). Furthermore, amino acids 86-173 of EIN3 were identified as crucial for mediating EIN2 binding. While the *in vitro* binding studies and Y2H analysis suggested the necessity of the complete C-terminal domain (residues 479-1294) for EIN3 interaction, *in planta* FLIM-FRET data revealed an additional interaction between EIN3 and the distal EIN2 region (residues 1042-1294), suggesting that EIN2 contains multiple binding interfaces for EIN3. However, these results did not resolve whether the distal C-terminal domain of EIN2 is sufficient to activate ethylene responses or whether the complete cytosolic domain is required. Since only BD-EIN2$^{479-1294}$, but none of the shorter EIN2 constructs, exhibited unexpected reporter activity in Y2H studies, it is reasonable to assume that the complete C-terminal domain of EIN2 is necessary for mediating ethylene responses through a prospective role in transcriptional activation together with EIN3 (Chapter 3.2, Figure 5B). The inability of the distal EIN2 region to activate ethylene responses is additionally reflected by the distinct binding mode outside of the EIN3 core binding domain. However, further investigation is needed to confirm this hypothesis and determine the minimal EIN2 sequence necessary for activating ethylene responses. This question could be addressed by performing rescue experiments using EIN2 truncations to complement ethylene-insensitive *ein2* mutants and restore the triple response phenotype. Based on the results, *ein2* mutants are expected to be rescued by expression of EIN2$^{479-1294}$, which has been previously shown in our lab (Bisson and Groth, 2010), but not by substantially shorter truncations of EIN2. As the used EIN2 constructs span a large gap between residues 663 and

1042, the precise determination of the minimal sequence required for phenotypic rescue might be limited. Thus, introducing additional truncations between residues 663 and 1042 may allow a more refined mapping of this region.

Following the identification of direct EIN2-EIN3 interaction, the proposed role of ENAP1 within this regulatory complex was subsequently investigated. The previously reported binding of ENAP1 to both EIN2 and EIN3 was confirmed by our studies (Zhang et al., 2017). Moreover, the binding affinities of ENAP1-EIN2 and ENAP1-EIN3 complexes were comparable (Chapter 3.2, Figure 3). Notably, ENAP1-EIN3 interaction did not increase the initial fluorescence, in contrast to experiments using EIN2 as a fluorophore. Elevation of initial fluorescence is usually attributable to direct binding of the dye or changes in the electrostatic surrounding of the fluorophore. The latter may be caused by either conformational changes or ligand binding in close proximity to the dye (Jerabek-Willemsen et al., 2011; Seidel et al., 2013). However, control experiments excluded dye-binding artifacts, suggesting changes in the electrostatic environment as the most likely explanation for the observed fluorescence increase (Chapter 3.2, Figure S1). If EIN2 undergoes conformational transitions, this information could be pioneering for future structural elucidation efforts, including potential trapping approaches to increase EIN2 stability. Therefore, whether the increase in fluorescence is induced by conformational changes or due to spatial proximity to the dye should be further investigated. This might be approached by using dyes with different reactive groups, leading to alternate labeling positions in the EIN2 fluorophore. If the initial fluorescence still increases upon EIN3 titration, this would support conformational transitions rather than ligand binding in dye proximity. However, binding in dye proximity may still occur even when using alternative dyes due to lack of labeling control. Therefore, methods such as NMR, hydrogen-deuterium exchange coupled with mass spectrometry (HDX-MS), or EPR with methanethiosulfonate spin labeled (MTSSL) cysteine residues should be considered to unravel potential conformational dynamics within EIN2 (Ishima and Torchia, 2000; Kaltashov and Eyles, 2002; Kugele et al., 2022). Furthermore, competitive MST binding studies revealed concentration-dependent competition between ENAP1 and EIN3 for binding of EIN2 (Chapter 3.2, Figure 4). This is in line with the fact that both ENAP1 and EIN3 exhibited the highest affinity towards the longest EIN2 construct, and therefore, might compete for the same EIN2 binding site. These results suggest a model involving several binary

complexes comprising either ENAP1, EIN2, and EIN3, rather than the simultaneous formation of a single ternary complex to regulate transcriptional activity. However, it remains unclear whether a ternary complex is formed or whether binding occurs sequentially. This question could be addressed by techniques such as size exclusion chromatography coupled with multi-angle light scattering (SEC-MALS), which allows the characterization of protein complexes (Some et al., 2019). In addition, surface-bound binding assays, which are highly suitable for determining kinetics, such as surface plasmon resonance (SPR) or biolayer interferometry (BLI) may provide further mechanistic insights into the binding events (Bates et al., 2025; Lipschultz et al., 2000).

Together, these findings provide the first evidence that EIN2 directly interacts with EIN3. Furthermore, the observed concentration-dependent competition between EIN3 and ENAP1 refines the current model of the ethylene signaling pathway by suggesting that transcriptional regulation may involve sequential protein interactions rather than the formation of a stable ternary complex.

A comprehensive understanding of the ethylene pathway additionally requires the characterization of the functional architecture of EIN3. Although it has not been conclusively demonstrated that EIN3 binds DNA as a homodimer, the dimeric form binds DNA with higher affinity than monomeric EIN3, indicating that dimerization promotes stable DNA recognition (Song et al., 2015). To date, the dimerization of EIN3 has been experimentally proven to involve amino acids 113-257 (Solano et al., 1998). Furthermore, the DNA core binding domain (residues 174-306) was identified and structurally solved by X-ray crystallography (PDB: 4ZDS) (Song et al., 2015). Besides, little is known about EIN3 and its functional regions. The work of this thesis provided evidence of a highly functional EIN3 region (amino acids 86-173) responsible for mediating protein-protein interactions with distinct proteins. As observed in Y2H studies, the same region was sufficient for homodimerization of EIN3, thereby further mapping the dimerization domain of EIN3 to amino acids 113-173 (Chapter 3.2, Figure 5D). This supports the hypothesis of a multi-step process for regulation of transcriptional activity since binding of EIN3, EIN2, and ENAP1 within the EIN3 core binding domain (residues 86-173) is unlikely to occur simultaneously. Consistent with this hypothesis, docking analyses refined the predicted EIN2-EIN3 binding interface to residues 120-173, overlapping with the EIN3 homodimerization

domain (residues 113-173). However, whether the protein interactions are all mediated by the same amino acids within this region has to be further investigated e.g. by introducing additional protein truncations to precisely determine the minimal amino acid sequence for binding. Additionally, structural prediction tools combined with sequence analysis could be used to generate potential loss-of-function mutants to obtain information about the distinct binding modes. Moreover, the Y2H data suggest that the major transcriptional activation domain of EIN3 is located in its C-terminal region beyond amino acid 471 (Chapter 3.2, Figure 5C). While the reporter activity of BD-EIN3$^{1-471}$ was completely abolished by 0.5 mM 3-AT, the auto-activation of full-length EIN3 remained unaffected under the same conditions. This interpretation is further supported by previous Y2H studies showing that BD-EIN3$^{1-299}$ lacks reporter activity (Wawrzyńska and Sirko, 2016). Sequence analysis using PredictNLS (Cokol et al., 2000) together with *in planta* localization data suggest that EIN3 contains two putative NLSs located at amino acids 59-66 and 377-384. The phenomenon of a protein containing several NLSs instead of a single one is also found for other transcription factors. Several mutagenesis studies of various transcription factors revealed synergistic effects regarding nuclear import (Luo et al., 2004; Theodore et al., 2008). However, since deletion of the C-terminal NLS (amino acids 377-384) markedly reduced nuclear accumulation, whereas deletion of the N-terminal NLS (amino acids 59-66) did not substantially affect nuclear localization, such synergistic effects are unlikely for EIN3 (Chapter 3.2, Figure 6). The functional mapping of EIN3 achieved in this thesis is pioneering for future studies to gain even deeper insights into the roles of its distinct domains. Applying the aforementioned rescue approach to complement *ein3* mutants with various EIN3 truncations would enable a more precise dissection of transcription-related domains in a physiological environment. Besides phenotypical analysis, these complemented plant lines could also be used for qPCR analysis of genes that are directly or indirectly regulated by EIN3, such as *ERF1*, *EDF1-4*, or *EBF2* (Chang et al., 2013b; Konishi and Yanagisawa, 2008; Solano et al., 1998), thereby further elucidating EIN3 regions required for transcriptional regulation. Notably, the requirement to retain both the DNA-binding domain and the NLS in these rescue experiments restricts the range of truncations that can be analyzed, potentially limiting the conclusions that can be drawn. Nevertheless, these constraints still permit the investigation of substantial N- and C-terminal regions flanking the DNA-binding

domain and the NLS to gain valuable insights into EIN3-mediated transcriptional regulation.

Taken together, the functional mapping of EIN3 presented in this thesis establishes a functional framework for understanding how distinct EIN3 regions contribute to protein-protein interactions, homodimerization, nuclear import, and transcriptional regulation.

The research regarding ethylene signaling provided in this thesis aimed at strengthening our understanding of the underlying molecular mechanisms and paving the way to contribute to translational science. As mentioned, due to its pivotal role in seed germination, leaf senescence, and fruit ripening, the ethylene signaling pathway is a suitable target for the agricultural economy. One possibility to influence fruit ripening would be the generation of transgenic lines with altered proteins (e.g. IMPα proteins) exhibiting stronger or weaker interactions, which might be coupled to faster or slower ethylene responses and thus faster or slower fruit ripening, respectively. However, apart from the lack of controllability, the use of transgenic lines for practical application may face regulatory challenges within the EU. Moreover, due to the strong redundancy within the IMPα superfamily regarding nucleocytoplasmic transport of EIN2, targeting this superfamily may not represent an effective strategy to modulate fruit ripening. Another, more suitable option for practical applications would be the use of peptide-based active compounds, similar to NOP-1, as inhibitors for specific protein interactions. NOP-1 is an octa-peptide derived from the NLS of EIN2, which has been shown to delay floral senescence in cut flowers and fruit ripening in tomato (Bisson et al., 2016; Hoppen et al., 2019a). Compared to established ethylene inhibitors such as aminoethoxyvinyl-glycine (AVG) or 1-methylcyclopropene (1-MCP), which inhibit ethylene biosynthesis or ethylene perception (Sisler and Serek, 1997; Yu and Yang, 1979), respectively, peptide-based inhibitors offer the opportunity to selectively target individual protein-protein interactions within the ethylene pathway (Apostolopoulos et al., 2021). 1-MCP has been associated with impaired ethylene-dependent defense responses and increased disease susceptibility in several plant species (Blankenship and Dole, 2003). In contrast, the increased target specificity of peptide-based active compounds potentially reduces undesired effects on other ethylene-regulated processes. Regardless of the molecular target, the application of active compounds allows fine-tuned control of the fruit ripening process by adjusting the timing and

concentration of treatment. The domain mapping of EIN3 presented in this thesis may facilitate the development of additional peptide inhibitors. A peptide library containing peptides derived from the identified protein-protein interaction domain (residues 86-173) could be applied to climacteric fruits and vegetables such as apples, tomatoes, or bananas to assess their effects on fruit ripening. Successful candidates could be iteratively modified to identify peptides that affect fruit ripening with enhanced efficacy. Notably, since the resulting active compounds would be derived from EIN3, they would likely exert their effect by inhibiting binding between EIN2 and EIN3 in the nucleus. This requires the active compound to be cell-penetrating and additionally capable of nuclear localization. Given the usual size of peptides, passive diffusion into the nucleus is considered feasible and therefore may not require an explicitly encoded NLS (Fei et al., 2011). However, cellular uptake could be facilitated by established cell-penetrating peptide sequences (Milletti, 2012). EIN3-derived peptides may be able to bind EIN2 even in the cytoplasm, thereby preventing IMPα docking and subsequent nuclear trafficking, as EIN3 is hypothesized to induce conformational changes in EIN2. Hence, this would not require nuclear localization of EIN3-derived peptides, similar to NOP-1. However, the NLS of EIN2, from which NOP-1 is derived, has been reported to fulfill multiple functions beyond mediating nucleocytoplasmic transport. It is involved in regulatory processes, including binding of EBF1/2 mRNA, and has also been shown to interact with other components of the ethylene signaling pathway, such as ETR1 (Bisson and Groth, 2015; Li *et al.*, 2015). Consequently, EIN3-derived peptides may enable more specific interference with individual protein-protein interactions.

In conclusion, the work presented in this thesis substantially advances the current molecular understanding of the ethylene signaling pathway by addressing previously unresolved questions regarding nucleocytoplasmic transport of EIN2 and subsequent nuclear events involving the central transcription factor EIN3. The Importin-α superfamily together with Importin-β proteins were identified as mediators that bridge the ethylene signal, perceived at the ER membrane, to the nucleus. Upon nuclear entry, EIN2 directly interacts with EIN3, while competition between EIN3 and ENAP1 for the EIN2 binding site suggests that transcriptional regulation is mediated through multi-step protein interactions and is thereby more dynamic than previously anticipated. Finally, functional mapping of EIN3 established the contribution of distinct

regions to homodimerization, protein-protein interactions, nuclear localization, and transcriptional regulation.

5 Literature

Aasland, R. (1996). The SANT domain: a putative DNA-binding domain in the SWI-SNF and ADA complexes, the transcriptional co-repressor N-CoR and TFIIIB. Trends Biochem. Sci. **21**:87-88.
Abeles, F. (1992). Roles and physiological effects of ethylene in plant physiology: dormancy, growth, and development. Ethylene in plant biology.
Abramson, J., Adler, J., Dunger, J., Evans, R., Green, T., Pritzel, A., Ronneberger, O., Willmore, L., Ballard, A.J., and Bambrick, J. (2024). Accurate structure prediction of biomolecular interactions with AlphaFold 3. Nature **630**:493-500.
Allen, M.D., Yamasaki, K., Ohme-Takagi, M., Tateno, M., and Suzuki, M. (1998). A novel mode of DNA recognition by a β-sheet revealed by the solution structure of the GCC-box binding domain in complex with DNA. The EMBO journal **17**:5484-5496.
Alonso, J.M., Hirayama, T., Roman, G., Nourizadeh, S., and Ecker, J.R. (1999). EIN2, a bifunctional transducer of ethylene and stress responses in Arabidopsis. Science **284**:2148-2152.
Alonso, J.M., Stepanova, A.N., Solano, R., Wisman, E., Ferrari, S., Ausubel, F.M., and Ecker, J.R. (2003). Five components of the ethylene-response pathway identified in a screen for weak ethylene-insensitive mutants in Arabidopsis. Proceedings of the National Academy of Sciences **100**:2992-2997. doi:10.1073/pnas.0438070100.
An, F., Zhao, Q., Ji, Y., Li, W., Jiang, Z., Yu, X., Zhang, C., Han, Y., He, W., and Liu, Y. (2010). Ethylene-induced stabilization of ETHYLENE INSENSITIVE3 and EIN3-LIKE1 is mediated by proteasomal degradation of EIN3 binding F-box 1 and 2 that requires EIN2 in Arabidopsis. The Plant Cell **22**:2384-2401.
Apostolopoulos, V., Bojarska, J., Chai, T.-T., Elnagdy, S., Kaczmarek, K., Matsoukas, J., New, R., Parang, K., Lopez, O.P., Parhiz, H., et al. (2021). A Global Review on Short Peptides: Frontiers and Perspectives. Molecules **26**:430.
Bakshi, A., Shemansky, J.M., Chang, C., and Binder, B.M. (2015). History of research on the plant hormone ethylene. Journal of Plant Growth Regulation **34**:809-827.
Bates, T.A., Gurmessa, S.K., Weinstein, J.B., Trank-Greene, M., Wrynla, X.H., Anastas, A., Anley, T.W., Hinchliff, A., Shinde, U., and Burke, J.E. (2025). Biolayer interferometry for measuring the kinetics of protein–protein interactions and nanobody binding. Nature protocols **20**:861-883.
Bayliss, R., Littlewood, T., and Stewart, M. (2000). Structural basis for the interaction between FxFG nucleoporin repeats and importin-β in nuclear trafficking. Cell **102**:99-108.
Bhattacharjee, S., Lee, L.-Y., Oltmanns, H., Cao, H., Veena, n., Cuperus, J., and Gelvin, S.B. (2008). IMPa-4, an Arabidopsis importin α isoform, is preferentially involved in Agrobacterium-mediated plant transformation. The Plant Cell **20**:2661-2680.
Binder, B.M. (2020). Ethylene signaling in plants. Journal of Biological Chemistry **295**:7710-7725.
Bischoff, F., Krebber, H., Smirnova, E., Dong, W., and Ponstingl, H. (1995). Co-activation of RanGTPase and inhibition of GTP dissociation by Ran-GTP binding protein RanBP1. The EMBO journal **14**:705-715.
Bischoff, F.R., and Görlich, D. (1997). RanBP1 is crucial for the release of RanGTP from importin β-related nuclear transport factors. FEBS letters **419**:249-254.
Bisson, M.M., and Groth, G. (2010). New insight in ethylene signaling: autokinase activity of ETR1 modulates the interaction of receptors and EIN2. Molecular Plant **3**:882-889.
Bisson, M.M., and Groth, G. (2011). New paradigm in ethylene signaling: EIN2, the central regulator of the signaling pathway, interacts directly with the upstream receptors. Plant signaling & behavior **6**:164-166.
Bisson, M.M., and Groth, G. (2015). Targeting Plant Ethylene Responses by Controlling Essential Protein-Protein Interactions in the Ethylene Pathway. Mol Plant **8**:1165-1174. 10.1016/j.molp.2015.03.014.

Bisson, M.M., Kessenbrock, M., Müller, L., Hofmann, A., Schmitz, F., Cristescu, S.M., and Groth, G. (2016). Peptides interfering with protein-protein interactions in the ethylene signaling pathway delay tomato fruit ripening. Scientific reports **6**:30634.

Blankenship, S.M., and Dole, J.M. (2003). 1-Methylcyclopropene: a review. Postharvest biology and technology **28**:1-25.

Bleecker, A.B., and Kende, H. (2000). Ethylene: a gaseous signal molecule in plants. Annual review of cell and developmental biology **16**:1-18.

Bleecker, A.B., Estelle, M.A., Somerville, C., and Kende, H. (1988). Insensitivity to ethylene conferred by a dominant mutation in Arabidopsis thaliana. Science **241**:1086-1089.

Chang, C.-W., Couñago, R.M., Williams, S.J., Boden, M., and Kobe, B. (2013a). The distribution of different classes of nuclear localization signals (NLSs) in diverse organisms and the utilization of the minor NLS-binding site inplantnuclear import factor importin-α. Plant signaling & behavior **8**:5074-5088.

Chang, C., Kwok, S.F., Bleecker, A.B., and Meyerowitz, E.M. (1993). Arabidopsis ethylene-response gene ETR1: similarity of product to two-component regulators. Science **262**:539-544.

Chang, K.N., Zhong, S., Weirauch, M.T., Hon, G., Pelizzola, M., Li, H., Huang, S.-s.C., Schmitz, R.J., Urich, M.A., and Kuo, D. (2013b). Temporal transcriptional response to ethylene gas drives growth hormone cross-regulation in Arabidopsis. elife **2**:e00675.

Chao, Q., Rothenberg, M., Solano, R., Roman, G., Terzaghi, W., and Ecker, J.R. (1997). Activation of the ethylene gas response pathway in Arabidopsis by the nuclear protein ETHYLENE-INSENSITIVE3 and related proteins. Cell **89**:1133-1144.

Chen, Y.-F., Randlett, M.D., Findell, J.L., and Schaller, G.E. (2002). Localization of the ethylene receptor ETR1 to the endoplasmic reticulum of Arabidopsis. Journal of Biological Chemistry **277**:19861-19866.

Chen, Y.-F., Gao, Z., Kerris III, R.J., Wang, W., Binder, B.M., and Schaller, G.E. (2010). Ethylene receptors function as components of high-molecular-mass protein complexes in Arabidopsis. PLoS One **5**:e8640.

Chi, N.C., and Adam, S.A. (1997). Functional domains in nuclear import factor p97 for binding the nuclear localization sequence receptor and the nuclear pore. Molecular biology of the cell **8**:945-956.

Chook, Y., and Blobel, G. (2001). Karyopherins and nuclear import. Current opinion in structural biology **11**:703-715.

Cingolani, G., Petosa, C., Weis, K., and Müller, C.W. (1999). Structure of importin-β bound to the IBB domain of importin-α. Nature **399**:221-229.

Cingolani, G., Bednenko, J., Gillespie, M.T., and Gerace, L. (2002). Molecular basis for the recognition of a nonclassical nuclear localization signal by importin β. Molecular cell **10**:1345-1353.

Clark, K.L., Larsen, P.B., Wang, X., and Chang, C. (1998). Association of the Arabidopsis CTR1 Raf-like kinase with the ETR1 and ERS ethylene receptors. Proceedings of the National Academy of Sciences **95**:5401-5406.

Cokol, M., Nair, R., and Rost, B. (2000). Finding nuclear localization signals. The EMBO Reports **1**:411-415.

Conti, E., and Kuriyan, J. (2000). Crystallographic analysis of the specific yet versatile recognition of distinct nuclear localization signals by karyopherin α. Structure **8**:329-338.

Damelin, M., and Silver, P.A. (2000). Mapping interactions between nuclear transport factors in living cells reveals pathways through the nuclear pore complex. Molecular cell **5**:133-140.

Davis, L.I. (1995). The nuclear pore complex. Annual review of biochemistry **64**:865-896.

Dey, V., and Patankar, S. (2018). Molecular basis for the lack of auto-inhibition of Plasmodium falciparum importin α. Biochemical and biophysical research communications **503**:1792-1797.

Dingwall, C., and Laskey, R.A. (1991). Nuclear targeting sequences—a consensus? Trends in biochemical sciences **16**:478-481.

Dluhosch, D., Kersten, L.S., Schott-Verdugo, S., Hoppen, C., Schwarten, M., Willbold, D., Gohlke, H., and Groth, G. (2024). Structure and dimerization properties of the plant-specific copper chaperone CCH. Scientific Reports **14**:19099.

Dolgikh, V.A., Pukhovaya, E.M., and Zemlyanskaya, E.V. (2019). Shaping ethylene response: the role of EIN3/EIL1 transcription factors. Frontiers in Plant Science **10**:1030.

Ecker, J.R. (1995). The ethylene signal transduction pathway in plants. Science **268**:667-675.

Fei, L., Ren, L., Zaro, J.L., and Shen, W.-C. (2011). The influence of net charge and charge distribution on cellular uptake and cytosolic localization of arginine-rich peptides. Journal of Drug Targeting **19**:675-680.

Feng, Y., Xu, P., Li, B., Li, P., Wen, X., An, F., Gong, Y., Xin, Y., Zhu, Z., and Wang, Y. (2017). Ethylene promotes root hair growth through coordinated EIN3/EIL1 and RHD6/RSL1 activity in Arabidopsis. Proceedings of the National Academy of Sciences **114**:13834-13839.

Floer, M., Blobel, G., and Rexach, M. (1997). Disassembly of RanGTP-karyopherin β complex, an intermediate in nuclear protein import. Journal of Biological Chemistry **272**:19538-19546.

Fontes, M.R., Teh, T., and Kobe, B. (2000). Structural basis of recognition of monopartite and bipartite nuclear localization sequences by mammalian importin-α. Journal of molecular biology **297**:1183-1194.

Fontes, M.R., Teh, T., Jans, D., Brinkworth, R.I., and Kobe, B. (2003). Structural basis for the specificity of bipartite nuclear localization sequence binding by importin-α. Journal of Biological Chemistry **278**:27981-27987.

Forbes, D.J., Travesa, A., Nord, M.S., and Bernis, C. (2015). Nuclear transport factors: global regulation of mitosis. Current opinion in cell biology **35**:78-90.

Fu, L., Liu, Y., Qin, G., Wu, P., Zi, H., Xu, Z., Zhao, X., Wang, Y., Li, Y., and Yang, S. (2021). The TOR–EIN2 axis mediates nuclear signalling to modulate plant growth. Nature **591**:288-292.

Funabiki, H. (2005). Two birds with one stone—dealing with nuclear transport and spindle assembly. Cell **121**:157-158.

Gallie, D., and Young, T. (2004). The ethylene biosynthetic and perception machinery is differentially expressed during endosperm and embryo development in maize. Molecular Genetics and Genomics **271**:267-281.

Gamble, R.L., Coonfield, M.L., and Schaller, G.E. (1998). Histidine kinase activity of the ETR1 ethylene receptor from Arabidopsis. Proceedings of the National Academy of Sciences **95**:7825-7829.

Gao, Z., Chen, Y.-F., Randlett, M.D., Zhao, X.-C., Findell, J.L., Kieber, J.J., and Schaller, G.E. (2003). Localization of the Raf-like Kinase CTR1 to the Endoplasmic Reticulum of Arabidopsis through Participation in Ethylene Receptor Signaling Complexes *. Journal of Biological Chemistry **278**:34725-34732. 10.1074/jbc.M305548200.

Goldfarb, D.S., Corbett, A.H., Mason, D.A., Harreman, M.T., and Adam, S.A. (2004). Importin α: a multipurpose nuclear-transport receptor. Trends in cell biology **14**:505-514.

Görlich, D., and Kutay, U. (1999). Transport between the cell nucleus and the cytoplasm. Annual review of cell and developmental biology **15**:607-660.

Görlich, D., Henklein, P., Laskey, R.A., and Hartmann, E. (1996a). A 41 amino acid motif in importin-alpha confers binding to importin-beta and hence transit into the nucleus. The EMBO journal **15**:1810-1817.

Görlich, D., Panté, N., Kutay, U., Aebi, U., and Bischoff, F.R. (1996b). Identification of different roles for RanGDP and RanGTP in nuclear protein import. The EMBO journal **15**:5584-5594.

Grefen, C., Städele, K., Růžička, K., Obrdlik, P., Harter, K., and Horák, J. (2008). Subcellular localization and in vivo interactions of the Arabidopsis thaliana ethylene receptor family members. Molecular plant **1**:308-320.

Grossman, E., Medalia, O., and Zwerger, M. (2012). Functional architecture of the nuclear pore complex. Annual review of biophysics **41**:557-584.

Guan, T., Kehlenbach, R.H., Schirmer, E.C., Kehlenbach, A., Fan, F., Clurman, B.E., Arnheim, N., and Gerace, L. (2000). Nup50, a nucleoplasmically oriented nucleoporin with a role in nuclear protein export. Molecular and cellular biology **20**:5619-5630.

Guo, A., He, K., Liu, D., Bai, S., Gu, X., Wei, L., and Luo, J. (2005). DATF: a database of Arabidopsis transcription factors. Bioinformatics **21**:2568-2569. 10.1093/bioinformatics/bti334.

Guo, H., and Ecker, J.R. (2003). Plant responses to ethylene gas are mediated by SCFEBF1/EBF2-dependent proteolysis of EIN3 transcription factor. Cell **115**:667-677.

Guo, H., and Ecker, J.R. (2004). The ethylene signaling pathway: new insights. Current opinion in plant biology **7**:40-49.

Guzman, P., and Ecker, J.R. (1990). Exploiting the triple response of Arabidopsis to identify ethylene-related mutants. The Plant Cell **2**:513-523.

Haasen, D., and Merkle, T. (2002). Characterization of an Arabidopsis thaliana Homologue of the Nuclear Export Receptor CAS by its Interaction with Importin α. Plant Biology **4**:432-439.

Hall, B.P., Shakeel, S.N., and Schaller, G.E. (2007). Ethylene receptors: ethylene perception and signal transduction. Journal of Plant Growth Regulation **26**:118-130.

He, H., and Lehming, N. (2003). Global effects of histone modifications. Briefings in Functional Genomics **2**:234-243.

Hirayama, T., Kieber, J.J., Hirayama, N., Kogan, M., Guzman, P., Nourizadeh, S., Alonso, J.M., Dailey, W.P., Dancis, A., and Ecker, J.R. (1999). RESPONSIVE-TO-ANTAGONIST1, a Menkes/Wilson disease-related copper transporter, is required for ethylene signaling in Arabidopsis. Cell **97**:383-393. 10.1016/s0092-8674(00)80747-3.

Hoppen, C., Müller, L., Albrecht, A.C., and Groth, G. (2019a). The NOP-1 peptide derived from the central regulator of ethylene signaling EIN2 delays floral senescence in cut flowers. Scientific reports **9**:1287.

Hoppen, C., Müller, L., Hänsch, S., Uzun, B., Milić, D., Meyer, A.J., Weidtkamp-Peters, S., and Groth, G. (2019b). Soluble and membrane-bound protein carrier mediate direct copper transport to the ethylene receptor family. Scientific reports **9**:10715.

Ishima, R., and Torchia, D.A. (2000). Protein dynamics from NMR. Nature structural biology **7**:740-743.

Jäkel, S., and Gürlich, D. (1998). Importin β, transportin, RanBP5 and RanBP7 mediate nuclear import of ribosomal proteins in mammalian cells. The EMBO journal **17**:4491-4502.

Jerabek-Willemsen, M., Wienken, C.J., Braun, D., Baaske, P., and Duhr, S. (2011). Molecular interaction studies using microscale thermophoresis. Assay and drug development technologies **9**:342-353.

Ju, C., Yoon, G.M., Shemansky, J.M., Lin, D.Y., Ying, Z.I., Chang, J., Garrett, W.M., Kessenbrock, M., Groth, G., and Tucker, M.L. (2012). CTR1 phosphorylates the central regulator EIN2 to control ethylene hormone signaling from the ER membrane to the nucleus in Arabidopsis. Proceedings of the National Academy of Sciences **109**:19486-19491.

Jumper, J., Evans, R., Pritzel, A., Green, T., Figurnov, M., Ronneberger, O., Tunyasuvunakool, K., Bates, R., Žídek, A., and Potapenko, A. (2021). Highly accurate protein structure prediction with AlphaFold. nature **596**:583-589.

Kalderon, D., Roberts, B.L., Richardson, W.D., and Smith, A.E. (1984a). A short amino acid sequence able to specify nuclear location. Cell **39**:499-509.

Kalderon, D., Richardson, W.D., Markham, A.F., and Smith, A.E. (1984b). Sequence requirements for nuclear location of simian virus 40 large-T antigen. Nature **311**:33-38.

Kaltashov, I.A., and Eyles, S.J. (2002). Studies of biomolecular conformations and conformational dynamics by mass spectrometry. Mass spectrometry reviews **21**:37-71.

Kieber, J.J., Rothenberg, M., Roman, G., Feldmann, K.A., and Ecker, J.R. (1993). CTR1, a negative regulator of the ethylene response pathway in Arabidopsis, encodes a member of the raf family of protein kinases. Cell **72**:427-441.

Ko, J., and Lee, J. (2021). Can AlphaFold2 predict protein-peptide complex structures accurately? BioRxiv:2021.2007. 2027.453972.
Kobe, B. (1999). Autoinhibition by an internal nuclear localization signal revealed by the crystal structure of mammalian importin α. Nature structural biology **6**:388-397.
Konishi, M., and Yanagisawa, S. (2008). Ethylene signaling in Arabidopsis involves feedback regulation via the elaborate control of EBF2 expression by EIN3. The Plant Journal **55**:821-831.
Kosugi, S., Hasebe, M., Matsumura, N., Takashima, H., Miyamoto-Sato, E., Tomita, M., and Yanagawa, H. (2009). Six classes of nuclear localization signals specific to different binding grooves of importin α. Journal of Biological Chemistry **284**:478-485.
Kugele, A., Uzun, B., Müller, L., Schott-Verdugo, S., Gohlke, H., Groth, G., and Drescher, M. (2022). Mapping the helix arrangement of the reconstituted ETR1 ethylene receptor transmembrane domain by EPR spectroscopy. RSC advances **12**:7352-7356.
Kutay, U., Bischoff, F.R., Kostka, S., Kraft, R., and Görlich, D. (1997). Export of importin α from the nucleus is mediated by a specific nuclear transport factor. Cell **90**:1061-1071.
Lacey, R.F., and Binder, B.M. (2014). How plants sense ethylene gas—The ethylene receptors. Journal of inorganic biochemistry **133**:58-62.
Lange, A., Mills, R.E., Lange, C.J., Stewart, M., Devine, S.E., and Corbett, A.H. (2007). Classical nuclear localization signals: definition, function, and interaction with importin α. Journal of biological chemistry **282**:5101-5105.
Lee, S.J., Matsuura, Y., Liu, S.M., and Stewart, M. (2005). Structural basis for nuclear import complex dissociation by RanGTP. Nature **435**:693-696.
Li, W., Ma, M., Feng, Y., Li, H., Wang, Y., Ma, Y., Li, M., An, F., and Guo, H. (2015). EIN2-directed translational regulation of ethylene signaling in Arabidopsis. Cell **163**:670-683.
Lipschultz, C.A., Li, Y., and Smith-Gill, S. (2000). Experimental design for analysis of complex kinetics using surface plasmon resonance. Methods **20**:310-318.
Liu, H.-H., Xiong, F., Duan, C.-Y., Wu, Y.-N., Zhang, Y., and Li, S. (2019). Importin β4 mediates nuclear import of GRF-interacting factors to control ovule development in Arabidopsis. Plant Physiology **179**:1080-1092.
Lorenzo, O., Piqueras, R., Sánchez-Serrano, J.J., and Solano, R. (2003). ETHYLENE RESPONSE FACTOR1 integrates signals from ethylene and jasmonate pathways in plant defense. The Plant Cell **15**:165-178.
Lott, K., and Cingolani, G. (2011). The importin β binding domain as a master regulator of nucleocytoplasmic transport. Biochimica et Biophysica Acta (BBA)-Molecular Cell Research **1813**:1578-1592.
Lu, K., Zhang, L., Qin, L., Chen, X., Wang, X., Zhang, M., and Dong, H. (2023). Importin β1 mediates nuclear entry of EIN2C to confer the phloem-based defense against aphids. International Journal of Molecular Sciences **24**:8545.
Lüdke, D., Roth, C., Kamrad, S.A., Messerschmidt, J., Hartken, D., Appel, J., Hörnich, B.F., Yan, Q., Kusch, S., and Klenke, M. (2021). Functional requirement of the Arabidopsis importin-α nuclear transport receptor family in autoimmunity mediated by the NLR protein SNC1. The Plant Journal **105**:994-1009.
Luo, M., Pang, C.M., Gerken, A.E., and Brock, T.G. (2004). Multiple nuclear localization sequences allow modulation of 5-lipoxygenase nuclear import. Traffic **5**:847-854.
Ma, B., Zhou, Y., Chen, H., He, S.-J., Huang, Y.-H., Zhao, H., Lu, X., Zhang, W.-K., Pang, J.-H., and Chen, S.-Y. (2018). Membrane protein MHZ3 stabilizes OsEIN2 in rice by interacting with its Nramp-like domain. Proceedings of the National Academy of Sciences **115**:2520-2525.
Marfori, M., Lonhienne, T.G., Forwood, J.K., and Kobe, B. (2012). Structural basis of high-affinity nuclear localization signal interactions with importin-α. Traffic **13**:532-548.
Matsuura, Y., and Stewart, M. (2005). Nup50/Npap60 function in nuclear protein import complex disassembly and importin recycling. The EMBO journal **24**:3681.

Mayerhofer, H., Panneerselvam, S., Kaljunen, H., Tuukkanen, A., Mertens, H.D., and Mueller-Dieckmann, J. (2015). Structural model of the cytosolic domain of the plant ethylene receptor 1 (ETR1). Journal of Biological Chemistry **290**:2644-2658.

Mehla, J., Caufield, J.H., and Uetz, P. (2018). Making the right choice: critical parameters of the Y2H systems. In Two-Hybrid Systems: Methods and Protocols, (Springer: pp. 17-28.

Milletti, F. (2012). Cell-penetrating peptides: classes, origin, and current landscape. Drug discovery today **17**:850-860.

Moroianu, J. (1997). Molecular mechanisms of nuclear protein transport. Critical Reviews™ in Eukaryotic Gene Expression **7**.

Moroianu, J. (1999). Nuclear import and export pathways. Journal of cellular biochemistry **75**:76-83.

Moroianu, J., Blobel, G., and Radu, A. (1996). Nuclear protein import: Ran-GTP dissociates the karyopherin alphabeta heterodimer by displacing alpha from an overlapping binding site on beta. Proceedings of the National Academy of Sciences **93**:7059-7062.

Moussatche, P., and Klee, H.J. (2004). Autophosphorylation Activity of the Arabidopsis Ethylene Receptor Multigene Family *. Journal of Biological Chemistry **279**:48734-48741. 10.1074/jbc.M403100200.

Müller-Dieckmann, H.-J., Grantz, A.A., and Kim, S.-H. (1999). The structure of the signal receiver domain of the Arabidopsis thaliana ethylene receptor ETR1. Structure **7**:1547-1556.

Nakano, T., Suzuki, K., Fujimura, T., and Shinshi, H. (2006). Genome-wide analysis of the ERF gene family in Arabidopsis and rice. Plant physiology **140**:411-432.

Neville, M., Stutz, F., Lee, L., Davis, L.I., and Rosbash, M. (1997). The importin-beta family member Crm1p bridges the interaction between Rev and the nuclear pore complex during nuclear export. Current Biology **7**:767-775.

O'Reilly, A.J., Dacks, J.B., and Field, M.C. (2011). Evolution of the karyopherin-β family of nucleocytoplasmic transport factors; ancient origins and continued specialization. PloS one **6**:e19308.

Palma, K., Zhang, Y., and Li, X. (2005). An importin α homolog, MOS6, plays an important role in plant innate immunity. Current Biology **15**:1129-1135.

Park, M.Y., Wu, G., Gonzalez-Sulser, A., Vaucheret, H., and Poethig, R.S. (2005). Nuclear processing and export of microRNAs in Arabidopsis. Proceedings of the National Academy of Sciences **102**:3691-3696.

Potuschak, T., Lechner, E., Parmentier, Y., Yanagisawa, S., Grava, S., Koncz, C., and Genschik, P. (2003). EIN3-dependent regulation of plant ethylene hormone signaling by two Arabidopsis F box proteins: EBF1 and EBF2. Cell **115**:679-689.

Pumroy, R.A., and Cingolani, G. (2015). Diversification of importin-α isoforms in cellular trafficking and disease states. Biochemical Journal **466**:13-28.

Pumroy, R.A., Ke, S., Hart, D.J., Zachariae, U., and Cingolani, G. (2015). Molecular determinants for nuclear import of influenza A PB2 by importin α isoforms 3 and 7. Structure **23**:374-384.

Qiao, H., Chang, K.N., Yazaki, J., and Ecker, J.R. (2009). Interplay between ethylene, ETP1/ETP2 F-box proteins, and degradation of EIN2 triggers ethylene responses in Arabidopsis. Genes & development **23**:512-521.

Qiao, H., Shen, Z., Huang, S.-s.C., Schmitz, R.J., Urich, M.A., Briggs, S.P., and Ecker, J.R. (2012). Processing and subcellular trafficking of ER-tethered EIN2 control response to ethylene gas. Science **338**:390-393.

Quimby, B., and Corbett, A. (2001). Nuclear transport mechanisms. Cellular and Molecular Life Sciences CMLS **58**:1766-1773.

Riechmann, J.L., Heard, J., Martin, G., Reuber, L., Jiang, C.-Z., Keddie, J., Adam, L., Pineda, O., Ratcliffe, O., and Samaha, R. (2000). Arabidopsis transcription factors: genome-wide comparative analysis among eukaryotes. science **290**:2105-2110.

Rodrıguez, F.I., Esch, J.J., Hall, A.E., Binder, B.M., Schaller, G.E., and Bleecker, A.B. (1999). A copper cofactor for the ethylene receptor ETR1 from Arabidopsis. Science **283**:996-998.

Rout, M.P., Aitchison, J.D., Suprapto, A., Hjertaas, K., Zhao, Y., and Chait, B.T. (2000). The yeast nuclear pore complex: composition, architecture, and transport mechanism. The Journal of cell biology **148**:635-652.

Sadigov, R. (2022). Rapid growth of the world population and its socioeconomic results. The Scientific World Journal **2022**:8110229.

Sakuma, Y., Liu, Q., Dubouzet, J.G., Abe, H., Shinozaki, K., and Yamaguchi-Shinozaki, K. (2002). DNA-binding specificity of the ERF/AP2 domain of Arabidopsis DREBs, transcription factors involved in dehydration-and cold-inducible gene expression. Biochemical and biophysical research communications **290**:998-1009.

Sang, Q., Pajoro, A., Sun, H., Song, B., Yang, X., Stolze, S.C., Andrés, F., Schneeberger, K., Nakagami, H., and Coupland, G. (2020). Mutagenesis of a quintuple mutant impaired in environmental responses reveals roles for CHROMATIN REMODELING4 in the Arabidopsis floral transition. The Plant Cell **32**:1479-1500.

Schaller, G.E., and Bleecker, A.B. (1995). Ethylene-binding sites generated in yeast expressing the Arabidopsis ETR1 gene. Science **270**:1809-1811.

Schott-Verdugo, S., Müller, L., Classen, E., Gohlke, H., and Groth, G. (2019). Structural model of the ETR1 ethylene receptor transmembrane sensor domain. Scientific reports **9**:8869.

Seidel, S.A., Dijkman, P.M., Lea, W.A., van den Bogaart, G., Jerabek-Willemsen, M., Lazic, A., Joseph, J.S., Srinivasan, P., Baaske, P., and Simeonov, A. (2013). Microscale thermophoresis quantifies biomolecular interactions under previously challenging conditions. Methods **59**:301-315.

Shi, Y., Tian, S., Hou, L., Huang, X., Zhang, X., Guo, H., and Yang, S. (2012). Ethylene signaling negatively regulates freezing tolerance by repressing expression of CBF and type-A ARR genes in Arabidopsis. The Plant Cell **24**:2578-2595.

Sisler, E.C., and Serek, M. (1997). Inhibitors of ethylene responses in plants at the receptor level: recent developments. Physiologia plantarum **100**:577-582.

Solano, R., Stepanova, A., Chao, Q., and Ecker, J.R. (1998). Nuclear events in ethylene signaling: a transcriptional cascade mediated by ETHYLENE-INSENSITIVE3 and ETHYLENE-RESPONSE-FACTOR1. Genes & development **12**:3703-3714.

Solsbacher, J., Maurer, P., Bischoff, F.R., and Schlenstedt, G. (1998). Cse1p is involved in export of yeast importin α from the nucleus. Molecular and cellular biology **18**:6805-6815.

Some, D., Amartely, H., Tsadok, A., and Lebendiker, M. (2019). Characterization of proteins by size-exclusion chromatography coupled to multi-angle light scattering (SEC-MALS). J vis Exp **148**:e59615.

Song, J., Zhu, C., Zhang, X., Wen, X., Liu, L., Peng, J., Guo, H., and Yi, C. (2015). Biochemical and structural insights into the mechanism of DNA recognition by Arabidopsis ETHYLENE INSENSITIVE3. PLoS One **10**:e0137439.

Strasser, B., Sánchez-Lamas, M., Yanovsky, M.J., Casal, J.J., and Cerdán, P.D. (2010). Arabidopsis thaliana life without phytochromes. Proceedings of the National Academy of Sciences **107**:4776-4781.

Ström, A.-C., and Weis, K. (2001). Importin-beta-like nuclear transport receptors. Genome biology **2**:reviews3008. 3001.

Su, M., and Hou, S. (2024). Ethylene insensitive 2 (EIN2) destiny shaper: The post-translational modification. Journal of Plant Physiology **295**:154190.

Takizawa, C.G., Weis, K., and Morgan, D.O. (1999). Ran-independent nuclear import of cyclin B1–Cdc2 by importin β. Proceedings of the National Academy of Sciences **96**:7938-7943.

Tamura, K., and Hara-Nishimura, I. (2014). Functional insights of nucleocytoplasmic transport in plants. Frontiers in Plant Science **5**:118.

Theodore, M., Kawai, Y., Yang, J., Kleshchenko, Y., Reddy, S.P., Villalta, F., and Arinze, I.J. (2008). Multiple nuclear localization signals function in the nuclear import of the transcription factor Nrf2. Journal of Biological Chemistry **283**:8984-8994.

Thirugnanasambantham, K., Durairaj, S., Saravanan, S., Karikalan, K., Muralidaran, S., and Islam, V.I.H. (2015). Role of ethylene response transcription factor (ERF) and its regulation in response to stress encountered by plants. Plant Molecular Biology Reporter **33**:347-357.

UniProt Consortium, T. (2018). UniProt: the universal protein knowledgebase. Nucleic acids research **46**:2699-2699.

Vogel, M.O., Gomez-Perez, D., Probst, N., and Dietz, K.-J. (2012). Combinatorial signal integration by APETALA2/Ethylene Response Factor (ERF)-transcription factors and the involvement of AP2-2 in starvation response. International Journal of Molecular Sciences **13**:5933-5951.

Wang, D.Y., Wang, L., Mi, A., and Wang, J. (2025). AI-Assisted Protein–Peptide Complex Prediction in a Practical Setting. Journal of Computational Chemistry **46**:e70137.

Wang, W., Esch, J.J., Shiu, S.-H., Agula, H., Binder, B.M., Chang, C., Patterson, S.E., and Bleecker, A.B. (2006). Identification of Important Regions for Ethylene Binding and Signaling in the Transmembrane Domain of the ETR1 Ethylene Receptor of Arabidopsis. The Plant Cell **18**:3429-3442. 10.1105/tpc.106.044537.

Wang, X., Wu, Y., Liu, Z., Liu, T., Zheng, L., and Zhang, G. (2021). The pip1s quintuple mutants demonstrate the essential roles of PIP1s in the plant growth and development of Arabidopsis. International Journal of Molecular Sciences **22**:1669.

Wawrzyńska, A., and Sirko, A. (2014). To control and to be controlled: understanding the Arabidopsis SLIM1 function in sulfur deficiency through comprehensive investigation of the EIL protein family. Frontiers in Plant Science **Volume 5 - 2014**10.3389/fpls.2014.00575.

Wawrzyńska, A., and Sirko, A. (2016). EIN3 interferes with the sulfur deficiency signaling in Arabidopsis thaliana through direct interaction with the SLIM1 transcription factor. Plant Science **253**:50-57.

Wen, X., Zhang, C., Ji, Y., Zhao, Q., He, W., An, F., Jiang, L., and Guo, H. (2012). Activation of ethylene signaling is mediated by nuclear translocation of the cleaved EIN2 carboxyl terminus. Cell research **22**:1613-1616.

Wirthmueller, L., Roth, C., Fabro, G., Caillaud, M.C., Rallapalli, G., Asai, S., Sklenar, J., Jones, A.M., Wiermer, M., and Jones, J.D. (2015). Probing formation of cargo/importin-α transport complexes in plant cells using a pathogen effector. The Plant Journal **81**:40-52.

Wu, K., He, J., Pu, W., and Peng, Y. (2018). The role of exportin-5 in microRNA biogenesis and cancer. Genomics, proteomics & bioinformatics **16**:120-126.

Wynen, F., Maika, J.E., Eberle, R.J., Jahnke, N., Wiermer, M., Hartmann, L., Simon, R., and Groth, G. (2025). The importin-alpha superfamily engages in ethylene signaling by shuttling ETHYLENE INSENSITIVE 2 from the endoplasmic reticulum to the nucleus. The FEBS Journal.

Xie, F., Liu, Q., and Wen, C.-K. (2006). Receptor signal output mediated by the ETR1 N terminus is primarily subfamily I receptor dependent. Plant Physiology **142**:492-508.

Xiong, F., Groot, E.P., Zhang, Y., and Li, S. (2021). Functions of plant importin β proteins beyond nucleocytoplasmic transport. Journal of Experimental Botany **72**:6140-6149.

Xiong, F., Duan, C.-Y., Liu, H.-H., Wu, J.-H., Zhang, Z.-H., Li, S., and Zhang, Y. (2020). Arabidopsis KETCH1 is critical for the nuclear accumulation of ribosomal proteins and gametogenesis. The Plant Cell **32**:1270-1284.

Xu, D., Farmer, A., and Chook, Y.M. (2010). Recognition of nuclear targeting signals by Karyopherin-β proteins. Current opinion in structural biology **20**:782-790.

Yu, Y.-B., and Yang, S.F. (1979). Auxin-induced ethylene production and its inhibition by aminoethyoxyvinylglycine and cobalt ion. Plant physiology **64**:1074-1077.

Zhai, Y., Fan, Z., Cui, Y., Gu, X., Chen, S., and Ma, H. (2022). APETALA2/ethylene responsive factor in fruit ripening: roles, interactions and expression regulation. Frontiers in Plant Science **13**:979348.

Zhang, B., Zhu, J., Chen, H.-F., and Liu, L.-N. (2026). AlphaFold-based peptide structure prediction: Opportunities, limitations, and future directions. Biotechnology Advances:108977.

Zhang, F., Wang, L., Ko, E.E., Shao, K., and Qiao, H. (2018). Histone deacetylases SRT1 and SRT2 interact with ENAP1 to mediate ethylene-induced transcriptional repression. The Plant Cell **30**:153-166.

Zhang, F., Qi, B., Wang, L., Zhao, B., Rode, S., Riggan, N.D., Ecker, J.R., and Qiao, H. (2016). EIN2-dependent regulation of acetylation of histone H3K14 and non-canonical histone H3K23 in ethylene signalling. Nature communications **7**:13018.

Zhang, F., Wang, L., Qi, B., Zhao, B., Ko, E.E., Riggan, N.D., Chin, K., and Qiao, H. (2017). EIN2 mediates direct regulation of histone acetylation in the ethylene response. Proceedings of the National Academy of Sciences **114**:10274-10279.

Zhang, L., Li, Z., Quan, R., Li, G., Wang, R., and Huang, R. (2011). An AP2 domain-containing gene, ESE1, targeted by the ethylene signaling component EIN3 is important for the salt response in Arabidopsis. Plant Physiology **157**:854-865.

Zhao, H., Yin, C.C., Ma, B., Chen, S.Y., and Zhang, J.S. (2021). Ethylene signaling in rice and Arabidopsis: new regulators and mechanisms. Journal of Integrative Plant Biology **63**:102-125.

Zheng, Y., and Zhu, Z. (2016). Relaying the ethylene signal: new roles for EIN2. Trends in plant science **21**:2-4.

Zhong, S., and Chang, C. (2012). Ethylene signalling: the CTR1 protein kinase. Annual Plant Reviews Volume 44: The Plant Hormone Ethylene **44**:147-168.

Zhong, S., Shi, H., Xue, C., Wang, L., Xi, Y., Li, J., Quail, P.H., Deng, X.W., and Guo, H. (2012). A molecular framework of light-controlled phytohormone action in Arabidopsis. Current biology **22**:1530-1535.

Zhou, F., Guo, S., Peng, X., Zhang, S., Men, C., and Duan, X. (2025). Benchmarking AlphaFold3-like Methods for Protein-Peptide Complex Prediction. bioRxiv 2025: 2025.03. 09.642277. Doi **10**:09.642277.

6 Acknowledgement

Mein besonderer Dank gilt meinem Doktorvater Herrn Prof. Dr. Georg Groth für das entgegengebrachte Vertrauen und die Möglichkeit, mich einem so wichtigen und herausfordernden Thema widmen zu können. Deine Tür steht jederzeit für Fragen offen und deine Lösungsansätze haben mich schon sehr oft davor bewahrt, einzelne Projekte in eine Sackgasse zu navigieren. Die wissenschaftlichen Diskussionen und Anmerkungen deinerseits haben mir immer sehr geholfen und mich als Wissenschaftler nachhaltig geformt. Ich bedanke mich für die jahrelange Unterstützung und selbstverständlich auch für die Übernahme des Erstgutachtens.

Bei Herrn Prof. Dr. Lutz Schmitt möchte ich mich vielmals für die Übernahme des Zweitgutachtens bedanken.

Bei Herrn Prof. Dr. Rüdiger Simon und seinem Team möchte ich mich für die Kollaboration, die im Rahmen dieser Dissertation entstanden ist, bedanken. Ganz besonders danke ich Jan und Meik für die Übernahme der Fluoreszenzstudien sowie für Erklärungen und Einarbeitungen in Experimente, die für mich vorher komplett fremd waren. Ich habe in dieser Zeit sehr viel neues Wissen erlangen und anwenden können.

Selbstverständlich möchte ich mich auch bei dem ganzen Institut für die wundervolle Arbeitsatmosphäre bedanken. Nici und Kerstin, ihr seid das Herzstück des Instituts. Ohne euch würde alles aus den Fugen geraten. Ivonne, vielen Dank für die positive Laune, die du verbreitest und die Hilfsbereitschaft, die du mir entgegengebracht hast, wenn ich bei administrativen Aufgaben wieder mal nicht weiterwusste.

Bei Alex und Raphael möchte ich mich für die stetigen Ratschläge und das Einbringen ihrer langjährigen Erfahrung in das Projekt bedanken. Vor allem du, Raphael, hast einen substanziellen Beitrag zu dieser Dissertation geleistet.

Buket, Dominik und Moritz, für mich seid ihr die „alte Doktorandengeneration“ des Instituts. Ihr habt mich seit meinem ersten Tag im Institut so herzlich empfangen und mir bei etlichen (un)wissenschaftlichen Fragen weitergeholfen. Ich danke euch für eure Hilfsbereitschaft, die lustigen Momente, die wir miteinander teilen konnten und wünsche euch für eure Zukunft alles Gute.

Bei dieser Gelegenheit möchte ich die „neue Doktorandengeneration“ aber natürlich auch nicht außen vorlassen. Marlene, Denise und Meike, ein großes Dankeschön für eure Unterstützung und eure positive Art, die das Institut bereichert. Ohne euch wäre die Zeit im Institut nicht ansatzweise so schön gewesen und ich wünsche euch viel Erfolg für das Verfassen eurer Dissertation.

Auch bei Niclas, Isabel, Maya und Hanna möchte ich mich für die fachliche Unterstützung meiner Projekte bedanken. Die Betreuung eurer Projekte hat mir die Möglichkeit gegeben, mich vor allem auch persönlich weiterzuentwickeln und ich hoffe, dass ihr auf die Zusammenarbeit mindestens genauso positiv zurückblickt wie ich.

Aber auch ein großes Dankeschön an Vinzent, Ece, Melina, Dana, Lucia, Daniel, Franziska, Yannis, Francesca, Sophie, Jacqueline (an dieser Stelle hoffe ich einfach,

dass ich niemanden vergessen habe) für die großartige Atmosphäre im Institut, die durch euch entstanden ist.

Ebenfalls möchte ich mich bei Flo bedanken. Ohne dich hätte das Biochemiestudium nicht mal halb so viel Spaß gemacht. Gegebenenfalls hätte ich das Studium aber auch nie beendet, wenn du mir nicht bei Mathe II geholfen hättest (und ich weiß, du ärgerst dich immer noch darüber, dass ich besser abgeschnitten habe, obwohl du mir alles beigebracht hast). Auch wenn wir uns heute nicht mehr regelmäßig sehen, bin ich dankbar für die Zeit und dafür, dass ich deine Hochzeit miterleben durfte. Ich wünsche dir und Nina alles erdenklich Gute für die Zukunft.

Natalie, dir möchte ich meinen besonderen Dank für die Geduld, den Zuspruch und die Wertschätzung aussprechen, die du mir stets entgegenbringst. Ich weiß, dass ich besonders in stressigen Phasen sehr schwierig sein kann und bin dir zutiefst dankbar für deine emotionale Unterstützung. Ich hoffe, ich bin für dich eine ebenso große Motivationsquelle wie du es für mich bist.

Dominik, Tobi, Karsten und Milad, ich weiß gar nicht wo ich da anfangen soll. Wir kennen uns schon so lange und haben so viel erlebt, dass ich hier mehrere Seiten füllen könnte, aber ich belasse es bei einem großen Dankeschön und spekuliere darauf, dass ihr wisst, wie wichtig ihr für mich seid.

Zu guter Letzt bedanke ich mich bei meiner Familie. Mama, ich kann in Worten gar nicht beschreiben, wie viel du mir bedeutest und wie dankbar ich dafür bin, dass du alles Erdenkliche versucht hast, um mir diesen Weg zu ermöglichen. Marc, vielen Dank für alles, was du in den letzten Jahren für uns getan hast. Auf dich ist immer Verlass. Lea, du hast ein genau so großes Herz wie du dickköpfig bist. Auch wenn wir uns ab und zu in die Haare kriegen, bin ich unglaublich froh darüber, dich als Schwester zu haben. Ich hoffe, dass meine beiden Neffen, Arian und Elian, dies eines Tages lesen werden.

7 Declaration

Ich versichere an Eides Statt, dass die Dissertation von mir selbständig und ohne unzulässige fremde Hilfe unter Beachtung der „Grundsätze zur Sicherung guter wissenschaftlicher Praxis an der Heinrich-Heine-Universität Düsseldorf“ erstellt worden ist. Weiterhin versichere ich, dass ich diese Dissertation weder in dieser noch in ähnlicher Form keiner anderen Fakultät oder Institution vorgelegt habe und dass ich keine vorherigen erfolglosen oder erfolgreichen Promotionsversuche unternommen habe.

Ort, Datum

Fabian Wynen